Reduced Order Modeling of Distillation Systems

Martina L.S. Welz

University of Cape Town
Department of Chemical Engineering
Dissertation in partial requirement for a Master of Science in Chemical Engineering

March 17, 2007

Abstract

The concept of distillation *separation feasibility* is investigated using *reduced-order models*.

Three different models of nonequilibrium rate-based packed distillation columns are developed, each with progressive levels of complexity. The final model is the most complex, and is based on the Maxwell-Stefan theory of mass transfer. The first and second models are used as building blocks in the approach to the final model, as various simplifying assumptions are systematically relaxed.

The models are all developed using orthogonal collocation. The order reduction properties of collocation are well documented. A low order model is desirable as the subsequent generation of data required for assessing the separation feasibility is fast.

The first model is the simplest as constant molar overflow is assumed. This assumption is relaxed in the subsequent models. The second and third models differ in their respective mass and energy transfer. The second model uses a *constant* bulk phase approximation for an overall gas phase transfer coefficient. The third model uses rigorous Maxwell-Stefan mass transfer coefficients, which *vary* throughout the column. In all models, the bootstrap equation for the energy balance across the two-phase film is used after the appropriate modifications are made based on the system assumptions.

Starting point solutions and minimum height and flows analysis are presented for all models. The first model is used to develop an azeotropic methodology for identifying and characterizing pinches. Different numerical techniques are also compared, and the accuracy of orthogonal collocation is verified.

Ternary and pseudo McCabe-Thiele diagrams are used to represent the results for the multicomponent models 2 and 3. The results for models 2 and 3 are similar. This is expected as they differ only in the mass and heat transfer definitions. An argument is made for a specific definition of an objective function for models 2 and 3, which is subsequently used to generate separation surfaces. This function is defined such that there will always be a solution and for this reason is deemed superior to any alternatives. Feasible regions are identified using a grid projection of the relevant sections of the separation surfaces. The data set contained within the feasible region will be used in an optimizer in future work.

In general, this work involves an understanding and application of the collocation mathematics to distillation systems. A further understanding of distillation systems, the associated mathematics and degrees of freedom is essential. A large section of this work is devoted to explaining and manipulating the available degrees of freedom, such that the desired end result of a *feasible region* for a *specific separation* can be obtained. Other complicating factors include the use of the collocation boundary conditions, and the relationship between these and the overall degrees of freedom for the system.

In the literature, collocation is largely applied to staged columns. The resulting feed stage discontinuities are smoothed out using various interpolation routines. Both of these approaches are incorrect. It is shown that the use of collocation in staged columns is fundamentally flawed due to the underlying theory of staged distillation and the implications of collocation assumptions. Further, the feed discontinuities present in all the results are intrinsic features of the system and should be preserved.

It is further concluded that Models 2 and 3 were correct in comparison with each other. Finally it was shown that the separation feasibility was successfully determined using the optimal objective function. This success was based on the accuracy and order reduction achieved through the use of collocation. Further work will involve optimizing the data found in the feasible region using Non-Linear Programming.

Acknowledgements

I would like to thank my supervisors Dr. Chakraborty and Prof. Möller for initially finding me the best possible project, as well as for their continued support and encouragement. Particular thanks to Prof. Möller for his open-door policy, programming advice and general enthusiasm and assistance wherever possible. The time spent as a post-graduate student has been incredibly beneficial and that is largely due to excellent supervision. Thank you also to my colleague Michael Hughes who was always ready to assist (and is an excellent proof-reader), and for showing me some of the short cuts!

The following organizations are thanked for providing funding for this research:

1. SASOL *ltd.* for providing a Researcher's Scholarship
2. The University of Cape Town Postgraduate Funding Office for awarding:
    - *UCT Senior Entrance Scholarship*
    - *Manuel and Luby Washkansky Scholarship*
    - *Council Postgraduate Scholarship*
    - *Harry Crossley Foundation*
3. The National Research Foundation

The chances are good that I would not have undertaken post-graduate studies if my older brothers was not around to offer support and dispense advice with a slightly sanctimonious air, which is of course the prerogative of older siblings. So, thank you Andreas for being an outstanding big brother! Thank you to my parents for the support they were able to offer. And of course to my best friend Meg and my second family 'the Britzes', thank you for everything!

Contents

List of Figures

List of Tables

Chapter 1

Introduction

The objective of this thesis is to develop an accurate *low order* model of a nonequilibrium rate-based packed distillation column. In the future, this model will be used to develop a flowsheet simulator which optimizes *separation feasibility*.

1.1 Optimizing Separation Feasibility: *Global Flowsheet Simulator*

It would be useful if there was a flowsheet simulator which could optimize a sequence of separation stages as envisioned in Figure 1.1. Given a feed, the flowsheet should be able to determine the optimal height as well as the separation feasibility[1]. Currently such a flowsheet simulator is not available for either separation or reaction-separation systems. Existing industrial simulators which use a trial-and-error approach, are limited as separation feasibility is not known prior to column design. Hence rigorous calculations may not converge if the separation is infeasible. Further, for a stiff system of equations, feasible designs may not converge. Therefore the flowsheet simulator would be a novel and useful tool. The first step forwards would be the development of an accurate low order model which would be repeatedly called within the simulator.

1.2 Optimizing Separation Feasibility: *Local Low Order Model*

Because the flowsheet simulator will repeatedly call the local low order model as shown in Figure 1.1[2], the *key concept* is that the model order must be as low as possible for faster processing time, without compromising accuracy. Orthogonal Collocation (OC) is an effective order-reduction

[1] There is an obvious trade-off between a taller column and the relative improvement in separation

[2] In this figure the smaller blocks represent the low order model, and the manner in which they are grouped is a global function of the flowsheet simulator.

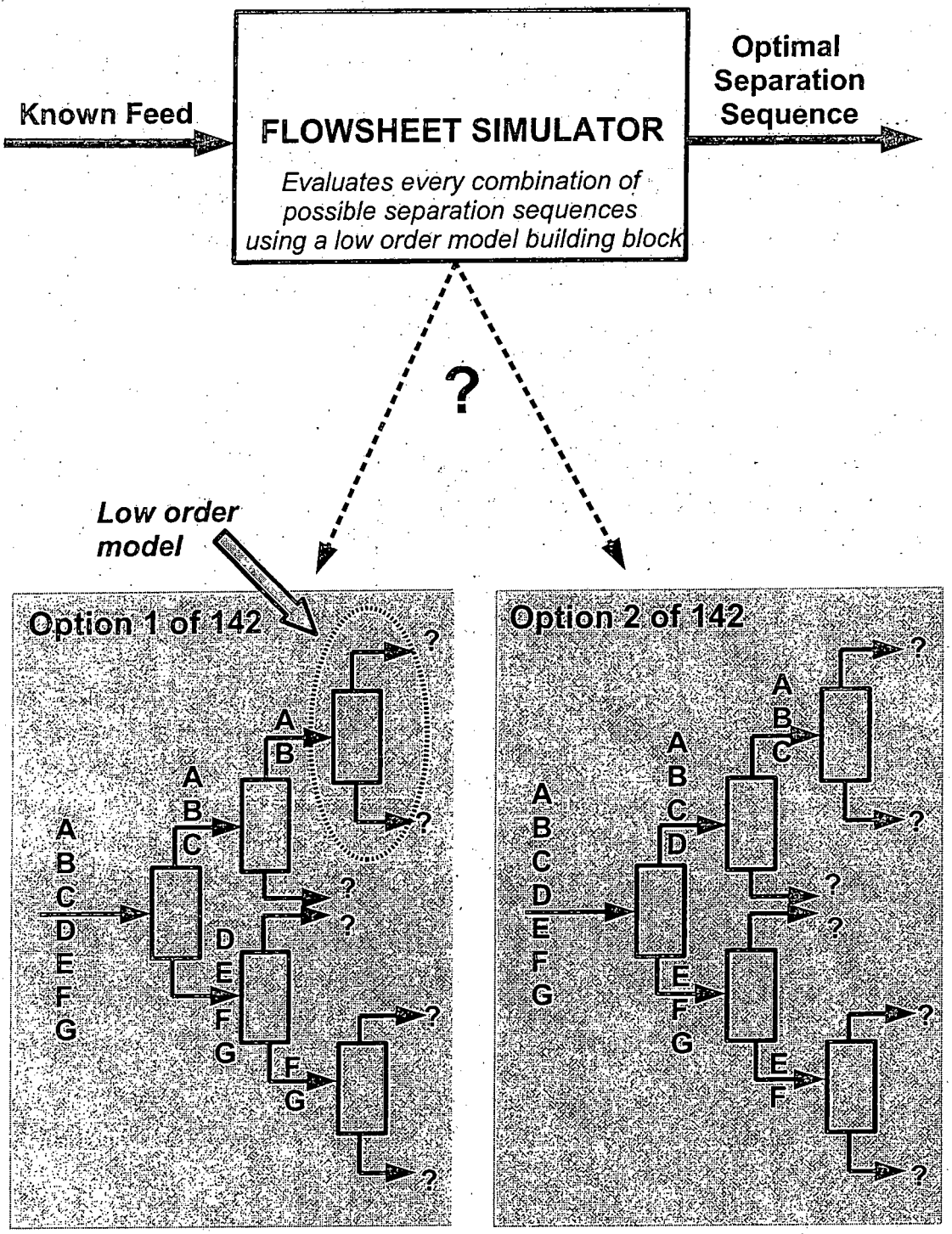

Figure 1.1: Proposing a flowsheet simulator for optimizing separation feasibility through the use of a low order model. The total number of possible separations sequences was estimated using Thompson and King's method [3]

modeling technique. It has been used extensively to model intransient staged columns, with minimal application to packed columns, and none to rigorous separation system sequencing. Collocation is also popular when modeling transient systems due to the high degree of stiffness. Generally distillation models have a high order, sometimes with thousands of equations. Without a reduction in order, plant models can quickly become large and difficult to solve. Flowsheet optimization[3] compounds the problem further. Hence a reduced order model is necessary.

1.2.1 Reducing the Model Order: *How does collocation work?*

The model order can be reduced through polynomial approximation of the state profiles. The polynomial order depends on the number of collocation points. These are the roots of the approximating polynomials. The state variables are calculated at each collocation point and not at each section of packing or stage. If there are fewer collocation points than there are sections of packing or number of stages, then the subsequent order of the model is reduced. The state variables associated with the real 'stages' are found by interpolation.

1.2.2 Packed Column vs. Staged Column?

From the start of work on this thesis, there was a debate as to which distillation system to model: staged or packed? The degree of order reduction possible is higher in a packed column as explained below. Further, the mathematical path followed between converting sets of equations from difference (staged) or differential (packed) equations into collocation format, suggest a packed column is more suitable. Finally, unlike a staged column height, a packed column has a continuous height which is better suited to polynomial approximation, making it the more intuitive choice.

1.2.2.1 Order of Magnitude Analysis

An order-of-magnitude analysis of the number of equations needed in a staged distillation column design is $N \cdot (2n_c + 7)$, where N is the number of stages, and n_c the number of components [18]. Typically, $10 \leq N \leq 100$ and $n_c < 50$. This estimation will be higher for packed columns as more calculation points are required.

1.2.2.2 Conversion between the Mathematical Equations

A staged column at steady state consists of Algebraic Equations (AE's) which need to be converted into Differential Equations (DE's) before collocation can be applied. The collocation pro-

[3]Optimization repeatedly evaluates various combinations of smaller models

cess converts the DE's back into a different set of AE's, which are subsequently solved. When considering a packed column, the equations are represented by DE's. Collocation is applied and the DE's are converted to AE's and solved[4]. To summarize, in comparison to a packed column, collocation applied to a staged column requires an additional mathematical conversion from AE's to DE's.

1.3 Research Questions

To conclude, this thesis aims to develop an accurate low order model of a rate-based nonequilbrium column, with the broader purpose of investigating separation feasibility. Therefore can a low order model with the following characteristics, be developed for future use in a flowsheet simulator:

- Vary the height or number of stages without affecting the order?
- Predict the state on any stage
- Not require a prior full-order solution
- Accept nonlinear and multicomponent problems
- Accept mass transfer correlations
- Allow free choice of thermodynamic subroutines?

[4]Alternatively finite differences can be used instead of collocation. However it has been shown that greater order reduction is possible when using collocation [10]

Chapter 2

Literature Review

This chapter first explains how collocation fits into a flowsheeting superstructure. A explanatory background to *distillation* and *collocation* is subsequently established, before looking at the more complex application of *collocation to distillation design*. While only the last section may truly be considered a literature review, it cannot stand without the prior background sections.

2.1 Flowsheeting Simulators and Building Blocks

The global aim is the development of a flowsheet simulator, which optimizes a separation sequence. This flowsheet superstructure will repeatedly call a single, low order model of a distillation system. While the low order is essential, high accuracy is also a prerequisite. The low order model can be thought of as a building block, and is the *focal point* of this work. The flowsheet superstructure is not included in the scope of this dissertation. However because it will constrain the building block to some extent, it is briefly mentioned in Section 2.1.1. In the literature, several similar flowsheets have been developed. As will be shown in Section 2.1.4, they are either insufficiently rigorous due to limiting simplifying assumptions, or inappropriate (i.e. absorption systems).

2.1.1 MINLP Superstructure for use in a Flowsheet Simulator

Mixed Integer Non-Linear Programming (MINLP) can optimize a system of non-linear equations containing continuous and integer variables. For example, MINLP can optimize feed tray location, the number of stages (or packed column height), and the number of column interactions [2], making it useful for process synthesis, retrofitting and optimization. However MINLP problems are difficult to solve unless a special structure can be exploited. A general MINLP problem is

described by the following objectives and constraints [3]:

$$Min \qquad Z = c^T \cdot y + f(x) \qquad st \qquad h(x) = 0 \tag{2.1}$$

$$g(x) + M \cdot y \leq 0 \tag{2.2}$$

$$x \in X \qquad y \in Y \tag{2.3}$$

In the above set of equations, x is a vector of continuous design variables and y is a vector of integer decision variables. They can be solved directly or be reduced through the use of several simplifications. For example, if the discrete variables are removed, a Non-Linear Problem (NLP) results. If the discrete variables remain yet the constraints are all linear, the MINLP reduces to a Mixed Integer Linear Problem (MILP). The MILP can be further reduced to a Linear Problem (LP), if the discrete variables are also excluded. These simplifications will prove important within this work. For example, if a packed column is modeled, the otherwise discrete staged height is replaced by a continuous height function. This has the favorable effect of reducing an MINLP to a NLP.

2.1.2 Using Collocation within a MINLP context

The primary advantage of collocation is the reduction in model order. If the order is varied by varying the degree of the approximating polynomials, solutions of varying accuracy and dimensionality can be obtained. The number of equations is directly proportional to the approximation order. When considering a staged column design without variable transformation, the diameter, feed tray position and stage number are discrete variables. This leads to numerical problems in the regions of pinches as the height tends toward infinity. Using collocation these discrete variables are transformed into continuous variables, allowing for continuous variable optimization i.e. the MINLP is reduced to a NLP [13, 6].

Previously the column height had to be supplied. Using collocation, it can be solved for. From an optimization perspective, it is inconvenient to have a mixture of discrete and continuous variables [21]. Therefore, if discrete variables need not be introduced for height optimization, the combinatorial optimization issues are avoided, thereby justifying the use of collocation [1].

2.1.3 Defining a Portable Collocation Model

A collocation model can be easily adapted into an optimization superstructure. The characteristics defining applicability as building block within such a superstructure are [1]:

- The packed height is obtained from the solution of the NLP and not the MINLP problem. This eliminates the combinatorial nature of the column design problem.
- The packed column model equations in an algebraic format (MERQS) are applied at the collocation points only, thereby reducing the NLP order.
- For a staged column, as the number of collocation points approaches the number of stages, the full-order solution is recovered.

In the future, the collocation building block will be used in a superstructure, as shown in Figures 1.1 & 2.1. The global aim is the development of an automatic, globally convergent, flowsheet simulator which efficiently and effectively optimizes separation sequences. In short, given a known feed, generate the best distillation train which achieves the required purity specifications at minimum cost (or some other objective function).

2.1.4 Existing Separation Feasibility Flowsheet Simulators

A multicomponent distillation network synthesis tool was developed using a transformation to dimensionless tray temperature [41]. The low order model (i.e. building block) used temperature collocation [40]. The resulting MINLP was solved using a Genetic Algorithm (GA). The flowsheet simulator was tested using multicomponent azeotropic separations. The assumptions made in the low order model constrained the flowsheet simulator results. In this case, the distillation systems were equilibrium staged columns with constant molar overflow (CMO) assumptions.
A further flowsheet for the synthesis of reactive absorption column exists. The low order model used OC to avoid combinatorial issues as mentioned previously in Section 2.1.2. Various simplifying assumptions were made, which can be referenced in the original text [1].

2.1.4.1 Smaller Optimization Problems

An optimization routine was developed for an equilibrium staged distillation model. The low order model was developed using OC and solved at steady state using NLP solvers. Two columns were simultaneously optimized. The key result showed that it was possible to converge to the optimal solution from a larger region of initial guesses, as opposed to the full order model. This was attributed to the successful retainment of gradient information, which is crucial for convergence to the same optimum as that of the rigorous model [23].
A similar optimization routine for an equilibrium staged distillation model *with reaction* was also developed. The low order model also used OC. Additionally, the rate of reaction was evaluated at the collocation points. The superstructure consisted of two columns and was optimized using a NLP solver. A detailed sensitivity analysis defined a range of design conditions such that a feasible operation was achieved for a given magnitude of possible parameter variations [21].

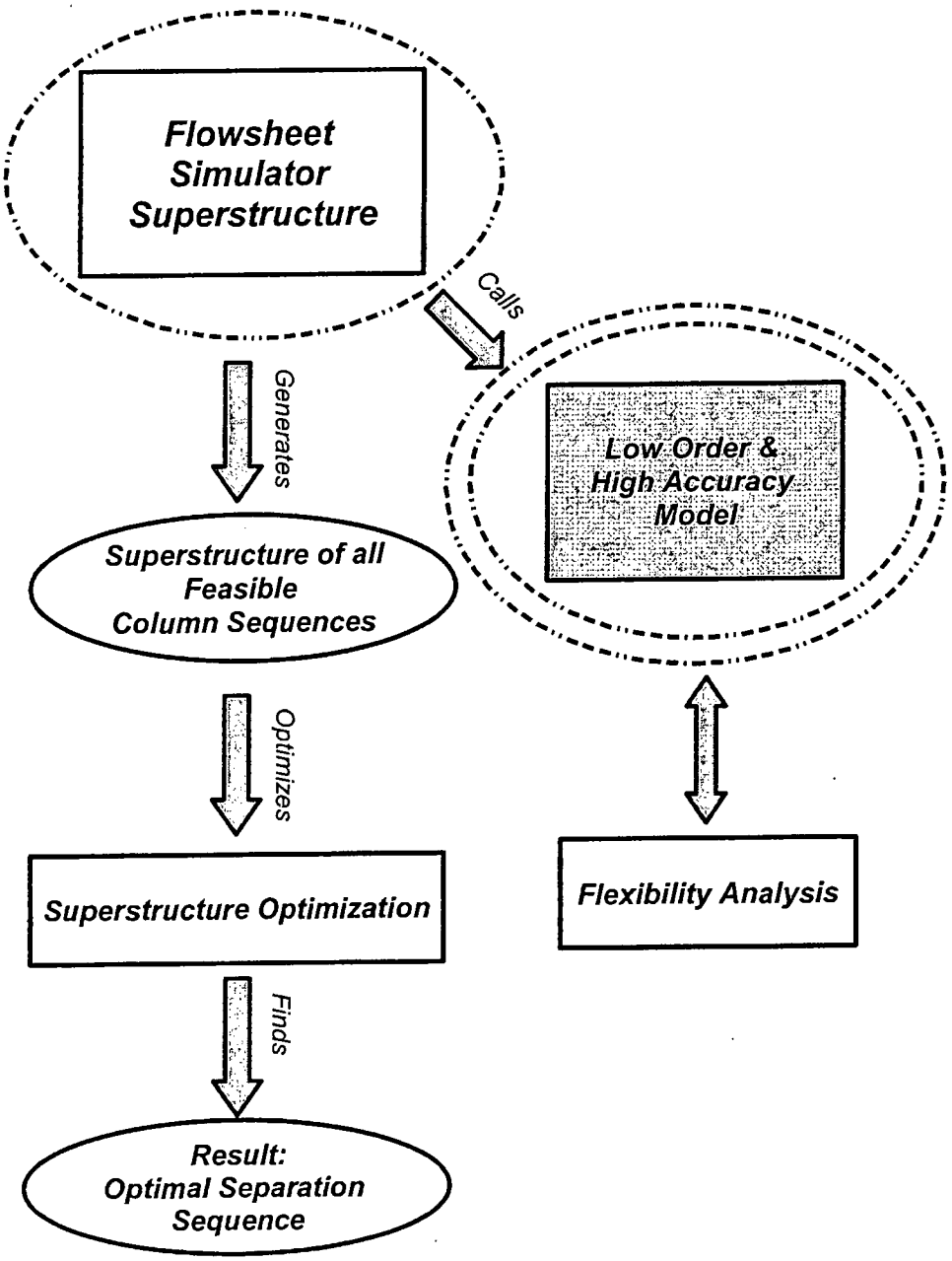

Figure 2.1: Methodology suggested for the development of a flowsheet simulator superstructure

2.1.5 Collocation and Flowsheeting: Summary

The first section of the literature has been completed. The intention was to flesh out the very broad idea of a flowsheet simulator which could optimize a separation sequence. The examples of current optimization superstructures highlighted the gaps in the literature. This motivated the development of a rigorous separation sequencing flowsheet simulator. The first developmental step requires the construction of a low order model. Collocation was suggested as an order reduction technique, as the link between MINLP and collocation based on simplifications of the superstructure was shown. The next section provides an overview of relevant distillation theory, which will be used extensively in Chapter 3, where the models are developed.

2.2 Distillation Theory: *Binary Systems*

McCabe-Thiele analysis is a common approach to modeling binary staged distillation columns. The assumptions used are [15]:

1. Liquid and vapor phases perfectly mixed
2. Constant molar overflow (CMO)
3. Adiabatic column
4. Isobaric column

Of the above assumptions, CMO is the most restrictive as it translates into constant liquid and vapor flowrates within each column section. Constant molar latent heat of vaporization of a mixture results in CMO in an adiabatic column, as identical amounts of energy are required to condense or vaporize a mole of material. Figure 2.2 shows a typical schematic of a McCabe-Thiele column with the stages numbered as n. The overall mass balance is:

$$F = D + B \tag{2.4}$$

The balance over the light component across the feed is:

$$F \cdot z_F = D \cdot z_D + B \cdot z_B \tag{2.5}$$

where z is a mole fraction of either phase. The steady state balances for the total molar flows in the top of the column (envelope 1 in Figure 2.2) are:

$$y_{n-1} = \frac{L_n}{V_{n-1}} \cdot x_n + \frac{D}{V_{n-1}} \cdot z_D \qquad \text{for } n = n+1, n, n-1, \ldots, \text{feed stage} + 1 \tag{2.6}$$

The above equation is known as the rectifying operating line. In the stripping section (envelope 2 in Figure 2.2), a similar balance gives the stripping operating line:

$$y_n = \frac{L_{n+1}}{V_n} \cdot x_{n+1} - \frac{B}{V_n} \cdot z_B \qquad \text{for } n = 0, 1, 2, \ldots, \text{feed stage} - 1 \tag{2.7}$$

2.2.1 Minimum Flows and Height

The minimum reflux ratio depends on the difficulty of the desired separation. Typically a column is operated at an optimum reflux ratio, which lies between 1.2 to 1.5 times the minimum [24]. The minimum height is determined at infinite reflux. For either a staged or a packed column, the

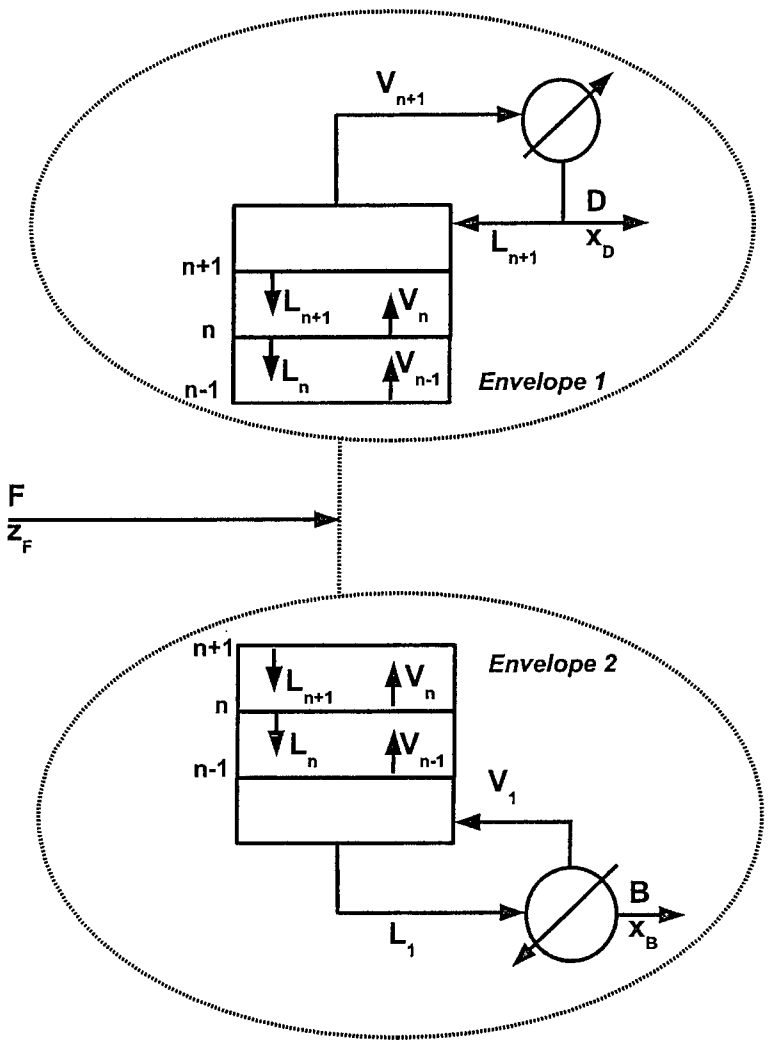

Figure 2.2: Schematic of McCabe-Thiele column with the rectifying and stripping sections indicated as envelopes 1 and 2 respectively

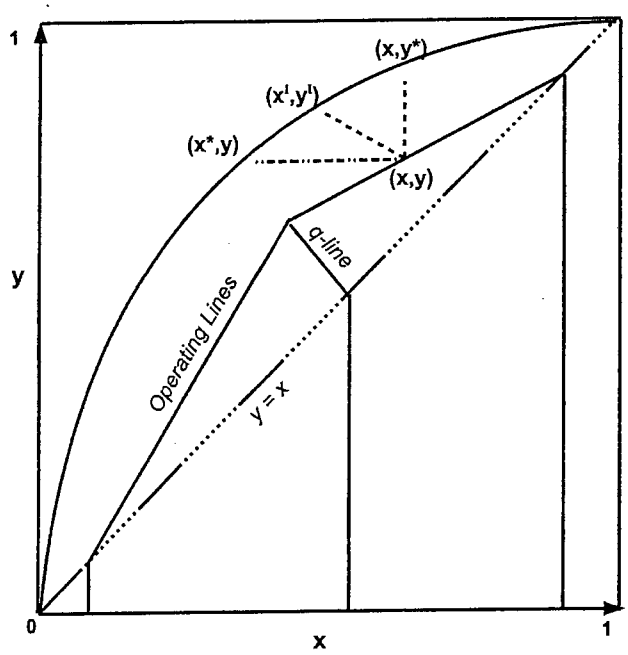

Figure 2.3: Binary distillation in a packed column with McCabe-Thiele assumptions

minimum height and minimum reflux ratio calculations are the same, as the position of the operating lines do not change. For minimum height, the operating lines must coincide with the $y = x$ line. For minimum flows, the operating lines must pinch at the equilibrium line. A significant point to be made is that these **limiting conditions must be determined at a fixed separation** i.e. one of the product purities must be specified. This will have the effect of tying down one of the operating lines. If this is not done, the position of the operating lines will shift making it difficult to establish whether or not limiting conditions have been met.

The minimum height and flows analysis is shown below for a packed column. The staged analogy can be referenced in [9] and [15] if required. If CMO is assumed, mass balances over an incremental section of packing are given as:

$$V \cdot dy = k_y a \cdot (y - y^{\mathrm{I}}) \cdot S \cdot dz \tag{2.8}$$

$$L \cdot dx = k_x a \cdot (x^{\mathrm{I}} - x) \cdot S \cdot dz \tag{2.9}$$

The column height is found by integrating over the rectifying and stripping sections as shown in Figure 2.3. For *minimum height* the operating lines coincide with the $y = x$ line:

$$Height^R = \int_0^{(Height^R)} dz = \int_{z_F}^{z_D} \frac{V \cdot dy}{k_y a \cdot S \cdot (y - y^I)} = \int_{z_F}^{z_D} \frac{L \cdot dx}{k_x a \cdot S \cdot (x^I - x)} \tag{2.10}$$

The area under the curve represented in the above equation, can be integrated numerically or graphically if α is constant.

2.2.2 Degrees of Freedom Analysis: *Binary or Multicomponent System*

In the following analysis, it is assumed that the feed composition, quality and the pressure are known, and that the mole fractions in each phase sum to unity. A simple column has four degrees of freedom, typically three product compositions and a desired reflux ratio [40], [9] & [32]. As the feed is fully specified, the following variables remain:

Reflux Ratio: 1 variable

Reboil Ratio: 1 variable

Distillate composition: $c - 1$ variables

Bottoms composition: $c - 1$ variables

Stripping section height: 1 variable

Rectifying section height: 1 variable

The total number of variables is subsequently $2 \cdot C + 2$, where C is the total number of components. The following constraints exist:

Overall energy balance: 1 constraint

Relations between the product compositions: $c - 2$ constraints *(shown in below equation)*

$$\frac{z_{i,B} - z_{i,F}}{z_{j,B} - z_{j,F}} = \frac{z_{i,D} - z_{i,F}}{z_{j,D} - z_{j,F}} \qquad \text{where } i, j \text{ are any two components} \tag{2.11}$$

Profiles must intersect at q-line and within VLE: $c - 1$ constraints *(shown in below equation)*

$$x^R_{i,Height^R} = x^S_{i,Height^S} \qquad \text{where } i = 1, ..., C \tag{2.12}$$

The total number of constraints is subsequently $2 \cdot C - 2$. Therefore, there are $(2 \cdot C + 2) - (2 \cdot C - 2) = 4$ degrees of freedom. Note that these degrees of freedom are independent of the number of components.

2.2.2.1 Typical Design Specifications

The *performance problem* predicts distillate and bottoms compositions for a given feed and known column configuration. The following are the most common design specifications for a binary mixture:

- Reboil ratio
- Reflux ratio
- Stripping section height
- Rectifying section height

The *inverse design problem* seeks optimal column dimensions and operating conditions for achieving the product purities. Typical design specifications for the inverse problem are:

- Distillate composition for 1 component
- Bottoms composition for 1 component
- Stripping section height
- Rectifying section height

The latter is the more difficult to converge numerically and may only exist for certain specifications due to thermodynamic separation barriers [40]. One technique for solving the inverse design problem rigorously has been proposed [40, 41]. The realizability of a given separation target (i.e. three product purity specifications and the desired reflux) can be determined using liquid tray composition profiles expressed in terms of equilibrium tray temperatures as independent variables. This approach is detailed in Section 2.11.2.

2.3 Distillation Theory: *Multicomponent Systems*

Ternary systems can be visualized using ternary diagrams [9], as well as by using pseudo McCabe-Thiele diagrams. Quaternary systems can be viewed using tetrahedral diagrams. However, unless components are similar and can be grouped together, it becomes more difficult to graphically represent multicomponent separations exceeding four components. Planar operating and equilibrium lines are replaced by multi-dimensional surfaces.

2.3.1 Pseudo McCabe-Thiele Diagrams

McCabe-Thiele diagrams can be modified for multicomponent systems. The diagrams can be constructed from the mole fractions of any two components, although usually the light key is normalized with respect to the heavy key. This is the most useful representation, allowing for the optimal feed position to be determined. The mole fractions are normalized so that each axis extends from 0 to 1. The operating and equilibrium lines may be strongly curved [32].

2.3.2 Degrees of Freedom Analysis: *Multicomponent System*

The degrees of freedom available in distillation design is independent of the number of components, and is subsequently the same as presented in Section 2.2.2 on page 13, namely **4 degrees of freedom** for a multicomponent mixture.

2.3.3 Minimum Flows and Height: *Multicomponent System*

The minimum reflux ratio in a multicomponent system can be found using the Underwood method. However it is restrictive due to the required assumptions of CMO and constant relative volatility (CRV). It is also of little use in the design of distillation trains because of its extremely nonlinear behavior [40]. Otherwise the same determining principles for binary systems as shown in Section 2.2.1, apply to multicomponent systems.

2.3.4 Pinch Point Analysis

Pinches are important for two reasons. Firstly, they need to be identified to avoid numerical difficulties e.g. $height \rightarrow \infty$. Secondly, they are used to find minimum flows. Pinches are solved for by the intersection of the rectifying and stripping operating lines with the equilibrium line. In a C component mixture there are usually C pinches points. However the number may increase with increasing non-linearity, which may be due to an increasing number of components. The operating lines remain fixed by the vapor and liquid flows, but there are now multiple equilibrium lines which may pinch with these [9].

2.3.4.1 Saddle Pinch

A saddle pinch occurs when the composition is constant for a large section of packing. An example is shown in Figure 2.4. They are common in multicomponent mixtures, and are approached asymptotically with increasing height. The pinch location is sensitive to the compositional purity. Although saddle pinches correspond to an infinite height and constant composition, they do not

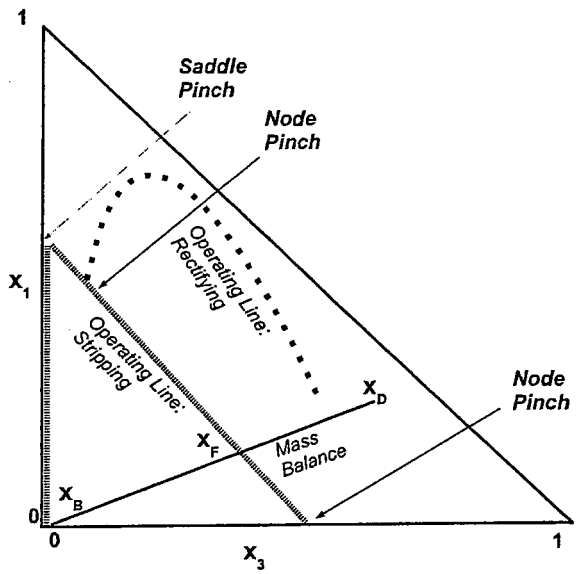

Figure 2.4: Triangle diagram showing the location of node and saddle pinches in a ternary system

necessarily correspond to the minimum reflux ratio in a multicomponent system. The reason is that while the stripping and rectifying profiles are fixed by the internal flows, there are additional equilibrium lines in a multicomponent system. And for an alternate component (different to the pinching component), the operating lines may still intersect for lower reflux values [9].

2.3.4.2 Node Pinch

While there is no analogy in binary systems for a saddle pinch, the pinches which appear at the upper and lower ends of the operating lines for binary mixtures, are known as node pinches in multicomponent systems. This is shown in Figure 2.4. The node pinch position depends on the ratio of the vapour to liquid flows i.e. reflux or reboil ratio.

2.3.4.3 Tangent Pinch

In a binary system, the tangent pinch lies between the operating line and the equilibrium curve. In a ternary system, the meeting of the equilibrium surface and operating line describes the tangent pinch. While it can be easily seen in a binary system, it is not apparent in a multicomponent one.

2.4 Distillation Theory: *Packed Columns*

Packed columns are used extensively in industry as a liquid-gas contacting system, mainly in absorption and distillation with small cross-sectional area requirements. There are three main modeling approaches. The simplest, most inaccurate and most frequently used are the HETP or HTU methods, where the packed column is divided into sections which are treated as stages. This is discussed in Section 2.4.1. Alternatively, differential balances are written for a small section of packing and solved numerically. This is more theoretically correct, but poses problems as the resulting models are frequently stiff. This is method is briefly mentioned in Section 2.4.2. The final approach used by ChemSep is a smart technique which takes the first order approximation to the set of differential equations. This resolves some of the numerical problems mentioned previously and is discussed further in Section 2.4.3.

2.4.1 HETP and HTU methods

Because packed columns are continuous differential contacting devices that do not have physically distinguishable stages, they are best analyzed using mass transfer considerations [15]. However in practice, they are often analyzed on the basis of equivalent equilibrium stages using a packed Height Equivalent to Theoretical Plate (HETP) defined as:

$$HETP = \frac{\text{Packed height}}{\text{Number of equivalent equilibrium stages}} = \frac{l_T}{N_t} \tag{2.13}$$

The HETP method assumes CMO and requires that the column be divided into discrete mass transfer sections, each of which is treated as a section in a staged column. The equilibrium stages are stepped off a binary McCabe-Thiele diagram. The mass transfer coefficients require field testing. Although this is widely used, it has no strict theoretical basis. This is a major limitation as the method cannot be scaled for use in different systems. The data is system specific from a *geometric* and *chemical* perspective. Therefore the accuracy of the results are in question, as they may not be in keeping with experimental results. Hence for packed columns, it is preferable to determine the packed height from a more theoretically based method using mass transfer coefficients for both phases [15]. The full derivation is not presented here, only the final result:

$$H_{OG} = \frac{V}{K_{og} \cdot a \cdot S} \tag{2.14}$$

$$N_{OG} = \int_{y_out}^{y_in} \frac{dy}{y - y*} \tag{2.15}$$

The Height of Transfer Unit (HTU) is defined as:

$$HTU = H_{OG} \cdot N_{OG} \tag{2.16}$$

The more theoretically based HTU method uses a McCabe-Thiele diagram to perform an integration over the packed height of each section. The smaller the resulting HTU, the better the contacting.

2.4.2 Rigorous Approach

The differential equations describing the model are solved directly in a rigorous approach. If finite differences are used the large dimensionality becomes a problem, unless the system is banded in which case an appropriate algorithm can be applied. Tridiagonal systems are common in staged distillation columns.

2.4.3 ChemSep Methodology

ChemSep's non-equilibrium model does not use the HETP method or efficiencies[1]. For binary mixtures these are useful techniques. However they do not translate well to multicomponent mixtures as HETP's are different for each component and may vary from $-\infty$ to $+\infty$ [32]. When modeling a packed column, ChemSep uses a first order approximation to the set of differential equations. The resulting set of algebraic equations is solved using a Newton method with a rigorously calculated Jacobian matrix. The methodology used for packed columns is similar to that of used for staged columns. Therefore the same solvers can be used for both systems.

2.5 Distillation Theory: *Summary*

The above three sections complete the literature discussion of distillation theory as thought necessary for this work. This alone is insufficient for the development of a low order model. The following section therefore deals with the more abstract concept of collocation as required. This section is highly mathematical and should be closely read as it provides the groundwork for Chapter 4, where the abstract concepts are applied in the solution methodology.

[1] HETP's and efficiencies are back-calculated from the results.

2.6 Collocation Background

Collocation is an approximation technique which belongs to the family of weighted residuals. An outline is presented below. To prevent any confusion with the nomenclature used in later chapters, a list of symbols used is presented at the conclusion of this section. The nomenclature list at the end of the thesis should not be referred to in conjunction with this section.

2.6.1 General Method of Weighted Residuals: An Approximation Routine

The methods of weighted residuals are used to approximate an implicitly defined continuous function. The approximate and true solutions both satisfy the differential equation at specified locations [12]. For a two-point scalar boundary value problem:

$$u'' = f(x, u, u') \qquad a < x < b \tag{2.17}$$

with boundary conditions:

$$u(a) = \omega \qquad u(b) = \psi \tag{2.18}$$

an approximate solution of the following form is required:

$$u(x) \approx v(x, \mathbf{a}) = \sum_{i=1}^{n} a_i \cdot \phi_i(x) \tag{2.19}$$

where ϕ_i are trial functions[2] defined on $[a, b]$ and $\mathbf{a}$ is an n-vector of undetermined parameters. The satisfaction of the boundary conditions is enforced as part of the process of choosing $\mathbf{a}$. To solve for the vector $\mathbf{a}$, the set of n collocation points are defined as [12]:

$$a = x_1 < \ldots < x_n = b \tag{2.20}$$

The approximate solution $v(x, a)$ is forced to satisfy the ordinary differential equation (ODE) at the interior and end[3] collocation points. In simpler and usually symmetric problems, the trial functions *may already satisfy the boundary conditions*. The approximate solution is consequently less constrained.

[2]While polynomials are the most popular choice, B-splines, trigonometric and other functions can be used provided that they are smooth and differentiable.

[3]The boundary conditions are satisfied at the end points.

Jacobi or Hahn polynomials are the most common choices for the collocation points (see Section 2.6.2 on page 21). Once the collocation points and trial functions have been chosen, the approximate solution and its derivatives are substituted into the ODE at each collocation point:

$$v''(x_i, \mathbf{a}) = f(x_i, v(x_i, \mathbf{a}), v'(x_i, \mathbf{a})) \qquad i = 2, \ldots, n-1 \tag{2.21}$$

The boundary conditions are included:

$$v(x_1, \mathbf{a}) = \omega \qquad v(x_n, \mathbf{a}) = \psi \tag{2.22}$$

The linearity of the resulting set of n equations in n unknowns depends on the whether $f(u, u')$ is linear or non-linear in u and u'. The set of equations are subsequently solved using either Gaussian reduction (if linear), or Newton's method (if non-linear). The resulting vector of parameters x determine the approximate solution function $v(x, \mathbf{a})$. The *key concept* is that a system of ODE's is converted into a set of AE's.

Instead of forcing the approximate solution to satisfy the DE at a finite number of points, the residual can be minimized over the integration interval. From (2.19) the residual is formed as:

$$r(x, \mathbf{a}) = v''(x, \mathbf{a}) - f(x) = \sum_i \phi_i''(x) - f(x) \tag{2.23}$$

The residual is a function of x. It therefore must be minimized over the entire domain. This requires a form of *averaging*:

$$\int_V r(x, \mathbf{a}) \cdot w_i(x) \cdot dx = 0 \qquad i = 1, \ldots n \tag{2.24}$$

In equation (2.24), V is the domain and w_i is a set of independent test functions. The integral is known as an *inner product*. There are n unknown coefficients a_i in the trial solution. Hence the inner product of the residual with the first n trial functions is set to zero:

$$(r, w_i) = 0 \qquad i = i, \ldots, n \tag{2.25}$$

The above set of equations is algebraically solved to obtain the coefficients a_i. There are several possibilities as to the choice of the test functions and definition of the inner product, of which equation (2.24) is only one [20]. There are five widely used variations of the method of weighted residuals. They are distinguished by their *test functions*:

1. Collocation Method (Section 2.6.1.1)
2. Least Squares Method

3. Galerkin Method
4. Moment Method
5. Subdomain Method

2.6.1.1 Collocation Method

The collocation principle is based on orthogonality of the polynomial, and not of the residual function which vanishes at the same points [36]. The test function is defined as the Dirac delta function at n collocation points:

$$w_i = \delta(x - x_i) \qquad 0 < x < V \tag{2.26}$$

where x_i is the i^{th} collocation point. The Dirac delta function is chosen because of the following property:

$$\int_{x_i^-}^{x_i^+} f(x) \cdot \delta(x - x_i) \cdot dx = f(x_i) \tag{2.27}$$

However, this view of collocation as a weighted residual method does not yield useful information as to how the collocation points should be chosen. A more useful approach is to select collocation points by optimizing the remainder term of an interpolation formula for the residual [29]. If the n interior collocation points are chosen as roots of an orthogonal Jacobi polynomial of n^{th} degree, the method is referred to as *orthogonal collocation*. While other orthogonal functions can be used, the Jacobi is the most popular as it is compact and contains only a few terms. Furthermore, the solution can be derived in terms of the dependent variable y, at the collocation points.

2.6.2 Collocation Point Placement

There are various options for the choice of collocation points. An increased number of points may not increase the accuracy. However, it will increase the stiffness ratio if the problem is non-linear, or the condition number if the problem is linear. This increases the computational time.

2.6.2.1 Jacobi Polynomials

When collocation points are chosen as the roots of Jacobian polynomials, very efficient collocation results [37]. The Jacobi polynomials are the solutions to the class of second order differential equations:

$$x \cdot (1 - x) \cdot \frac{d^2y}{dx^2} + [1 - (1 + b) \cdot x)] \cdot \frac{dy}{dx} + n \cdot (b + n) \cdot y = 0 \tag{2.28}$$

The above equation is satisfied by the following n^{th} order Jacobi polynomial:

$$y = P_n^{(\alpha,\beta)}(x) \tag{2.29}$$

The solution is well-behaved at $x = 0$:

$$P_n^{(\alpha,\beta)}(0) = 1 \tag{2.30}$$

The Jacobian polynomial can also be represented as a finite power series with n terms:

$$P_n^{(\alpha,\beta)}(x) = \sum_{i=0}^{n}(-1)^{n-i} \cdot \gamma_{n,i} \cdot x^i \tag{2.31}$$

In the above equation $\gamma_{0,i} = 1$ and the remaining non-zero values are obtained from a recursion relation as detailed in Section C.2.2.1. The variables α and β are defined in the weighting function described by:

$$W(x) = x^\beta \cdot (1-x)^\alpha \tag{2.32}$$

The remaining n coefficients are found from the orthogonality condition, which the Jacobi polynomials satisfy [20]:

$$\int_0^1 [x^\beta \cdot (1-x)^\alpha] \cdot P_j^{(\alpha,\beta)}(x) \cdot P_n^{(\alpha,\beta)}(x) \cdot dx = 0 \qquad \text{for } j = 0, 1, 2, ..., n-1 \tag{2.33}$$

2.6.2.2 Hahn Polynomials

Hahn polynomials are the *discrete analogue of Jacobi polynomials* [30]. As the number of points where the Hahn polynomial is calculated increases toward infinity, it approaches the Jacobian polynomial. They are further related through:

$$Q_k(x, \alpha, \beta, n) = \frac{P_k^{(\alpha,\beta)}(1 - 2 \cdot x)}{P_k^{(\alpha,\beta)}(1)} \tag{2.34}$$

2.6.2.3 Other Collocation Polynomials

The Legrende polynomial is a special case of the Jacobi polynomial. They are one solution to:

$$x \cdot (1-x) \cdot \frac{d^2y}{dx^2} - 2x \cdot \frac{dy}{dx} + n \cdot (n+1) \cdot y = 0 \tag{2.35}$$

The Chebyshev polynomial is also occasionally used [20]. They are one solution to:

$$(1-x^2) \cdot \frac{d^2y}{dx^2} - x \cdot \frac{dy}{dx} + n^2 \cdot y = 0 \tag{2.36}$$

2.6.3 Lagrange Interpolation Polynomials

The Jacobi or Hahn polynomials provide the collocation point position. Since these points are usually not equally spaced,Lagrangian interpolation polynomials are used to provide an approximate solution. There are $(n+1)$ building blocks, which are n^{th} degree polynomials. The Lagrange interpolation polynomial is defined as:

$$y_n(x) = \sum_{i=1}^{n+1} y(x_i) \cdot l_i(x) \tag{2.37}$$

In the above equation, y_n is the n^{th} degree polynomial, y_i is the value of y at the point x_i, and $l_i(x)$ is called the Lagrangian polynomial and is defined as:

$$l_i(x_j) = \begin{cases} 0 & i \neq j \\ 1 & i = j \end{cases}$$

The Lagrange interpolation polynomial is a useful building block. There are $(n+1)$ building blocks, which are n^{th} degree polynomials. The building blocks are given as:

$$l_i(x) = \prod_{\substack{j=1 \\ j \neq i}}^{n+1} \frac{(x - x_j)}{(x_i - x_j)} \tag{2.38}$$

The construction of the Lagrange interpolation polynomial is as follows:

- $n+1$ interpolation points must be chosen
- $n+1$ building blocks must be constructed
- If the functional values of y at those $n+1$ points are known, the interpolation polynomial is given by equation (2.37)

The definitions of Jacobi and Lagrangian polynomials allows for development of computational methods, which are expanded on in Section C.2 on page 155. In brief, the 1^{st} and 2^{nd} derivatives of the interpolation polynomials at the interpolation points are taken [20]. Vector form is used for compactness and the following matrices result:

$$y' = A \cdot y \tag{2.39}$$

$$y'' = B \cdot y \tag{2.40}$$

$$A = \left\{ a_{ij} = \frac{dl_j(x_i)}{dx} \qquad i,j = 1,2,...,n,n+1 \right\} \tag{2.41}$$

$$B = \left\{ b_{ij} = \frac{d^2 l_j(x_i)}{dx^2} \qquad i,j = 1,2,...,n,n+1 \right\} \tag{2.42}$$

A and B are $(n+1, n+1)$ square matrices. If the $n+1$ interpolation points are chosen, the Lagrangian building blocks are defined (2.38), and A and B are known.

2.6.4 Quadrature

Quadrature allows for the evaluation of integrals using weighted discrete summations to a high accuracy. The weights are chosen according to the approximating polynomial used. Quadrature is not usually required when modeling distillation columns. It is often used in catalytic diffusion problems where integrals are required for average reaction rates over the particle volume.

2.6.4.1 Gauss-Jacobi

The quadrature relation is [20]:

$$\int_0^1 W(x) \cdot y_{n-1}(x) \cdot dx = \sum_{i=1}^{n} y_i \int_0^1 l_i(x) \cdot W(x) \cdot dx = w^T \cdot y \tag{2.43}$$

The weights are defined:

$$w_i = \int_0^1 l_i(x) \cdot W(x) \cdot dx \tag{2.44}$$

If a Jacobi polynomial is used, the quadrature weights becomes:

$$w_i = \int_0^1 x^\beta \cdot (1-x)^\alpha \cdot l_j(x) \cdot dx \tag{2.45}$$

For Gauss-Jacobi quadrature and weights, n collocation points must be chosen as the n roots of the n^{th} degree Jacobian polynomial. Adding one more point to the interpolation process will not increase the accuracy of the quadrature if the n interior collocation points are chosen as the roots of the n^{th} degree Jacobian polynomial $P_n^{(\alpha,\beta)}$. To improve the accuracy when one or two boundary points are used as extra interpolation points, an alternative quadrature formula is needed [20].

2.6.4.2 Radau and Lobatto

If an additional interpolation point is to be included e.g. $x_{n+1} = 1$, the first n interior collocation points should be chosen as the roots of the Jacobi polynomial $P_n^{(\alpha+1,\beta)}$. Similarly, if an additional point at $x = 0$ is required; the interior points must be chosen as the roots of $P_n^{(\alpha,\beta+1)}$. If both boundary conditions are included, then $P_n^{(\alpha+1,\beta+1)}$ is used. End-point collocation gives superior results to interior-point collocation [34]. The stability of the system is also improved. However, the approximation polynomials are one degree higher.

2.6.5 Trial Functions

Collocation specifies a criterion for determining the coefficients of the trial functions. As shown in equation (2.19), the trial functions are used to build the approximate solution to the DE. Collocation does not constrain the choice of trial functions. The simplest choice of collocation points is an equally-spaced mesh, although when using polynomials as trial functions, accuracy is improved if alternative points are chosen.

2.6.5.1 Spectral Trial Functions

Trial functions are chosen as polynomials or trigonometric functions, which are non-zero over the domain. The trial functions are eigenfunctions of a differential operator. These methods have a high accuracy in relation to the number of points used. However the resulting system of equations are dense and computationally expensive [12].

2.6.5.2 Finite Element Trial Functions

The trial functions are non-zero over only a small portion of the problem domain e.g. B-splines. The resulting set of equations are well conditioned and display almost orthogonal behavior, with their sparsity reducing computational effort. However as the number of basis functions increase, the set of equations becomes increasingly ill conditioned. An acceptable accuracy may require a larger set of equations [12].

2.6.5.3 Comparison between Collocation and Finite Differences

While both methods have approximate solutions chosen from a finite space, the nature of the solutions are different. The collocation solution parameters are coefficients of a linear combination of trial functions. Because two or more functions can have the same gradient at a point without having agreement in function values, satisfying the DE is not the same as agreeing with the exact

solution. Hence, collocation solutions are not anticipated to be exact, nor mimic all properties of true solutions. Collocation uses global information across all points in the domain to find a solution at a single point. Finite differencing uses local information adjacent to the current point being solved for. The order of the finite difference approximation is an indication of the number of adjacent points used in the local approximation.

Finite difference solution parameters are approximate values of the solution. They require small spatial steps, which increases the stiffness [25]. However, they are effective over non-symmetric domains, as well as in multidimensional problems. Finite difference methods improve in accuracy and convergence as the number of points increase. The resulting solution is however only defined at discrete points, and is subsequently not differentiable nor continuous [12].

A case study examined mass and energy diffusion in a catalyst pellet with both a small and a large value for the Thiele modulus (Φ) [4]. For reaction to take place, heat and mass needs to diffuse into the catalyst pellet. The resulting mathematical equation is a two point nonlinear boundary value problem (BVP). If the diffusion is very fast (and Φ is correspondingly small), the concentration of each species is everywhere close to its boundary value. If Φ increases, the concentration profiles develop a boundary layer near the pellet surface, and the concentration at the interior of the pellet is at a modified equilibrium.

OC can be combined with finite difference methods to solve these type of problems when Φ is large. Physically, this translates into a steep concentration gradient near the pellet surface. If only collocation was used, a large number of points would be required to obtain a reasonable accuracy. The orthogonal collocation on finite elements (OCFE) method combines the rapid convergence of OC with the convenience associated with finite difference methods of locating grid points or elements where the solution is important, or has large gradients

The set of equations was solved using both OC, OCFE and finite differences. It was shown that for small Φ, OC was more effective than OCFE, but both were more efficient than finite differences. The reduction in error achievable when using OCFE is h^{2n}, while for finite differences, the error reduction is lower at h^n. For a large Φ, OCFE was the most suitable method for the steep gradients.

Therefore collocation had superior accuracy and faster computational times. However if the severity of the gradients was increased, finite differences took half the computational time required for collocation methods. Hence collocation achieves its dramatic improvement as it uses fewer terms, although in this instance, compromising on accuracy. Generally if a problem has steep gradients, then a finite difference method is preferable [10]. A similar analysis was performed on a packed bed reactor with radial dispersion. Results obtained using finite differences

were compared with those found using OC. The OC results were more accurate e.g. 21 finite difference grid points were needed in comparison to 3 collocation points, in order to achieve the same accuracy [10].

2.7 Collocation and Separation Systems

Collocation gains application when it is considered in conjunction with the set of equations describing a distillation column. The choice of collocation roots should be made in consideration with the physical system.

2.7.1 Background: *The need for order reduction strategies*

Distillation models have large dimensionality, consisting of large, stiff systems of nonlinear algebraic and differential equations [30]. Simulation packages are limited by the number of equations. A low order model approximates the composition profiles using polynomials. The number of equations are reduced as they are dependent on the number of collocation points and not the height or number of stages [6, 1].

2.7.1.1 Single Systems

Low order models can be much smaller for very large columns. For example, a model was developed which is equivalent to an 18-staged column, irrespective of the actual number of trays [13]. Reduced order models can be used in steady-state simulation and optimization if they identify the same optimal solution as the full order model. However the values of the state variables associated with the real stages, are only obtained through interpolation of those associated with the pseudo stages i.e. at the collocation points [5].

2.7.1.2 Multiple Systems

Low order models have use in simulation and optimization of large multicomponent distillation columns or trains. They can allow for the study of dynamic systems previously considered too difficult due to high dimensionality. Other related applications include process interaction analysis, troubleshooting of start-up and shut-down, safety and reliability analysis and design and testing of control strategies [6].

2.7.2 Choice of Polynomials

The location of collocation points is determined by:

1. The type of polynomial
2. The choice of weighting function

There are different strategies for collocation point placement. No particular polynomial gives optimal point positioning. Most approaches are based on trial and error. The number of collocation points should be sufficient to represent the physical phenomena, but not so great as to lead to numerical problems e.g. oscillatory behavior [1, 26]. The full order model is recovered if the number of collocation points equals the number of stages.

2.7.2.1 Hahn Polynomials

Because they are defined over a set of integers (see Section 2.6.2.2 on page 22), Hahn polynomials are more suitable for models based on difference equations e.g. staged columns. Based on empirical observation, it was suggested that $\alpha = 0$ and $\beta = 0$ are the optimal weighting functions for Hahn polynomials [30].

2.7.2.2 Jacobi Polynomials

The zeros of Jacobi polynomials can be used for collocation point placement (see Section 2.6.2.1 on page 21). The point location is determined by α and β. The default choice of $\alpha = 0$ and $\beta = 0$ results in symmetrically positioned points. The points can be moved toward either side of the collocation element by increasing both parameters while keeping them equal. The best choice depends on the nature of the problem; more points should be placed in regions with steeper gradients.

For three collocation points, if one is placed in the middle and the other two symmetrically away from the middle, Jacobi placement results. If the points are biased toward the ends of the sections, roughly 70 % of the distance from the middle to the end, more accurate answers are obtained. However, the reduction in error from 6×10^{-5} to 8×10^{-6}, does not justify the additional complications of non-Jacobian placement.

It has been argued that Jacobi polynomials are unnatural for staged calculations as they satisfy an integral orthogonality relation as shown in equation (2.33). This corresponds to a minimization of the residuals on a continuous interval, rather than on the actual stages [13]. If this argument is valid[4], then Jacobi polynomials are best suited to packed columns as height is continuous.

2.7.2.3 Other Polynomials

Three orthogonal polynomials were investigated [36]; Legrende, Tschebysheff and Radau. The resulting accuracy varied depending on the weight functions used and no definitive conclusions could be drawn. Legrende polynomials were also successfully used to model a dynamic binary distillation column [17].

2.7.2.4 Literature Case Studies

Table 2.1 summarizes the use of collocation points. Hahn polynomials are generally preferred, although the justification refers back to a non-exhaustive, single source [30], which is in dispute with [26]. The latter source investigated a wider range of weighting values.

2.8 Collocation: *Summary and List of Symbols Used*

An overview of collocation as a mathematical technique has been given in the previous two sections. There is an extensive field of knowledge in the subject, which presents difficulties when trying to identify the salient points. The reference texts should be consulted if more clarity is required. A list of the nomenclature used in the above section is presented shortly. It only refers to the prior section. The rest of this chapter deals with the more interesting application of collocation to engineering design.

[4] This is not necessarily true, although it has been shown that a staged column model using Hahn polynomials [30] had errors 10 times smaller than a similar model using Jacobi polynomials [6].

Table 2.1: Summary of collocation point placements

Reference		Polynomial Type	Justification or Result
[22]	Seferlis & Hrymak 1994a	Hahn	In the limit where the number of collocation points equals the number of stages, the locations of the collocation points coincide with that of the stages i.e. the full order model is exactly recovered
[31, 5]	Swart & Stewart 1987; Carta *et al* 1995a	Hahn	Based on result reported in [30]
[26]	Strivastava & Joseph 1985a	Jacobi and Hahn	Performed extensive analysis of both polynomials as well as various weighting functions, and found that they were roughly equivalent
[30]	Stewart *et al* 1985	Jacobi and Hahn	Performed extensive analysis of both polynomials with two different weighting functions and found Hahn polynomials to be an order of 10 more accurate
[25]	Strivastava & Joseph 1984	Jacobi	Based on polynomial used by [6]
[6]	Cho & Joseph 1983a	Jacobi	Refers to relation discussed in [37]
[17]	Karacan *et al* 1998	Jacobi and Legrende	Performed limited comparison between Legrende and Jacobi polynomials and found the former to be twice as effective
[39]	Wong & Luus 1980	Shifted Legrende	-
[38]	Wajge *et al* 1997	7^{th} Order Legrende	-
[13]	Huss & Westerberg 1996a	Jacobi	Variable transformation meant that the collocation points were not equally spaced (in which case Hahn polynomials would have been preferred as the full order, symmetrically spaced, discrete staged model can be exactly recovered)

Nomenclature

A First derivative matrix, equation (2.41)

$\mathbf{a}$ A vector of undetermined parameters

a Lower limit of boundary range (independent variable)

B Second derivative matrix, equation (2.42)

b Upper limit of boundary range (independent variable)

h Finite element size

$l_i(x)$ Lagrange interpolation polynomial, equation (2.37)

n Number of collocation or finite difference points

$P_n^{(\alpha,\beta)}$ Jacobi polynomial, equation (2.31)

$p_n(x)$ Rescaled Jacobi polynomial of degree n, equation (C.2)

$p_n'(x)$ First derivative of rescaled Jacobi polynomial of degree n, equation (C.4)

Q Hahn polynomial, equation (2.34)

r Residual difference between approximate and exact solution

u Exact solution to DE

u' First derivative of exact solution to DE

u'' Second derivative of exact solution to DE

V Domain of integration

v Approximate solution to DE

v' First derivative of approximate solution to DE

v'' Second derivative of approximate solution to DE

w Set of independent test functions

x Independent variable

y Dependent variable

Subscript:

i Collocation point

Greek Letters:

α Exponent in the weighting function of the Jacobi polynomial, equation (2.33)

β Exponent in the weighting function of the Jacobi polynomial, equation (2.33)

δ Delta function

$\gamma_{n,i}$ Coefficient of Jacobi polynomial of degree n

ϕ Trial functions

ψ Boundary condition

ω Boundary condition

Φ Thiele modulus

Table 2.2: Summary of collocation models of packed-bed separation processes from the earliest work on the subject [25]

Components	Key Model Features
Ethanol, water	Distillation system The energy balance was neglected A linear equilibrium relation was used
Methyl cyclohexane, toluene, p-xylene, m-xylene	Distillation system The energy balance was neglected A nonlinear equilibrium relation was used
Ammonia, water, air	Absorption system The energy balance was included

2.9 General Applications of Collocation to Process Design

Collocation has been used in the design of a variety of process units such as reactors and distillation columns. The primary motivation has been the reduction in the model order.

2.9.1 Packed-Bed Separation Processes: *Continuous*

There have been relatively few attempts at modeling packed distillation columns on an entirely continuous basis. Usually a mass and energy balance across such a system will result in a two point boundary problem i.e. a split boundary. An early study looked at three simple packed-bed separation processes and developed the models using collocation [25]. Table 2.2 summarizes the nonequilibrium rate-based model characteristics. They were all based on two-film theory of mass and energy transfer, although several simplifying assumptions were made e.g. all resistance to transfer was assumed to reside in the vapor phase. In this study, the transfer coefficients were determined from experimental correlations. Generally, the scarcity of these parameters is a limitation on this approach. Collocation and finite differences were compared with the former being the most efficient. The work was limited to a single feed and a single column section. This greatly simplifies the collocation problem as there are no discontinuities in the profile, which would usually be found if either a full column or side streams were included.

A later work investigated a dynamic model of a packed binary distillation column [17]. The system was more complex than the previous one [25], as axial dispersion was considered, and second order DE's result. OCFE was used to solve the equations, and the results compared favorably to experimental work.

2.9.2 Packed Column Distillation: *Batch*

Batch distillation is a more flexible and cheaper means of separation than a continuous staged column. A dynamic model requires distribution in time and in the axial direction. Therefore an efficient solution technique is necessary due to the high dimensionality. Conventional packages use a computationally expensive, equation tearing algorithm. A model using a differential contactor with mass transfer effects was developed [38]. This contactor was representative of a packed column. Typically finite differences would be used to solve the system, creating large systems of dense equations. The use of OCFE resulted in a low order, sparse system of equations i.e. block diagonal matrix. By exploiting the sparsity and using the correct order of approximating polynomial, the authors improved the degree of order reduction.

2.9.3 Staged Distillation: *Continuous*

The earliest work on collocation applied within a process unit context, developed a simple model for a dynamic staged absorber [39]. A few years later, a staged distillation model was developed with single collocation sections above and below the feed [6]. This was extended to include multiple feeds and side draws using OCFE [28, 27]. Steep and flat composition profiles were easily modeled as different polynomials were used in each column section. Local and global collocation points were used to represent non-key and key components respectively. A limitation was the requirement of a prior knowledge of the composition profiles i.e. a full-order solution. Later models have been developed using OCFE to simulate existing columns [22], as well as multiphase distillation [31]. These and others are comprehensively listed in Table 2.3.

2.9.4 Staged Distillation: *Reactive*

Reactive distillation enhances conversion of equilibrium controlled reactive systems with significant volatility differences between the reactants and products. Collocation was applied to an equilibrium staged model with kinetically controlled reactions [21]. The reactive column was coupled with a standard distillation unit. The steady-state model was based on the MESH equations. The reaction column had two feeds, and was subsequently divided into three stages using OCFE: rectifying, reaction section between the feeds, and stripping section. Although OCFE allows for some of the sections to have reaction and others not, reaction was assumed to occur in all three sections. Each section was further divided into finite elements, as is standard with OCFE (see Section 2.10.3). Hahn polynomials were used to position the collocation points. The size of each section was a degree of freedom with the constraint: the number of real stages needed to be greater than, or equal to the number of collocation points in that section. The collocation model was used in an optimization superstructure as mentioned in Section 2.1.4.1.

Table 2.3: Summary of chronological development of staged collocation distillation model features through the literature

References	Stages	Components	Key Model Features
Wong & Luus 1980	20 6	3	Dynamic gas absorber
Cho & Joseph 1983a	9 20	2	β values of 1,2 and 3
Cho & Joseph 1983b	10 10 21	2 3	Tray hydraulics (*Francis Weir*) Stage efficiencies non-linear composition profiles
Cho & Joseph 1983c	21 40 21	2 4 2	Tray hydraulics (*Francis Weir*) Known side stream Vaporization efficiency Liquid and vapor feed streams PI controllers in sump and accumulator Condenser and reboiler dynamics
Stewart *et al* 1985	30 40 15 19	2 6 3	Pinch at feed tray Averaged relative volatilities Stage efficiencies Non-ideal vapor-liquid equilibrium
Strivastava & Joseph 1985	76	5	Order reduction parameter
Swartz & Stewart 1987	10 16	3	2^{nd} liquid phase Heterogeneous azeotropic distillation
Seferlis & Hrymak 1994a	31 175 70	4 2	Economic objective utility function Regression to calculate equilibrium constants
Huss & Westerberg 1996a	46 33 23	2 3 5	Product purities each of 99 % Equimolar Known reflux
Huss & Westerberg 1996b	86 24	3	Cost optimization (*utility, heat exchange area*) Column optimization (*trays, diameter, feed tray*)
Strivastava & Joseph 1996	40 50 76	2 5	Spline fitting Level controllers in reflux drum and reboiler Global and local collocation points

2.9.5 Absorption: *Chromatography*

Modeling fixed bed absorption columns is difficult due to strong nonlinearities in the absorption equilibrium isotherms, interference effects, mass transfer resistances and fluid dispersion phenomena. These effects combine to produce steep concentration gradients which move along the column during the absorption process. A complex approach using moving finite elements, where the movement of the grid is initially calculated was developed [16]. Although similar, mobile finite elements are not the same as adaptive placement of breakpoints, as the movement is calculated *a priori*, and not as a result of error minimization.

2.9.6 Absorption: *Reactive*

Industrially reactive absorption processes are commonly used e.g. purification of synthesis gas. Reactive absorption processes are complex operations due to strong physiochemical interactions. When using rigorous staged models, the resulting equations are difficult to solve. To address this, collocation has been incorporated into a reactive absorber column superstructure [1].

2.9.7 Packed Bed Reactors: *Macroscopic*

A reasonable model would account for axial dispersion, inter-phase mass and energy transfer, as well as kinetics. Such models describing transient packed bed reactors have been developed using orthogonal collocation [11].

2.9.8 Packed Bed Reactors: *Microscopic*

For reaction to occur, heat and mass must diffuse into a catalyst pellet, resulting in a two point nonlinear BVP. OCFE can be used to solve these problems when the Thiele modulus (Φ) is large. Physically, this translates into a steep concentration gradient near the pellet surface. If only collocation was used, a large number of points would be required to obtain a reasonable accuracy. OCFE combines the rapid collocation convergence, with the convenience of finite difference methods, which locate grid points or elements where the solution is important, or has steep gradients [4]. This has been mentioned previously in Section 2.6.5.3.

2.10 Specific Applications of Collocation to Distillation

To identify the trends (if any) in collocation models of distillation systems, the literature was analyzed and categorized according to the stages used in distillation model development:

Table 2.4: Suggested categorization of collocation model assumptions primarily for staged columns (bulk of literature is focused on staged distillation)

Suggested Category	**Assumptions**
Thermodynamics	Liquid and gas ideal solutions No pressure drop No energy balance Constant relative volatility Linear equilibrium relationship
Heat Effects	Adiabatic Negligible heat effects
Mass Balance	Constant molar overflow
Mass Transfer (packed column)	Defined by overall gas phase transfer coefficient Resistance to energy and mass transfer on vapor side Component mass transfer coefficients equal
Tray Relations	Streams leaving trays in thermal equilibrium Efficiency relationships between streams leaving trays
Mixing	Liquid leaving tray well mixed Both phases well mixed
Efficiency	Ideal stages Murphree efficiency

1. Define assumptions: **Table 2.4**
2. Choose components: **Table 2.5**
3. Choose thermodynamic database: **Table 2.6**

And after model development:

4. Test and validate: **Tables 2.7 and 2.8**

As an aside, the referencing convention within the tables has been temporarily changed to include the author list and date, as this highlights the chronological development. The referencing within the text is restricted numbers for easier reading.

Table 2.5: Type of separation systems for which the collocation approach has been applied

References		Components
[6, 7]	Cho & Joseph 1983a & b	(*i*) Propane, n-butane (*ii*) Ethane, propane, n-butane
[8]	Cho & Joseph 1983c	(*i*) Methanol, acetone, ethanol, water
[30]	Stewart *et al* 1985	(*i*) Methane, ethane, propane, n-butane, n-pentane, n-hexane (*ii*) Methanol, ethanol, water
[31]	Swartz & Stewart 1987	(*i*) Propanol, butanol, water (*ii*) Acrylanitrile, acetonitrile, water
[22]	Seferlis & Hrymak 1994a	(*i*) Propane, i-butane, n-butane, pentane (*ii*) Propylene, propane (*iii*) Styrene, ethylbenzene
[13]	Huss & Westerberg 1996a	(*i*) Methanol, water (*ii*) Acetone, chloroform, benzene (*iii*) Acetone, ethanol, propanol, isobutyl alcohol, butanol
[14]	Huss & Westerberg 1996b	(*i*) Propanol, isobutyl alcohol, butanol (*ii*) Acetone, chloroform, benzene

Table 2.6: Thermodynamic models used in the collocation approach

References		Thermodynamics
[8]	Cho & Joseph 1983c	Wilson's equation
[6, 7, 8]	Cho & Joseph 1983a,b & c	Ideal solution with Antoine equation
[30]	Stewart *et al* 1985	UNIQUAC
[31]	Swartz & Stewart 1987	Non-ideal 3 phase mixture (empirical)
[22]	Seferlis & Hrymak 1994a	Regression of data
[13]	Huss & Westerberg 1996a	UNIFAC / Pitzer
[38]	Wajge *et al* 1997	Empirical

Table 2.7: Types of simulations performed on some of the collocation models

References		Simulations: Steady State
[6]	Cho & Joseph 1983a	Step increase in liquid feed concentration
[6, 7]	Cho & Joseph 1983a & b	Random change in liquid feed concentration
[25]	Strivastava & Joseph 1984	Varied number of collocation points Varied reflux ratios
[30]	Stewart *et al* 1985	External reflux ratio variation Distillate-to-feed ratio variation
[22]	Seferlis & Hrymak 1994a	Product purities as degrees of freedom Reflux ratio and reboiler duty as degrees of freedom Distillate flowrate and reboiler duty as degrees of freedom
[13]	Huss & Westerberg 1996a	Distillate-to-feed ratio incrementally increased
[14]	Huss & Westerberg 1996b	Feed position, distillate flowrate and reflux ratio alternatively varied
		Simulations: Unsteady State
[8]	Cho & Joseph 1983c	Changing liquid feed temperature and reboil ratio Change in reflux ratio Composition control by manipulating bottoms flowrate
[26]	Strivastava & Joseph 1985a	Varied number of collocation points until error <10% Step change in liquid flowrate at top
[28]	Strivastava & Joseph 1986	Step change in liquid composition entering from top Step change in vapor composition entering from bottom 10% and 30% step increases in feed flowrates

Table 2.8: Approaches taken to validate the collocation solution

References		Comparisons of numerical values between:
[6, 7]	Cho & Joseph 1983a & b	Full and low order rectifying model
[8]	Cho & Joseph 1983c	Full and low order model Simulator and low order model
[25]	Strivastava & Joseph 1984	Analytical solution and low order model
[26]	Strivastava & Joseph 1985a	Order reduction parameter (ORP) was compared to number of collocation points required to maintain fixed error (found by comparing full and low order model)
[30]	Stewart *et al* 1985	Intransient responses of full and low order model (i.e. unsteady state)
[28] [31] [22]	Strivastava & Joseph 1986 Swartz & Stewart 1987 Seferlis & Hrymak 1994a	Full and low order model

The most obvious gap in the literature is the development of a rigorous nonequilibrium packed column model using MaxWell-Stefan equations. This will be addressed through this work. What is also concerning is the level of attention devoted to developing interpolation methodologies for smoothing out profile discontinuities e.g. feed and side-streams. This is seen largely in the papers by Strivastava and Joseph as documented in Table 2.8. It seems to indicate a lack of distillation understanding rather than a mathematical mistake. This will be elaborated on in the following section.

Much of the work listed in Table 2.7 used dynamic responses to validate the collocation model. The collocation equations are integrated with respect to time, and the resulting problem set requires differentiation in one spatial direction only i.e. time instead of both time and height. This is a smart application of collocation and has clearly been recognized as such by the numerous authors.

There do not appear to be any obvious trends in the choice of components or thermodynamic models as shown in Tables 2.5 and 2.6 respectively.

The final point of interest is that the majority of the collocation models used equilibrium-based *staged* columns. This is surprising as collocation is fundamentally tied to mathematical problems involving DE's. Staged columns are characterized by difference equations. An approximation is therefore made to convert the difference equations to DE's before collocation is applied. This may have implications in the definition of a *continuous* equilibrium between the *discrete* stages. At this point, it is sufficient to note that the almost exclusive use of staged columns raises a red flag. Further comment will be made in Chapter 3.

2.10.1 Model Attributes: *Feeds, Multiple Feeds and Side Streams*

The entry of a feed or side stream causes discontinuities in the column profiles. This can be seen in Figure 2.5 where the total liquid flow in either a staged or packed column is considered[5]. The two types of discontinuities introduced are:

$$L(z_f^-) \neq L(z_f^+) \tag{2.46}$$

$$\frac{dL}{dz}|_{(z_f^-)} \neq \frac{dL}{dz}|_{(z_f^+)} \tag{2.47}$$

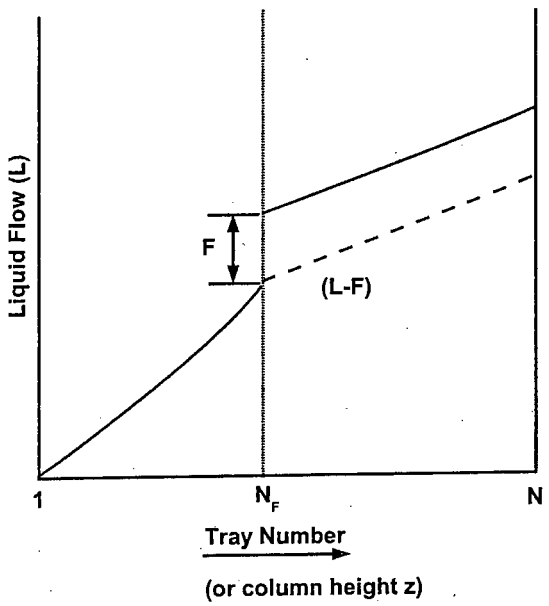

Figure 2.5: Discontinuity in liquid flow due to liquid feed at stage N_F [28]

[5]A vapor or mixed feed could also be used

It is possible to manage the first discontinuity in equation (2.46) by transferring the state variable L to $(L - F)$ for $z > z_f$ as suggested by [8]. The complete profile is subsequently approximated using a continuous polynomial:

$$L \cdot x(z) = \sum_{k=1}^{n1} l_k(z) \cdot (L \cdot x_k) + \sum_{k=n1}^{n+2} l_k(z) \cdot (L \cdot x_k - F \cdot x_f) \tag{2.48}$$

In other words, a single continuous polynomial was used to approximate the entire profile. While this reduces the model order, the column profiles incur error which is insensitive to the model order [28]. The accuracy deteriorates further as collocation points move away from the feed as:

1. The discontinuity in equation (2.47) was not accounted for
2. The discontinuity in equation (2.46) was accounted for at the nearest collocation point and not at the feed location.

Separate regions exist because the DE's in each section are not the same. They therefore need to be linked through *boundary conditions*, instead of using a continuous profile. Hence the following suggestion for using two sections above and below the feed (or side stream), where each section is approximated by a different polynomial, is more correct. Unfortunately, instead of using boundary conditions to link the two sections, a spline technique was favored. Both discontinuities were accounted for by placing one collocation point at the feed location and approximating the complete profile by splines. The derivation is in [28]. This logic is flawed as the natural discontinuity introduced by additional streams should be preserved and not smoothed out through imaginative interpolation. Some other similarly flawed and confusing suggestions included [19]:

1. *Sectional OC without extrapolation:* In each column section, the extreme point (condenser, reboiler, feed or side stream) and internal collocation points are all taken as interpolation points. The polynomials of each section meet on the feed plate.
2. *Sectional OC with extrapolation:* To reduce the difference between the mass balances resulting from the use of the top and bottom polynomial respectively, these two expressions are 'fused' into one.
3. *Global OC:* A single interpolating polynomial is used along the entire column. Collocation and interpolation points are used at the extreme points, the feed plate and internal points. This is basically the same as the method shown in Figure 2.5, as used by [8]
4. *Orthogonal spline interpolation:* The motivation was to make the mass balances on the feed stage the same when calculated with either polynomial of the rectifying or stripping

section. The system is solved as standard with a feed discontinuity. The rectifying and stripping profiles were extrapolated such that they met exactly at the q-line, with the actual feed stage being used as an interpolation point for both profiles. This method seems to be fairly similar suggested by [28] in a critical response to the idea of a global polynomial used by [8] and shown in Figure 2.5.

However the most logical suggestion made, was to treat the points in the column in which discontinuities occur as discrete equilibrium stages by applying separate, lateral mass and energy balances [23]. This can be simplified further by not treating the feed as an additional stage, but rather adding the liquid and vapor part of the feed stream to the liquid and vapor streams connecting the two sections [30]. Of course, this is only strictly true for an adiabatic column with CMO, but nonetheless is an acceptable approximation.

2.10.2 Model Attributes: *Heterogeneous Azeotropes*

In an extension of some of the collocation models mentioned in the preceding sections, a distillation system with more than one liquid phase, was modeled using OCFE [31]. The uncertainty of the locations of the multiphase regions was an obstacle. The phase miscibility boundaries were subsequently treated as unknown variables in order to circumvent that. The length of the finite elements representing each multiphase section were therefore variable and unknown, while the physical column sections were determined by the position of feeds and side streams. An initial guess for the location of the multiphase elements was found by solving the system in much that same manner as discussed previously i.e. single liquid and vapor phases.

2.10.3 Model Structure: *Orthogonal Collocation on Finite Elements (OCFE)*

A column can be divided into elements and orthogonal collocation applied to each [17, 30, 22]. This is a more intelligent application of collocation as:

1. Finite element length can be chosen such that results correspond exactly to experimentally measured points [17].
2. Multiple elements allows for more collocation points to be used in areas where gradients change rapidly.
3. Several low order polynomials are more efficient than a single high order polynomial [31].

If the composition profiles are known (either exactly or approximately), the finite elements can be chosen such that there are more in regions of steep gradient change. A standard model

Table 2.9: Number of finite elements used in the collocation approach

References		Number of elements
[26]	Strivastava & Joseph 1985a	Single
[30]	Stewart *et al* 1985	
[39]	Wong & Luus 1980	
[17]	Karacan *et al* 1998	Single and Multiple
[38]	Wajge *et al* 1997	Multiple
[13]	Huss & Westerberg 1996a	
[5]	Carta *et al* 1995a	
[28]	Strivastava & Joseph 1986	
[22]	Seferlis & Hrymak 1994a	Multiple (*adaptive breakpoints*)
[31]	Swartz & Stewart 1987	Multiple (*breakpoints at phase discontinuities*)

formulation is shown in Figure 2.6. Each column section is divided into 2 collocation sections with 2 nodes in each. A fractionation system could consist of a set of such multi-stage elements linked to condensers, reboilers, feed and product lines etc. For each element, these linkages are expressed through the states and flows at the collocation points.

A model with 4 collocation sections each containing 2 nodes as well as a feed tray, reboiler and condenser, would have 11 'stage' calculations. Because collocation 'stages' are not connected analogously to those in a staged, full order model, there are more equations in the reduced order model than what there would be in an 11-staged model. Collocation is only effective as an order reduction technique when the full order model has more equations. In this case, beyond an 18-staged column [13]. The usefulness of collocation for pinch analysis should be apparent. In a pinching system, the packed column height or number of stages, becomes very large causing numerical difficulties in rigorous models. If collocation models are used instead, the height can be 'stretched' while maintaining the same number of collocation points i.e. the order of the system is constant Table 2.9 summarizes the use of collocation elements.

2.10.3.1 Adaptive Placement of Breakpoints

Collocation accuracy can improved by adaptively placing the break-points between elements such that the approximation error is equally distributed. These breakpoints become additional degrees of freedom [22]. The break-point location is dependent on the profiles. Smaller elements are used in regions where there are rapid changes in profiles. The accuracy of the low order model subsequently depends on the shape and complexity of the profiles. By adjusting the break-point positions, the element lengths are also changed. These lengths are not restricted to integers. The procedure for optimal element length is implemented in the code COLSYS (see Section C.2.1).

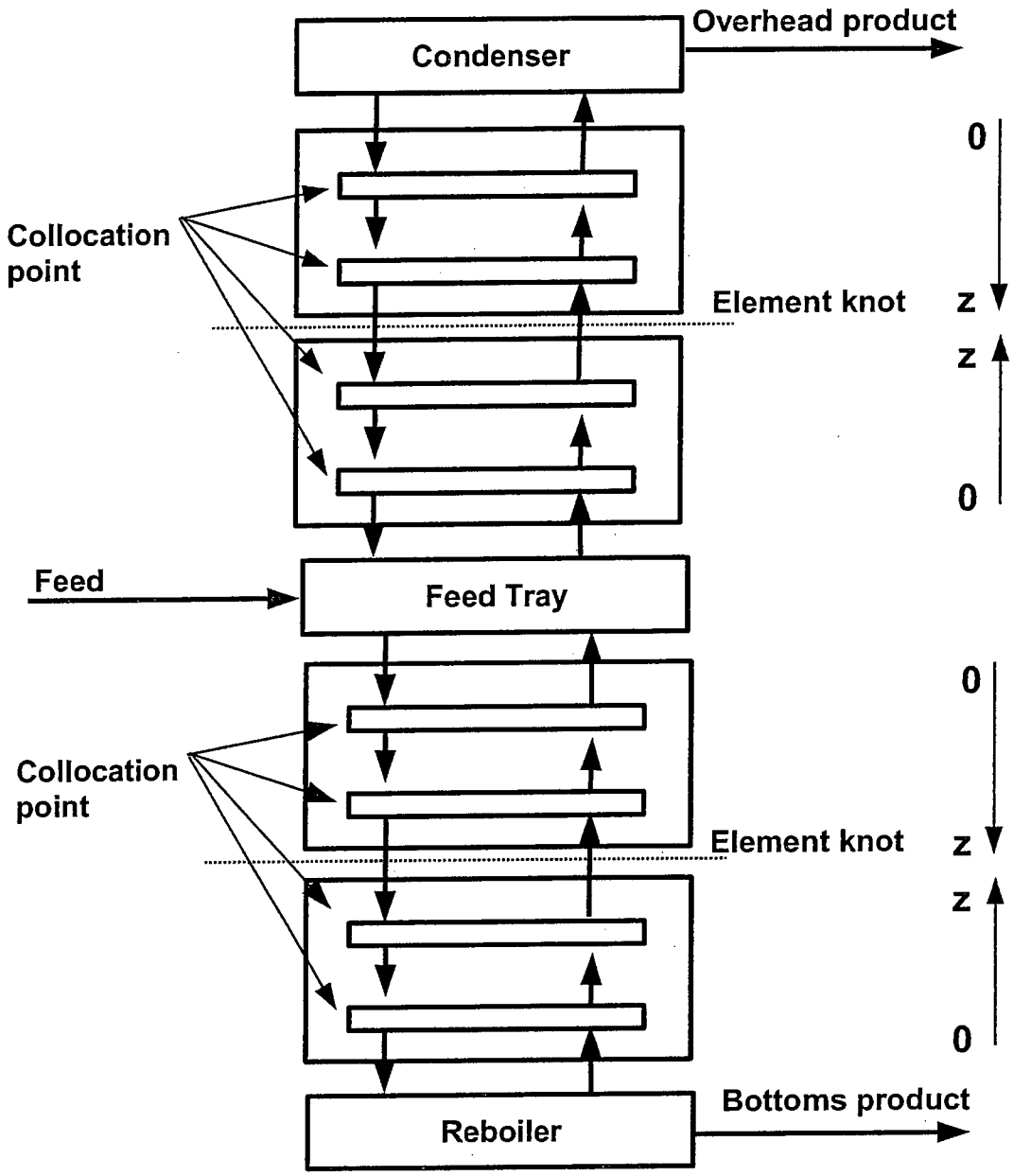

Figure 2.6: Column configuration showing OCFE [22]

2.11 Solution Techniques based on *Transformations*

Numerical difficulties encountered when solving reduced order models, can be reduced by re-defining the variables.

2.11.1 Transformation of Tray Number

In distillation columns, flat profiles may occur in the middle of large columns, or where concentrations approach 0 or 1. Polynomials do not fit these flattened trajectories well. In order to transform them, an index is required which tends to a finite number as the tray number tends to infinity. Hence, an exponential transformation of tray number[6] could be used. With an exponential transformation which maps zero to an infinite number of trays onto the range $0-1$, four collocation points accurately simulated a large column section [13]. The exponential transformation was given as:

$$z = 1 - e^{-a \cdot s} \tag{2.49}$$

A less effective transformation in comparison to (2.49) is:

$$z = \frac{s}{s+a} \tag{2.50}$$

In two above equations, a is a parameter for the exponential transformation of stage location (s). For the simulation of high purity column, a hyperbolic tangent transformation of the mole fractions could be used:

$$2 \cdot x_i - 1 = tanh(x_i) \tag{2.51}$$

If the component is present in very small amounts, the Lagrange interpolation polynomials may oscillate, reducing accuracy. Because the nonlinearity is increased if equation (2.51) is used, another transformation is suggested [21]:

$$\widehat{L} \cdot x_k = ln(L \cdot x_k) \tag{2.52}$$

Equation (2.52) is a transformation of the component liquid flow rate, and is applied to components with very low compositions; usually near the column endpoints. The transformed variable can take on negative numbers, allowing the Lagrange interpolating function more room to accommodate very low composition values for non-key components. An alternative approach is to remove inert components with low concentrations from the mass and energy balances in selected elements. While the elimination approach is the easier option, in the presence of disturbances that strongly affect the trace-component composition, it should not be used [21].

[6] The same concept can be applied to a packed column height

2.11.2 Dimensionless Temperature

The inverse design problem can be solved rigorously. The feasibility of a given separation target (i.e. three product purity specifications and the desired reflux) can be determined using liquid tray composition profiles. These are expressed in terms of equilibrium tray temperatures, as independent variables.

Singularities in the profiles near pinch points cause numerical difficulties. These occur even in ideal mixtures. These can be overcome by transforming the profiles into the space of *dimensionless bubble point temperatures*, and then minimizing a bubble point distance function. Dimensionless temperature could be used as an independent variable[7]. It ranges between $[0, 1]$, is well-behaved and avoids singularities at the pinches. Composition profiles exhibit strict temperature monotonicity preventing profiles from intersecting the same bubble point surface twice, irrespective of the solution non-ideality.

If the separation is of a high purity, the rectifying and stripping profiles approach a saddle point, which divides the profiles into 2 branches. These are only attainable if there are an infinite number of equilibrium trays. The bubble points associated with the distillate, bottoms and stable pinch points, span the *Attainable Temperature Window* (ATW), delineating all possible tray temperatures. By comparing the ATW in the stripping and rectifying sections, design specifications can be excluded without performing rigorous staged computations. If the ATW overlaps, a detailed analysis is required.

The *Bubble Point Distance* (BPD) is defined as the distance between 2 equilibrium compositions of the stripping and rectifying profiles, with the same bubble point. A feasible specification requires that a pair of compositions have a BPD of zero. However, a BPD of zero does not distinguish between a feasible separation and one which has been over-designed. In summary, this definition translates into an intersection of the operating lines.

Using the above concepts, an algorithm was developed to assess separation feasibility [40]. Applications to column sequencing were illustrated, and a separation sequencing superstructure was developed in a further study [41]. However, the concept was limited to non-azeotropic and quaternary mixtures[8], as well as CMO assumptions [40].

[7] The column height is mapped into a dimensionless bubble point temperature

[8] This graphical approach restricts the number of components to 4, beyond which hyper-surfaces are required and physical meaning is lost.

2.12 Solution Techniques based on *Profile Information*

These strategies are based on a prior knowledge of the column profiles. Such information can be found in the form of an Order Reduction Parameter (ORP) index [27, 26]. This index predicts *a priori* the extent of order reduction achievable, which is a factor of [7]:

Column size: the larger the column, the greater the reduction

Required accuracy: the higher the accuracy, the lower the reduction

Nonlinearity: the higher the nonlinearity, the lower the reduction

The extent of the steepness and flatness of the component flow rates is indicated by the ORP:

$$ORP(i) = N \cdot ln\left(\frac{L}{K_i \cdot V}\right) \qquad i = 1, 2, ..., NC \tag{2.53}$$

Columns with steep and flat composition profiles exhibit high ORP values and require high order approximating polynomials[9]. Component compositions which do not change over a column section can be approximated as a constant. This prevents oscillations resulting from using high order polynomials to approximate straight lines.

Because composition profiles are fitted with polynomials tailored to each component, the software complexity increases. Alternatively, global collocation points could be used to approximate key component profiles, and local collocation for non-key component profiles [25]. This reduces the order further as previously, the entire equation set was solved at each collocation point.

[9] Collocation may not be the best method of solution and alternative order reduction strategies could be investigated.

Chapter 3

Model Development

Each of the three models developed in this thesis represent adiabatic *nonequilibrium rate-based distillation columns*. The models differ according to the level of simplifying assumptions made. Although three models were developed, the final model is the one of interest due to the high degree of complexity. The previous models are motivated as progressive building blocks used to develop the final model. In other words, as with any complex model it is advisable to start with the simplest case and work toward the more complex one. In this chapter, each model is developed in such a manner that the successive model progression is emphasized.

Figure 3.1 provides an overview of the model development. While Models 1 and 2 both make simplifying assumptions at the liquid phase interface, Model 1 is further simplified by assuming constant molar overflow (CMO). This allows for the energy balance to be neglected. Model 2 progresses by including the energy balance, while assuming an ideal thermal film. Model 3 advances further by dropping the assumptions made at the liquid phase interface and thermal film.

The model development is structured such that the theory used when developing the equations is presented first, followed by the assumptions, data used, and system schematic. Each model concludes with a summary of the variables and associated equations. This chapter and the next contain numerous equations, some of which are in matrix format. The approach used for the nomenclature is as follows:

$$\Theta^{L,V,\mathrm{I},R,S}_{\textit{component number, collocation point}}$$

where Θ is any state variable and a combination of L (*liquid*), V (*vapor*), I (*interface*), R (*rectifying*) or S (*stripping*), can be used in the superscript. Usually k is used to represent the component number, and n the collocation point.

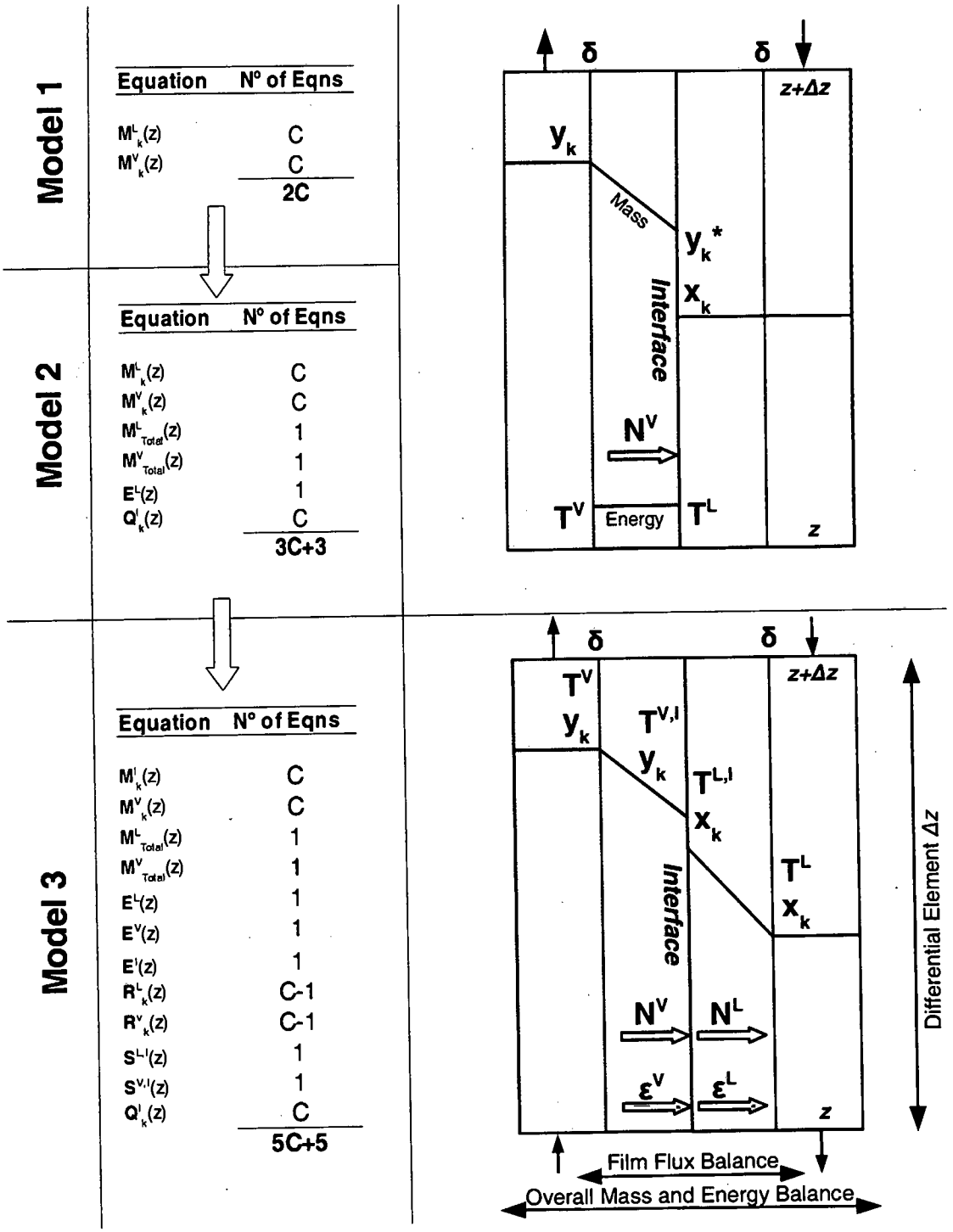

Figure 3.1: Equations and related film balance showing successive model development

Modeling Staged vs. Continuous Nonequilibrium Columns: Usually MERQS[1] equations are used to model the nonequilibrium stages. The MERQS equations for the interior stages are solved with equations for the reboiler, condenser, and any specification equations, to yield for each stage, vapor and liquid mole fractions, vapor and liquid flows, and temperature profiles. Vapor from the stage below and liquid from above, are brought into contact on the stage [32].

When collocation is applied to a packed column, the differential equations are converted into a series of algebraic equations located at discrete collocation points. In a sense, the resulting equations are identical to the MERQS equations in a staged column. The difference being that all relationships between the two phases (which previously related two streams leaving a stage), now apply at the collocation point. In other words, the relatively large height represented by a stage has been replaced by an infinitesimal one i.e. a point in space. Therefore, the state variables are expressed as polynomial functions of position in each column section.

As shown in Table 2.3 on page 34, distillation models using collocation have largely been developed using equilibrium-based *staged* columns. However, this may be fundamentally incorrect. Figure 3.2 represents a McCabe-Thiele solution for an equilibrium-based *staged* distillation system. The solution points found using collocation, as well as those from the full staged solution, are indicated on the diagram.

The key flaw when using collocation in such a system is that equilibrium only applies at the discrete stages and *not at the collocation points.* When collocation is applied, the operating lines are solved for at points other than the stages. However, no equilibrium is possible at these points as they *do not exist* in a staged system. This is shown in Figure 3.2. Therefore the resulting 'solution' is highly questionable. This argument does not apply to a packed column as the solution is fundamentally continuous. Hence equilibrium occurs at every point on the operating lines by definition i.e. a continuum.

[1] **M**ass balance, **E**nergy relations, **R**ate expressions , e**Q**uilbrium and **S**ummation equations

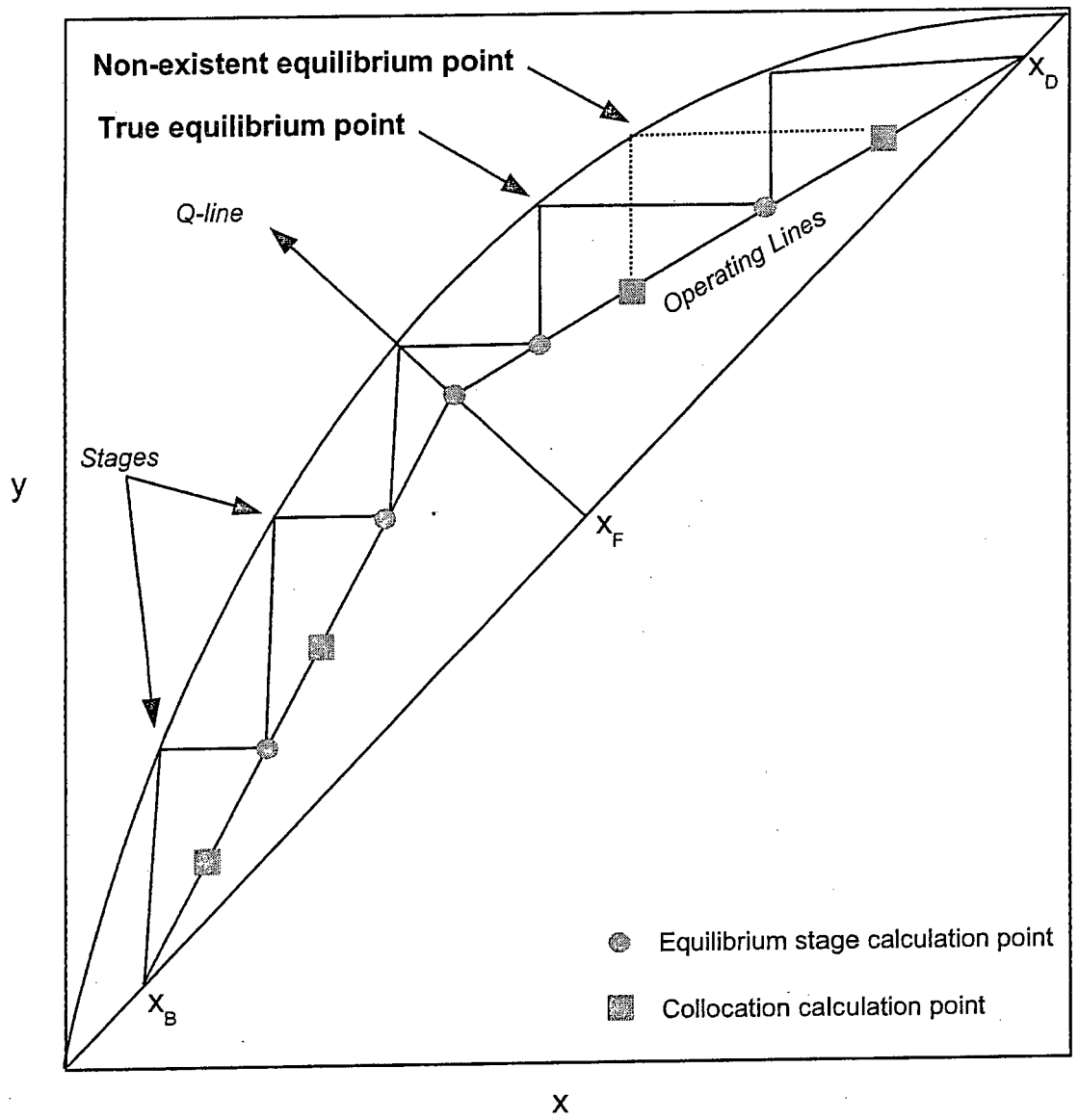

Figure 3.2: McCabe-Thiele construction for a staged system highlighting the *invalidity of collocation applied to staged systems*

3.1 Model 1: *Constant Molar Overflow & Vapor Phase Resistance*

The simplest model of a distillation column would have constant internal flows. This occurs when CMO is assumed, as was done in this model.

As an aside, this approach is similar to a staged column using McCabe -Thiele assumptions with efficiencies. A brief overview of McCabe -Thiele theory and assumptions is given in the literature review on page 10. When referring to a McCabe -Thiele column, it is understood to be at equilibrium at the stages. In attempt to account for a nonequilibrium column (which is almost always the case in practice), the McCabe -Thiele approach includes an efficiency factor e.g. Murphree efficiency. A graphical McCabe -Thiele analysis is a very useful tool when designing a column. While McCabe -Thiele strictly applies to a staged equilibrium column, the same analysis can be performed on a packed nonequilibrium column, as the location of the operating and equilibrium lines are the same irrespectively.

As mentioned in the chapter introduction, both Model 1 and Model 2 made simplifying assumptions at the liquid phase interface by assuming that all resistance to mass transfer occurred in the vapor phase, as shown in Figure 3.1. This approach was used as there is subsequently no need to determine the interface composition. In other words, a fictitious vapor mole fraction y^* was defined and assumed to be in equilibrium with the liquid mole fraction x in the bulk liquid. To simplify the model further, the equilibrium relationship between y^* and x was known, either from experimental correlations, or was defined in terms of known and constant α values. By assuming $\alpha = f(T)$ over a small temperature range, constant α was subsequently possible due a constant column temperature. The overall volumetric mass transfer coefficient was defined in terms of the overall driving force for the vapor phase[2]. This coefficient was likewise taken from an experimental correlation or estimated.

3.1.1 Theory-Based Equation Development

This section develops and presents the mass, energy, rate and equilibrium equations (MERQ) used in Model 1. In all the models within this thesis, the direction of integration is taken from the reboiler upwards. This is important when defining the signs used in the differential equations.

[2]The overall volumetric mass transfer coefficients can be defined in terms of either phase depending on where the relative resistance is highest.

3.1.1.1 Mass Balance

The following component mass balances are needed:

$$\frac{d(V \cdot y_k)}{dz} + N_k = 0 \qquad k = 1, ..., \text{Number of components} \tag{3.1}$$

$$\frac{d(L \cdot x_k)}{dz} + N_k = 0 \qquad k = 1, ..., \text{Number of components} \tag{3.2}$$

The below equation (3.3) could be used in place of either equation (3.2) or (3.1):

$$\frac{d(L \cdot x_k)}{dz} - \frac{d(V \cdot y_k)}{dz} = 0 \qquad k = 1, ..., \text{Number of components} \tag{3.3}$$

Whichever combination of equations (3.2), (3.1) and (3.3) is used, it is preferable to remove the constant values (V and L) from the differential equations. This improves the logic when implementing the collocation routines. As seen from the above mass balance equations, an extension to multicomponent systems is straightforward. Pseudo McCabe -Thiele diagrams can be used to represent a multicomponent system as mentioned in Section 2.3.1 on page 15.

The reflux (Re) and reboil (Rb) ratio definitions are presented in equations (3.4) and (3.5). They can be combined with a mass balance over the condenser and reboiler to provide the necessary boundary conditions for the differential mass balance equations. The resulting boundary conditions are subsequently shown in equations (3.6) and (3.7).

$$Re = \frac{L_{\text{ leaving the condenser}}}{D} \tag{3.4}$$

$$Rb = \frac{V_{\text{leaving the condenser}}}{B} \tag{3.5}$$

The reflux ratio definition in equation (3.4) is combined with the condenser mass balance to give the first boundary condition:

$$V_{\text{leaving the column}} = (Re + 1) \cdot D \tag{3.6}$$

Similarly, the reboil ratio definition in equation (3.5) is combined with the reboiler mass balance to give the second boundary condition:

$$L_{\text{ leaving the column}} = (Rb + 1) \cdot B \tag{3.7}$$

However, care must be taken when defining the reflux (Re) and reboil (Rb) ratios in this model with constant liquid and vapor flow rates. The ratios are related through the feed condition q, which is defined when the feed composition, temperature and pressure are known[3]:

$$\frac{D}{B} = \frac{Rb + 1 - q}{Re + q} \tag{3.8}$$

$$F = D + B \tag{3.9}$$

Therefore, if the feed is fully specified as well as the reflux ratio (Re), $L_{\text{leaving the condenser}}$ is solved for using equation (3.2) in conjunction with equation (3.1). Hence the distillate flow rate D is known from equation (3.4). If the total mass balance in equation (3.9) is considered, the bottoms flow rate B is also known. This results in a dependent value for (Rb) from equation (3.8). The boundary conditions will be covered in more detail in the following chapter.

3.1.1.2 Energy Balance

As explained previously, the assumption of *constant molar overflow* (CMO) renders a stage-by-stage energy balance unnecessary. However the overall energy balance for an adiabatic column, can be used to determine the condenser *or* reboiler heat duty if needed. The balance is:

$$F \cdot H_F + Q_R = D \cdot H_D + B \cdot H_B + Q_{Con} \tag{3.10}$$

3.1.1.3 Rates

The rate of mass transfer as used in equations (3.1) and (3.2) is derived below. The equilibrium expression for y^* is model specific and is discussed in Section 3.1.1.4.

Mass Transfer: Mass transfer of a species is usually assumed to be from the vapor to the liquid phase. A concentration gradient exists in each film. At the interface, equilibrium is assumed to exist. Mass transfer coefficients are typically based on volume, as the area for mass transfer in a packed bed is difficult to estimate. At steady state, the rate of mass transfer of the transferring species across the vapor-phase film must equal the rate across the liquid film. The component rate of mass transfer per unit of packed bed N_k, is written in terms of mole fraction driving forces [15]:

$$N_k = \kappa_y \cdot a \cdot (y_k - y_k^{\mathrm{I}}) = \kappa_x \cdot a \cdot (x_k^{\mathrm{I}} - x_k) \qquad k = 1, \ldots, \text{Number of components} \tag{3.11}$$

[3]Note that this relation is only strictly true for CMO assumptions.

The above equation can be rearranged to show that the composition at the interface is dependent on the typically large ratio $\frac{\kappa_x \cdot a}{\kappa_y \cdot a}$:

$$\frac{y - y^I}{x - x^I} = -\frac{\kappa_x \cdot a}{\kappa_y \cdot a} \tag{3.12}$$

The above equation represents a straight line with a slope of $-\frac{\kappa_x \cdot a}{\kappa_y \cdot a}$. The slope determines the relative resistances of the phases to mass transfer. In this model, all resistance was assumed to reside in the vapor phase i.e. $x \approx x^I$ and $K_{og} = \kappa_y$. As mentioned before, an overall volumetric mass transfer coefficient is defined in terms of the overall driving forces for the vapor phase. This is useful as the compositions at the interface do not have to be evaluated. Due to the assumption of CMO, the bulk flux contribution can be assumed to be negligible. The resulting rate equation follows:

$$N_k = K_{og}a \cdot S \cdot (y_k - y_k^*) \qquad k = 1, ..., \text{Number of components} \tag{3.13}$$

- y_k^* is the fictitious vapor mole fraction in equilibrium with the liquid mole fraction x_k in the bulk phase
- N_k has units of $\left(\frac{kmol}{time.m}\right)$
- a is the interface surface area with units of $\left(\frac{m^2}{m^3}\right)$
- S is the surface area with units of (m^2)
- K_{og} has units of $\left(\frac{kmol}{time.m^2}\right)$
- $(K_{og}a \cdot S)$ is a lumped parameter

Equation (3.13) is only independent for $C - 1$ out of C equations, where C is the total number of components under consideration. To find the final remaining rate expression, the *bootstrap* needs to be used. In brief, the bootstrap method [33] is a form of the energy balance across the film and is affected by the model assumptions.

Energy Transfer Because there is no energy balance (due to CMO), there is clearly no rate of energy transfer. The correct bootstrap to use when defining the rate of component C would then be:

$$\sum_{k=1}^{k=C} N_k = 0 \tag{3.14}$$

3.1.1.4 Equilibrium

As will be explained, three similar variations on Model 1 were developed. Each used a different equilibrium relationship, which are listed below:

Model 1.A: Linear equilibrium relationship [35]:

$$y_k^* = a \cdot x_k + b \qquad a = 0.43755 \qquad b = 0.44142 \qquad k = 1,2 \tag{3.15}$$

Model 1.B: Nonlinear equilibrium with an azeotrope occurring at 52% $x_{pentane}$ [9]:

$$y_k^* = \frac{a \cdot x_k}{1 + (a-1) \cdot x_k} + b \cdot x_k \cdot (1 - x_k) \qquad a = 4.2 \qquad b = -1.2 \qquad k = 1,2 \tag{3.16}$$

Model 1.C: Nonlinear equilibrium (constant α):

$$y_k^* = \frac{\alpha_k \cdot x_k}{\sum_{k=1}^{k=4} \alpha_k \cdot x_k} \qquad k = 1, ..., 4 \tag{3.17}$$

3.1.2 Assumptions Made

Although some of the following assumptions have been mentioned elsewhere, they are nonetheless grouped again here. When using the Model 1 template, the following assumptions were always made:

1. Adiabatic distillation column
2. Constant and saturated liquid and vapor flow rates
3. Known equilibrium relationship
4. Known overall mass transfer coefficient
5. Constant α
6. Feed condition $q = 0$

3.1.3 Instances of Model 1: *Data used and schematic*

Model 1 describes a general template of a distillation system. Using this abstract class definition, three different models were derived from it. Each of these models retains the common equations and assumptions. They differ in the data used and number of components. Model 1 represents a rectifying section only. This largely motivated by the purpose of Model 1, namely developing the simplest model possible for learning purposes, yet while retaining meaning as a building block for Model 2 and Model 3. This purpose is subsequently met through considering a rectifying section alone. The instances of Model 1 are:

Table 3.1: Data used in the three models derived from **Model 1**

Parameter	Model 1.A	Model 1.B	Model 1.C
Components	Ethanol (1) Water (2)	Pentane (1) Dichloromethane (2)	Methyl Cyclohexane (1) Toulene (2) P-Xylene (3) M-Xylene (4)
Vapor feed flow rate $\left(\frac{gmol}{hr}\right)$	78.0	260	50
$K_{og}a \cdot S$ $\left(\frac{gmol}{cm.hr}\right)$	10		0.5
Feed composition	$y_1 = 0.52$ $y_2 = 0.48$	$y_1 = 0.3$ $y_2 = 0.7$	$y_1 = 0.23$ $y_2 = 0.37$ $y_3 = 0.21$ $y_4 = 0.19$
Feed volatility			$\alpha_1 = 2.8$ $\alpha_2 = 2.2$ $\alpha_3 = 1.95$ $\alpha_4 = 1.0$
Feed quality	$q = 0$		

Model 1.A: Binary System

- The mass transfer coefficient value was taken from a literature experimental study [35].
- The model was further advanced by [17].

Model 1.B: Binary Azeotropic System

Model 1.C: Multicomponent System [17]

The data used in the derived models is listed in Table 3.1. The schematic representative of all three of the derived models is shown in Figure 3.3.

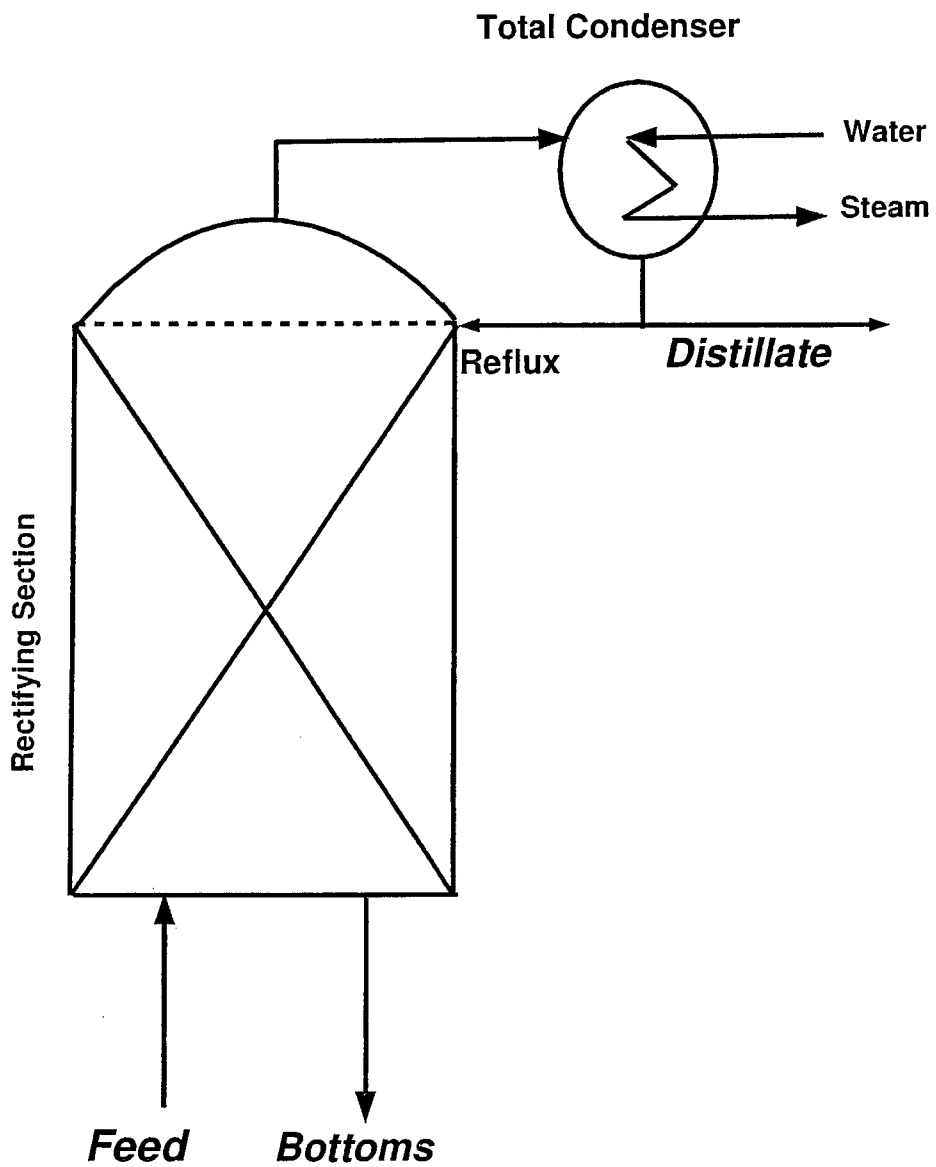

Figure 3.3: Schematic of the rectifying section of a packed distillation column used in **Model 1.A, 1.B & 1.C**

Table 3.2: Summary of equations used in **Model 1**, and their position in the text

Mass	Rate
Eqn (3.1), pg 54 Eqn (3.2), pg 54	Eqn (3.13), pg 56

3.1.4 List of Equations and Variables

Although the equations used in this model have been explained above, this section ties up the list of equations with the associated variables. This will be useful should the reader wish to reproduce the exact model. The $2 \cdot C$ variables at each collocation point in a nonequilibrium column, are ordered into a vector (g_n) as follows:

$$(g_n)^T = (x_{1,n}, x_{2,n}, ..., x_{C,n}, y_{1,n}, y_{2,n}, ..., y_{C,n}) \tag{3.18}$$

where $n = 1, ...,$ total number of collocation points and $C =$ total number of components. The corresponding $2 \cdot C$ equations for each collocation point are ordered into a vector (F_n) as follows:

$$(F_n)^T = (M^L_{1,n}, M^L_{2,n}, ..., M^L_{C,n}, M^V_{1,n}, M^V_{2,n}, ..., M^V_{C,n}) \tag{3.19}$$

The nonequilibrium model equations for the rectifying section can be expressed in the general functional form:

$$F \cdot g = 0 \tag{3.20}$$

where (F) is defined as:

$$(F)^T = ((F_1)^T, (F_2)^T, ..., (F_n)^T) \tag{3.21}$$

The equations used in Model 1 are listed in Table 3.2.

3.2 Model 2: *Vapor Phase Resistance with Energy Balance*

Model 1 and Model 2 are similar. They both assume that all resistance to mass transfer occurred in the vapor phase, as explained in Section 3.1 and shown in Figure 3.1. However, Model 2 increases in complexity by relaxing the assumption of CMO. An energy balance at each collocation point is subsequently needed. This has the effect of introducing variant liquid and vapor temperatures, as well as changing total liquid and vapor flows throughout the column. Initially both the vapor and liquid temperatures were calculated in this model. This was however replaced by a single temperature, which is representative of the liquid phase[4].

To summarize, a fictitious vapor mole fraction y^* is once again defined and assumed to be in equilibrium with the liquid mole fraction x in the bulk liquid. As before, this approach is used to avoid determining the composition at the interface between the two phases. However unlike in Model 1, the equilibrium relationship between y^* and x is not known. This requires that as well as with the vapor and liquid flows and temperatures (V, L and T^{liq}), the bulk concentrations y^*, must be added to the list of unknowns being solved for.

3.2.1 Theory-Based Equation Development

This section develops and presents the mass, energy, rate and equilibrium equations (MERQ) used in Model 2.

3.2.1.1 Mass Balance

There are 2 sets of mass balance equations; the overall and the component mass balances. Each set contains 3 equations. However, because the mole fractions in both phases must sum to unity, only 2 of the 3 equations within each set are independent.

1. *Overall Mass Balances:*

$$\frac{dL}{dz} - \frac{dV}{dz} = 0 \tag{3.22}$$

$$\frac{dL}{dz} + \sum_{k=1}^{k=C} N_k = 0 \tag{3.23}$$

[4]The bubble point relationship is used to determine the temperature, instead of the dew point if the vapor phase was assumed to be representative

$$\frac{dV}{dz} + \sum_{k=1}^{k=C} N_k = 0 \tag{3.24}$$

2. *Component Mass Balances:*

$$\frac{d(L \cdot x_k)}{dz} - \frac{d(V \cdot y_k)}{dz} = 0 \qquad k = 1, ..., \text{Number of components} \tag{3.25}$$

$$\frac{d(L \cdot x_k)}{dz} + N_k = 0 \qquad k = 1, ..., \text{Number of components} \tag{3.26}$$

$$\frac{d(V \cdot y_k)}{dz} + N_k = 0 \qquad k = 1, ..., \text{Number of components} \tag{3.27}$$

3.2.1.2 Energy Balance

It was assumed that energy transfer across the thermal film is ideal i.e $T^L = T^V$ as shown in Figure 3.1. To determine the temperature, the liquid and vapor flows are assumed to be saturated. This allows for the use of the bubble point relationship as shown below:

$$\sum_{k=1}^{k=C} (K_k \cdot x_k) = 1 \tag{3.28}$$

Although it is obvious that the above equation is not differential, a subtle consequence is that collocation is not directly applied to it. Instead, the equation is evaluated at the collocation points as they stand i.e. unaltered. This means that boundary conditions cannot be applied at the end points as is standard for example, in the mass balance. In general, all reference points were taken at 298K. The average enthalpy of a simple liquid is an almost linear function of pressure (P) and temperature (T):

$$H^L = c_p^{L,average} \cdot (T - T^{Ref}) + v \cdot (P - P^{Ref}) \tag{3.29}$$

The pressure term can be ignored due to the small liquid volume (v), resulting in the following equation:

$$H^L = \sum_{k=1}^{k=C} (c_p^L \cdot (T - T^{Ref}) \cdot x_k) \tag{3.30}$$

Gases have higher enthalpies than liquids, and for a mixture of ideal gases at low pressures the average enthalpy is represented by:

$$H^V = \sum_{k=1}^{k=C} (H_k^V \cdot y_k) \tag{3.31}$$

In the above equation, the heat of vaporization dominates. If the heat capacities for both phases are small, the following is true:

$$H_k^V - H_k^L = \sum_{k=1}^{k=C} (\Delta H_k^{vap} \cdot y_k) \tag{3.32}$$

3.2.1.3 Rates

Unlike in Model 1, the rates of *both* the mass and energy transfer need to be considered.

Mass Transfer: The mass transfer used here is the same as that in Model 1 and can be referenced in Section 3.1.1.3.

Energy Transfer: Energy transfer was not considered in Model 1 as there was no energy balance. Model 2 includes an energy balance while assuming ideal heat transfer at the interface i.e. $T^V = T^L$. This is shown in Figure 3.1. The bootstrap equation subsequently required to find the C^{th} component flux is:

$$N_{k=C} = -\frac{\sum_{k=1}^{k=C-1}(N_k \cdot H_k^{vap})}{H_{k=C}^{vap}} \tag{3.33}$$

The derivation of equation (3.33) follows:
The complete bootstrap equation is shown below for a rigorous, nonequilbrium column with four distinct film temperatures i.e. $T^V \neq T^{V,I} \neq T^{L,I} \neq T^L$:

$$h^L \cdot a_h \cdot (T^I - T^L) \cdot S + \sum_{k=1}^{C} N_k \cdot H_k^L = h^V \cdot a_h \cdot (T^V - T^I) \cdot S + \sum_{k=1}^{C} N_k \cdot H_k^V \tag{3.34}$$

In equation (3.34), a_h is the area available for energy transfer, N_k is the rate of flux of component k, and $h^{L \text{ or } V}$ is the heat transfer coefficient. As explained before, the bootstrap equation is used to determine the C^{th} component flux as only $C-1$ flux equations are independent. It can be broken down into the vapor and liquid energy rates:

$$\epsilon^V = h_v \cdot a_h \cdot (T^V - T^{V,I}) \cdot S + \sum_{k=1}^{C} N_k \cdot H_k^V \tag{3.35}$$

$$\epsilon^L = h_l \cdot a_h \cdot (T^{L,I} - T^L) \cdot S + \sum_{k=1}^{C} N_k \cdot H_k^L \tag{3.36}$$

The energy fluxes across the films are also equal:

$$\epsilon^L - \epsilon^V = 0 \tag{3.37}$$

However Model 2 assumes that $T^L = T^V$, and that the interface temperatures are redundant. If we implement the assumptions then equation (3.34) reduces to:

$$\epsilon^V - \epsilon^L = 0 = \sum_{k=1}^{C} N_k \cdot \Delta H_k^{vap} \tag{3.38}$$

The rearrangement of equation (3.38) in terms of the remaining mass transfer rate ($N_{k=C}$) is subsequently shown in equation (3.33).

3.2.1.4 *Equilibrium*

The standard equilibrium relationship at the interface was used in Model 2:

$$y_k^* = K_k \cdot x_k \qquad k = 1, ..., \text{Number of components} \tag{3.39}$$

The equilibrium coefficient was evaluated by assuming an ideal gas phase:

$$K_k = \frac{P_k}{P_{total}} \qquad k = 1, ..., \text{Number of components} \tag{3.40}$$

In the above equation, the Antoine correlation is used to determine the component vapor pressures.

3.2.2 Assumptions Made

The following assumptions were made in this model:

1. Resistance to mass and energy transfer occurs in the vapor phase
2. Ideal energy transfer
3. Isobaric distillation column
4. Adiabatic distillation column
5. Thermal and mass equilibrium between phases
6. Saturated vapor and liquid flows
7. Vapor phase heat transfer coefficient (h^V) assumed to be negligibly small
8. A lumped parameter represents the overall vapor phase transfer coefficient ($K_{og}a \cdot S$)

$$\epsilon^L - \epsilon^V = 0 \tag{3.37}$$

However Model 2 assumes that $T^L = T^V$, and that the interface temperatures are redundant. If we implement the assumptions then equation (3.34) reduces to:

$$\epsilon^V - \epsilon^L = 0 = \sum_{k=1}^{C} N_k \cdot \Delta H_k^{vap} \tag{3.38}$$

The rearrangement of equation (3.38) in terms of the remaining mass transfer rate ($N_{k=C}$) is subsequently shown in equation (3.33).

3.2.1.4 *Equilibrium*

The standard equilibrium relationship at the interface was used in Model 2:

$$y_k^* = K_k \cdot x_k \qquad k = 1, ..., \text{Number of components} \tag{3.39}$$

The equilibrium coefficient was evaluated by assuming an ideal gas phase:

$$K_k = \frac{P_k}{P_{total}} \qquad k = 1, ..., \text{Number of components} \tag{3.40}$$

In the above equation, the Antoine correlation is used to determine the component vapor pressures.

3.2.2 Assumptions Made

The following assumptions were made in this model:

1. Resistance to mass and energy transfer occurs in the vapor phase
2. Ideal energy transfer
3. Isobaric distillation column
4. Adiabatic distillation column
5. Thermal and mass equilibrium between phases
6. Saturated vapor and liquid flows
7. Vapor phase heat transfer coefficient (h^V) assumed to be negligibly small
8. A lumped parameter represents the overall vapor phase transfer coefficient ($K_{og}a \cdot S$)

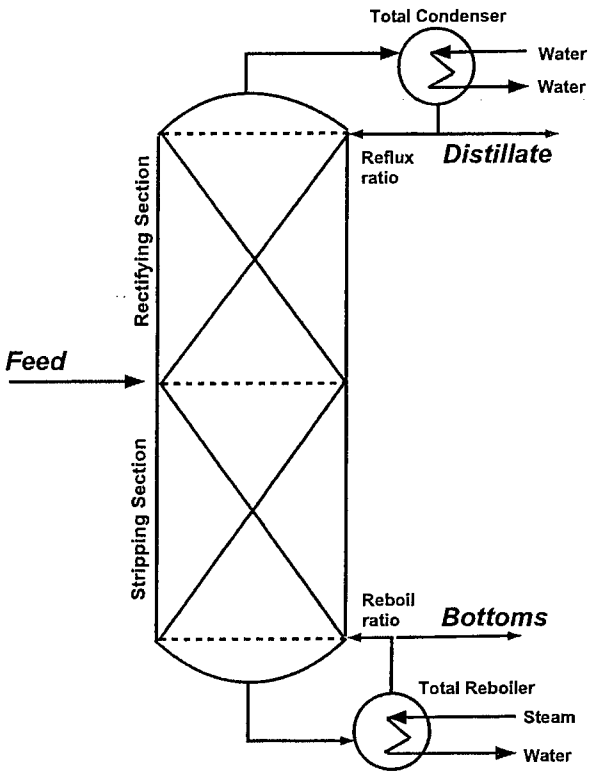

Figure 3.4: Schematic of the packed distillation column used in **Models 2 & 3**

3.2.3 An Instance of Model 2: *Data used and schematic*

In a similar manner to Model 1, Model 2 represents a general model of a distillation column based on certain assumptions. A specific instance of this broad definition was derived using a three component system with a rectifying and stripping section. The schematic representing the derived model is shown in Figure 3.4.

While the explanation surrounding the choice of degrees of freedom will be presented in the following chapter, at this point it is sufficient to note that should the feed be fully specified, a degree of freedom will be removed from the system. Because this approach was taken, a consistent feed was required. Table 3.3 lists the variables characterizing the feed. In Table 3.3, the second column characterizes the process stream fed to the column. Shortly before the stream reaches the column, it passes through a value which drops the pressure, resulting in the flashed conditions listed in the final two columns. When performing a flash calculation, two state variables must be defined. In this work, the vapor flow rates and temperature were assumed. The adiabatic Rachford Rice equations were used in the flash calculation.

Table 3.3: Specifications used to fully define the feed in **Model 2 & 3**

	Line to Column	*Flashed on Entry*	
Variables	*Feed*	*Liquid*	*Vapor*
T^V (K)	-	371	371
T^L (K)	368	371	371
Pressure (kPa)	300	200	200
V ($\frac{kmol}{min}$)	-	-	45
L ($\frac{kmol}{min}$)	100	55	-
Quality q	1	1	-
$y_{ethanol}$	-	-	0.3222
y_{water}	-	-	0.1789
$y_{methanol}$	-	-	0.4987
$x_{ethanol}$	0.3200	0.3170	-
y_{water}	0.2700	0.3810	-
$x_{methanol}$	0.4100	0.3014	-
Total flowrate ($\frac{kmol}{min}$)	100	45	55

3.2.4 List of Equations and Variables

The $3 \cdot C + 3$ variables at each collocation point n in a nonequilibrium column, are ordered into a vector (g_n) as follows:

$$(g_n)^T = \left(x_{1,n}, x_{2,n}, ..., x_{C,n}, L_n, T_n, y_{1,n}, y_{2,n}, ..., y_{C,n}, V_n, y^*_{1,n}, y^*_{2,n}, ..., y^*_{c,n}\right) \tag{3.41}$$

where $n = 1, ...,$ total number of collocation points and $C =$ total number of components. The corresponding $3 \cdot C + 3$ equations for each collocation point are ordered into a vector (F_n) as follows:

$$(F_n)^T = \left(M^L_{1,n}, M^L_{2,n}, ..., M^L_{C,n}, M^L_{Total,n}, E_n, M^V_{1,n}, M^V_{2,n}, ..., M^V_{C,n}, M^V_{Total,n}, Q^I_{1,n}, Q^I_{2,n}, ..., Q^I_{C,n}\right) \tag{3.42}$$

The nonequilibrium model equations for an entire column can be expressed in the general functional form:

$$F \cdot g = 0 \tag{3.43}$$

where (F) is defined as:

$$(F)^T = ((F_1)^T, (F_2)^T, ..., (F_n)^T) \tag{3.44}$$

Table 3.4 summarizes the equations used in Model 2.

Table 3.4: Summary of equations used in **Model 2**, and their position in the text

Mass	**E**nergy	**R**ate	**E**quilibrium
Eqn (3.22), pg 61 Eqn (3.23), pg 61 Eqn (3.25), pg 62 Eqn (3.27), pg 62	Eqn (3.28), pg 62 Eqn (3.33), pg 63	Eqn (3.13), pg 56	Eqn (3.39), pg 64

3.3 Model 3: *Rigorous Nonequilibrium Rate-Based Distillation*

This model progresses by dropping the equilibrium assumption made in Model 2. Previously, a fictitious vapor mole fraction was defined to be in equilibrium with the bulk liquid phase. This was done to avoid calculating the compositions at the interface between the two phases. By dropping this assumption in Model 3, a complete rigorous nonequilibrium model as described in any of the standard reference texts results.

Figure 3.5 shows a nonequilibrium section of a packed column. Vapor from the section below is brought into contact with liquid from the section above and allowed to exchange mass and energy across their common interface. The packed column consists of a sequence of these sections. Model 3 increases the complexity by requiring that the compositions at the interface are calculated. To do so, expressions for determining the mass and energy transfer coefficients are used. These expressions require a thorough knowledge of the column internals, as well as an extensive database of physical properties.

3.3.1 Theory-Based Equation Development

This section develops and presents the mass, energy, rate and equilibrium equations (MERQ) used in Model 3.

3.3.1.1 M*ass Balance*

The mass balances are the same as those used in Model 2 on page 61. There is a difference in the rate definitions which will be detailed in the proceeding sections.

3.3.1.2 E*nergy Balance*

The overall and phase balances are shown below in equations (3.45), (3.46) and (3.47), of which only two are independent. This shown by subtracting equation (3.46) from equation (3.47) and

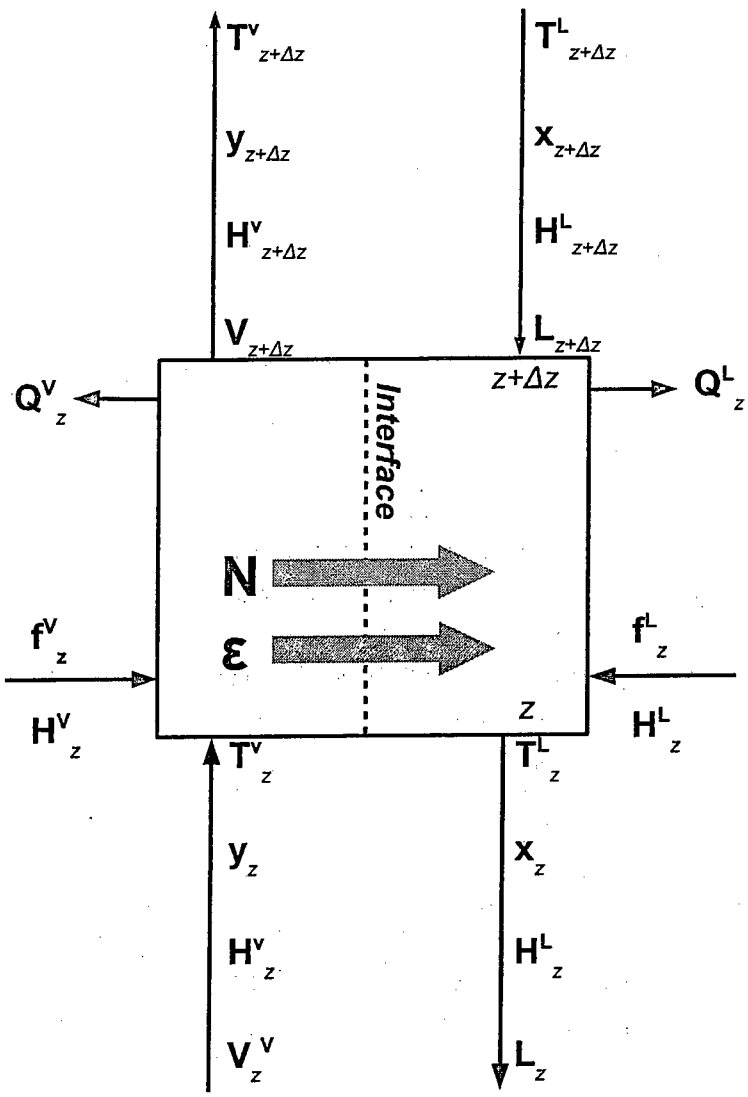

Figure 3.5: Section of a nonequilibrium column showing direction of mass and energy transfer and integration direction from the bottom upwards

noting that the energy rates are equivalent across the phases i.e. $\epsilon^V - \epsilon^L = 0$. Equation (3.45) subsequently results.

$$0 = \frac{d(L \cdot H^L)}{dz} - \frac{d(V \cdot H^V)}{dz} \tag{3.45}$$

$$\frac{d(V \cdot H^V)}{dz} + \epsilon^V = 0 \tag{3.46}$$

$$\frac{d(L \cdot H^L)}{dz} + \epsilon^L = 0 \tag{3.47}$$

3.3.1.3 Rates

Similarly to Model 2, the rates of both the mass and energy transfer need to be considered.

Mass Transfer For rate-based models, accurate predictions of heat and mass transfer rates are required. These rates depend on transport coefficients, interface area and driving forces. Mass transfer rates should account for component-coupling effects through binary interactions [15]. While they are often neglected, there are some phenomena such as reverse diffusion which can only be explained by the off-diagonal diffusion coefficients. Before the mass transfer rates can be calculated, the fluxes must be determined. This is shown in the below equation, where the liquid phase flux $J_i(z)$ is multiplied by an area $a(z)$ to find the rate of mass transfer $N_i(z)$.

$$N_i(z) = a(z) \cdot J_i(z) + x_i(z) \cdot N_T(z) \tag{3.48}$$

To find the fluxes, either Fick's law or Maxwell-Stefan (MS) equations can be used. Fick's law states that the diffusion flux is proportional to the concentration gradient and is shown in equation (3.49). MS equations are preferred in multicomponent systems [33] due to the component-coupling effects, and are shown in equation (3.50).

$$(J) = -c_t \cdot [D] \cdot \Delta(y) \tag{3.49}$$

$$(J) = -c_t \cdot [B]^{-1} \cdot [\Gamma] \cdot \Delta(y) \tag{3.50}$$

The term $[\Gamma]$ is a matrix of thermodynamic factors that corrects for non-ideality when using non-ideal VLE. This is often needed for the liquid phase but can mostly be neglected in the vapor phase. When using an activity-coefficient model Γ is defined by:

$$\Gamma^L_{ij} = \delta_{ij} + x_i \cdot \left(\frac{\partial ln(\gamma_i)}{\partial x_j}\right)_{T,P,x_k,k\neq j=1\ldots c-1} \tag{3.51}$$

The elements of $[B]$ in terms of general mole fractions, z_i are:

$$B_{ii} = \frac{z_i}{D_{iC}} + \sum_{\substack{k=1 \\ k\neq i}}^{C} \frac{z_k}{D_{ik}} \tag{3.52}$$

$$B_{ij} = -z_i \cdot \left(\frac{1}{D_{ij}} - \frac{1}{D_{iC}}\right) \tag{3.53}$$

The relation between equations 3.49 and 3.50 is:

$$[D] \equiv [B]^{-1} \cdot [\Gamma] \tag{3.54}$$

At infinite dilution, MS diffusivities are equal to Fick diffusion coefficients. If the solution is ideal, $[\Gamma]$ reduces to the identity matrix and the Fick diffusivities are equal to $[B]^{-1}$. This applies to gases at low to moderate pressures [32]. To continue the derivation, it is useful to consider the vapor phase fluxes in ternary systems:

$$J^V_1(z) = c^V_t \cdot \kappa^V_{11} \cdot (y_1 - y^I_1) + c^V_t \cdot \kappa^V_{12} \cdot (y_2 - y^I_2) \tag{3.55}$$

$$J^V_2(z) = c^V_t \cdot \kappa^V_{21} \cdot (y_1 - y^I_1) + c^V_t \cdot \kappa^V_{22} \cdot (y_2 - y^I_2) \tag{3.56}$$

The third component flux is derived using the definition of the molar diffusive flux:

$$\sum_{i=1}^{C} J_i = 0 \tag{3.57}$$

$$J^V_3 = -J^V_1 - J^V_2 \tag{3.58}$$

In the above equations, the matrix of binary-pair coefficients $[\kappa]$, are complex functions related to inverse rate functions. Using the MS approach, it is convenient to determine $[\kappa]$ from a reciprocal mass transfer coefficient function R, for an ideal gas solution [15]:

$$[\kappa^V] = [R^V]^{-1} \tag{3.59}$$

For a non-ideal liquid solution:

$$[\kappa^L] = [R^L]^{-1} \cdot [\Gamma^L] \tag{3.60}$$

The elements of $[R]$ in terms of general mole fractions, z_i are:

$$R_{ii} = \frac{z_i}{\kappa_{iC}} + \sum_{\substack{k=1 \\ k \neq i}}^{C} \frac{z_k}{\kappa_{ik}} \tag{3.61}$$

$$R_{ij} = -z_i \cdot \left(\frac{1}{\kappa_{ij}} - \frac{1}{\kappa_{iC}} \right) \tag{3.62}$$

In the above equations, j refers to the j^{th} component and values of k are binary-pair mass-transfer coefficients. Because ideal VLE was used, the thermodynamic factor Γ is 1. The vapor and liquid phase mass transfer coefficient matrices subsequently become:

$$[\kappa^{V \text{ or } L}] = [R^{V \text{ or } L}]^{-1} \tag{3.63}$$

The resulting fluxes are shown below :

$$\begin{pmatrix} J_1^V \\ J_2^V \end{pmatrix} = \begin{pmatrix} R_{1,1}^V & R_{1,2}^V \\ R_{2,1}^V & R_{2,2}^V \end{pmatrix}^{-1} \begin{pmatrix} (y_1^V - y_1^I) \\ (y_2^V - y_2^I) \end{pmatrix} \tag{3.64}$$

If the coupling effects are assumed to be negligible the following results:

$$\begin{pmatrix} J_1^V \\ J_2^V \end{pmatrix} = \begin{pmatrix} R_{1,1}^V & 0 \\ 0 & R_{2,2}^V \end{pmatrix}^{-1} \begin{pmatrix} (y_1^V - y_1^I) \\ (y_2^V - y_2^I) \end{pmatrix} \tag{3.65}$$

The elements of the vector $[\mathbb{R}]$ are ultimately represented by:

$$R_{1,1} = \frac{z_1}{\kappa_{1,3}^V} + \frac{z_2}{\kappa_{1,2}^V} + \frac{z_3}{\kappa_{1,3}^V} \tag{3.66}$$

$$R_{2,2} = \frac{z_2}{\kappa_{2,3}^V} + \frac{z_1}{\kappa_{2,1}^V} + \frac{z_3}{\kappa_{2,3}^V} \tag{3.67}$$

At this stage it is useful to refer back to the starting point in equation (3.48). The rates have been defined in terms of the area $a(z)$, fluxes and a matrix of mass transfer coefficients. To determine the mass transfer coefficient values, a knowledge of the column internals is required. The subsequent correlations used are explained in detail in section A.1. The final mass transfer expressions are shown:

$$N_k^L(z) = c_{total,k}^L \cdot [\kappa_k^L] \cdot a_j \cdot (x_k^I - x_k) + x_k \cdot N_{total}^L \qquad k = 1, \ldots C-1 \tag{3.68}$$

$$N_k^V(z) = c_{total,k}^V \cdot [\kappa_k^V] \cdot a_j \cdot (y_k - y_k^I) + y_k \cdot N_{total}^V \qquad k = 1, \ldots C-1 \tag{3.69}$$

As in Model 2, only $C-1$ of C rate expressions are independent. The final rate is likewise derived from the bootstrap method shown in equation (3.34) on page 63.

Energy Transfer With reference to Figure 3.1, Model 2 assumed $T^L = T^{L,I}$. Model 3 makes no such assumption and the rates of vapor and liquid energy transfer are subsequently described by equations (3.35) and (3.36) respectively on page 63. The correlations used to calculate the energy transfer coefficients are shown in Section A.2.

3.3.1.4 *Equilibrium*

As in Model 2, the standard equilibrium at the interface relationship at the interface was used in conjunction with equation (3.40) and the Antoine equation:

$$y_k^I = K_k x_k^I \qquad k = 1, ..., \text{Number of components} \tag{3.70}$$

However, the manner in which it was used is slightly different. Previously, the equilibrium was assumed to be across the bulk phases i.e. $y^* = f(x_{bulk})$. In this model, the complexity is increased by accounting for a separate set of interface compositions i.e. $y^I = f(x^I)$. The number of variables significantly increases as a result. To increase the number of equations likewise, the interface summations are also included:

$$\sum_{k=1}^{C} y_k^I = 1 \tag{3.71}$$

$$\sum_{k=1}^{C} x_k^I = 1 \tag{3.72}$$

The summations of the bulk compositions are not necessary as the overall mass balances account for that. The bulk mole fraction summations could alternatively be used as an error analysis tool.

3.3.2 Assumptions Made

The following assumptions were made in this model:

1. Isobaric distillation column
2. Adiabatic distillation column
3. No coupling effects in the mass transfer coefficients i.e. the mass transfer coefficient square matrix $[k]$ is reduced to the diagonal values
4. Thermodynamic factor Γ is assumed to be 1 in both phases i.e. ideal phases
5. Column has structured packing which is well represented by the Bravo correlation [33]

3.3.3 An Instance of Model 3: *Data used and schematic*

In a similar manner to the previous models, Model 3 represents a general model of a distillation column based on certain assumptions. A specific instance of this broad definition was derived using a three component system with a rectifying and stripping section. The schematic representing the derived model is the same as in Model 2 and can be referenced in Figure 3.4 on page 65.
A vast amount of data is required to represent this problem. Table B.1 lists the correlations and their sources used to calculate the physical properties. The feed data is the same as that used in Model 2, and is listed in Table 3.3 on page 66. The data used to describe the column internals can be found in Table A.1 on page 151.

3.3.4 List of Equations and Variables

As previously explained, the purpose of the section is to tie together all the equations used in the development of Model 3, with the associated variables. The $5 \cdot C + 5$ variables at each collocation point n in a nonequilibrium column, are ordered into a vector (g_n) as follows:

$$(g_n)^T = \left((g_{film\ balance,n})^T, (g_{mass\ balance,n})^T\right) \tag{3.73}$$

$$(g_{film\ balance,n})^T = \left(x^{\mathrm{I}}_{1,n}, x^{\mathrm{I}}_{2,n}, ..., x^{\mathrm{I}}_{C,n}, y^{\mathrm{I}}_{1,n}, y^{\mathrm{I}}_{2,n}, ..., y^{\mathrm{I}}_{C,n}, T^{\mathrm{I}}_n, N_{1,n}, N_{2,n}, ..., N_{C,n}\right) \tag{3.74}$$

$$(g_{mass\ balance,n})^T = \left(x_{1,n}, x_{2,n}, ..., x_{C,n}, L_n, T^L_n, y_{1,n}, y_{2,n}, ..., y_{C,n}, V_n, T^V_n\right) \tag{3.75}$$

where $n = 1, ...,$ total number of collocation points and $C =$ total number of components.

The corresponding $5 \cdot C + 5$ equations for each collocation point are ordered into a vector (F_n) as follows:

$$(F_n)^T = \left((F_{film\ balance,n})^T, (F_{mass\ balance,n})^T\right) \tag{3.76}$$

$$(F_{film\ balance,n})^T = \left(M^L_{1,n}, M^L_{2,n}, ..., M^L_{C,n}, M^L_{Total,n}, E^L_n, M^V_{1,n}, M^V_{2,n}, ..., M^V_{C,n}, M^V_{Total,n}, E^V_n\right) \tag{3.77}$$

$$(F_{mass\ bal.,n})^T = \left(Q^{\mathrm{I}}_{1,n}, Q^{\mathrm{I}}_{2,n}, ..., Q^{\mathrm{I}}_{C,n}, S^{V,\mathrm{I}}_n, S^{L,\mathrm{I}}_n, R^V_{1,n}, R^V_{2,n}, ..., R^V_{C-1,n}, R^L_{1,n}, R^L_{2,n}, ...R^L_{C-1,n}, E^{\mathrm{I}}_n\right) \tag{3.78}$$

Table 3.5: Summary of equations used in **Model 3**, and their position in the text

Mass	**E**nergy	**R**ate	E**Q**uilibrium	**S**ummation
Eqn (3.22)	Eqn (3.46)	Eqn (3.68)	Eqn (3.70)	Eqn (3.71)
Eqn (3.23)	Eqn (3.47)	Eqn (3.69)		Eqn (3.72)
Eqn (3.25)	Eqn (3.34)			
Eqn (3.27)				

The vector $(g_{film\ balance})$ has $C + C + 1 + C = 3 \cdot C + 1$ variables per collocation point, where C is the total number of components. The vector $(g_{mass\ balance})$ has $C + 1 + 1 + C + 1 + 1 = 2 \cdot C + 4$ variables per collocation point. In total, there are $5 \cdot C + 5$ equations per collocation point. The nonequilibrium model equations for an entire column can be expressed in the general functional form:

$$F \cdot g = 0 \tag{3.79}$$

where (F) is defined as:

$$(F)^T = ((F_1)^T, (F_2)^T, ..., (F_n)^T) \tag{3.80}$$

Table 3.5 summarizes the equations used in Model 3.

Chapter 4

Solution Methodology

Once the model equations have been developed, surely it should be a simple matter of solving them? Unfortunately this is not entirely true as there are still several solution steps to be followed.

The first question that could be raised is 'what is being solved for'? To answer this, an evaluation of the degrees of freedom is required. This is the first section covered in this chapter. It is an important section as the degrees of freedom need to be carefully considered and kept consistent throughout all the models, particularly as the approach followed here is usually not that of the reference books.

The second question that could be asked might be something along the lines of 'having the collocation equations and the correct number or specifications, how are the boundary conditions assigned'? This is the more difficult question and the response involves a clear definition of how the column model is segregated and where boundary conditions can be applied without violating the degrees of freedom. The second section in this chapter tackles this concept.

Finally, what may still be missing between having the model equations, identifying the variables being solved for and understanding the boundary conditions, is a explanation of how the collocation programs are used and examples of the actual collocation equations. These technical aspects do not contribute significantly to the argument in this chapter, and are subsequently presented in Appendix C.

4.1 Degrees of Freedom: What is being solved for?

An analysis of the degrees of freedom of a distillation column was given in Section 2.2.2. The result was that there were four degrees available once the feed was fully characterized. The more common usage was to define any two product specifications, the feed position and the column height. While it cannot be argued that four is the incorrect number of degrees of freedom, it can be suggested that the most common choice thereof is not necessarily the best depending on the design aims.

Throughout this thesis, there has been a key idea (kept largely in the background admittedly), of documenting the separation feasibility. This is an extremely vague concept and requires more definition. What is the best, or at least the most logical, manner to go about describing the separation? Is it smarter to fix an ideal product purity and then identify the combination of reflux *or* reboil ratios and section heights which can achieve this? Or is it a better idea to relax the product specifications and incrementally adjust the internal flows as well as the height, and try optimize the resulting product specifications?

There is possibly no correct answer to this problem and it becomes a matter of personal choice. In this case, it was decided to let the product specifications float i.e. the second option. This allowed for the following variables to be adjusted, while solving for the final compositions in the bottoms and distillate:

- Reflux ratio (Re)
- Reboil ratio (Rb)
- Rectifying section height
- Stripping section height

A subtle point is that the above degrees of freedom also intrinsically specify the feed location. This is fixed when the rectifying and stripping height are chosen. The separation feasibility is subsequently defined as the absolute difference between the component mole fraction in the feed, and the same component mole fraction in either the bottoms or distillate stream.

As will be shown in later chapters, this choice of degrees of freedom has serious ramifications. Because most of the reference books specify a product composition (i.e. the alternative approach to the one used here), some of their analysis will not hold i.e. minimum flows and coincidence of profiles. This point will be raised again in Chapter 5, Section 5.1.3.

Table 4.1: Boundary Conditions for **Model 1.A, 1.B & 1.C.**

Profile	*Position*	*Boundary condition*
x_k	$n+2$	$x^R_{k,n+2} = y^R_{k,n+2}$
y_k	1	$y^R_{k,1} = y^F_k$

4.2 The Structure of the Collocation Models

The structure of Models 1.A, 1.B & 1.C are the simplest, consisting of a single collocation block representing the rectifying section. The structure of Models 2 and 3 are the same, and consist of two collocation blocks representing the rectifying and stripping sections. The complexity increases in this latter structure due to the feed discontinuity. Both structures are discussed in more detail below.

4.2.1 Models 1.A, 1.B & 1.C

A single collocation block was used to represent the rectifying section. This is shown in Figure 4.1. The direction of integration is from the feed to the condenser, as is standard throughout this thesis. As explained in Section 4.1, the reflux ratio, height and feed location are known, and the feed is fully defined. The resulting boundary conditions represent a split boundary problem as the vapor mole fractions at the feed entry is one constraint; the other is the liquid mole fractions at the condenser. These boundary conditions are summarized in Table 4.1.

4.2.2 Models 2 & 3

As mentioned before, these models share the same structure; two collocation blocks representing the rectifying and stripping sections. It must be emphasized that these blocks are not finite elements. Neither the value of the composition variable nor the value of the first derivative thereof, is continuous across the interface i.e $x^R_1 \neq x^S_{n+2}$ and $\frac{dx^R_1}{dz} \neq \frac{dx^S_{n+2}}{dz}$. This is due to the discontinuities introduced by the feed.

The feed discontinuity is very possibly the most noteworthy source of programming headaches. Figure 4.2 was included to explain the problem. In the rectifying section, the liquid mole fractions were constrained at $n = n+2$ using the boundary condition of a total condenser. The vapor mole fractions needed to be constrained at $n = 1$. This point is situated shortly above the feed. However the vapor composition is not known at that point. It is dependent on the vapor composition exiting the stripping section at $n = n+2$, as well as the feed composition.

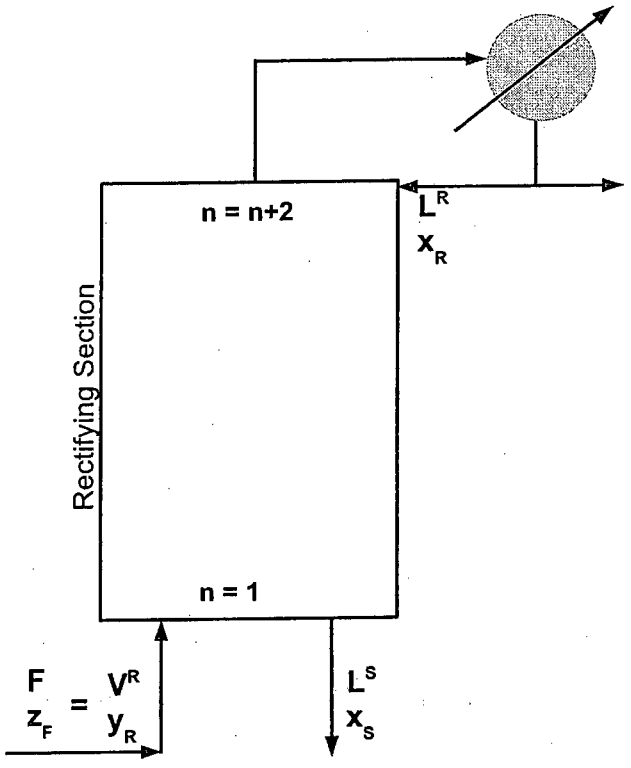

Figure 4.1: Collocation Structure for **Models 1.A, 1.B & 1.C**

Therefore, while two separate collocation blocks were used, they were dependent on each other according to the boundary conditions used at the feed entry point.

To continue the explanation, within the stripping section the vapor mole fractions were constrained at $n = 1$ using the partial reboiler as an additional stage. This leaves the stripping liquid mole fractions at $n = n + 2$, which are dependent on the entering liquid composition from the rectifying section as well as that of the feed composition. Once again, there is a link between the two collocation blocks. This is very tricky to handle and initially iterations were needed to find reasonable initial estimates. However, both of these models are fully automated in their final state i.e. require *no iteration*.

The same locations for the boundary conditions used for the vapor and liquid mole fractions, are also used for the total liquid and vapor flows. To tie up all of the variables, the temperature profiles must also be mentioned. While these represented differential equations, they were not constrained as the temperatures are implicitly known when the compositions are i.e. there is dependence between composition and temperature.

Unfortunately the problem has not been fully resolved at this point. The next major source of difficulty was deciding how to integrate the feed into the column. The literature is relatively thin on this subject, and only two clear references mentioned this problem in reasonable detail ([23] and [30]), and even then only for staged columns. It was decided to treat the feed as an adiabatic mixing stage. The feed was flashed at the same pressure as that of the column, and with the condition specified[1]. The resulting vapor stream was mixed with the vapor leaving the stripping section and vice versa for the liquid flows. The most obvious shortcoming is that this approach is only strictly true for adiabatic columns with constant molar overflow. While all the models were adiabatic, only Model 1 applied the necessary McCabe -Thiele assumptions.

But provided the temperature of the flashed feed matches the temperature of the column[2], there is little reason to dispute this approach. The reasoning goes back to the degrees of freedom discussion in Section 4.1, where it was decided not to force the product compositions. This now proves to be the correct approach. If the product compositions had been specified, the feed composition would change in order to satisfy them thereby complicating the mixing as the temperatures would also shift [23]. A more concrete reason for specifying the variables can now replace the previously instinctive choice made in Section 4.1. Table 4.2 summarizes the above argument by listing the boundary conditions used in both models.

[1] The ratio of vapor to liquid flows

[2] Or at least is very similar

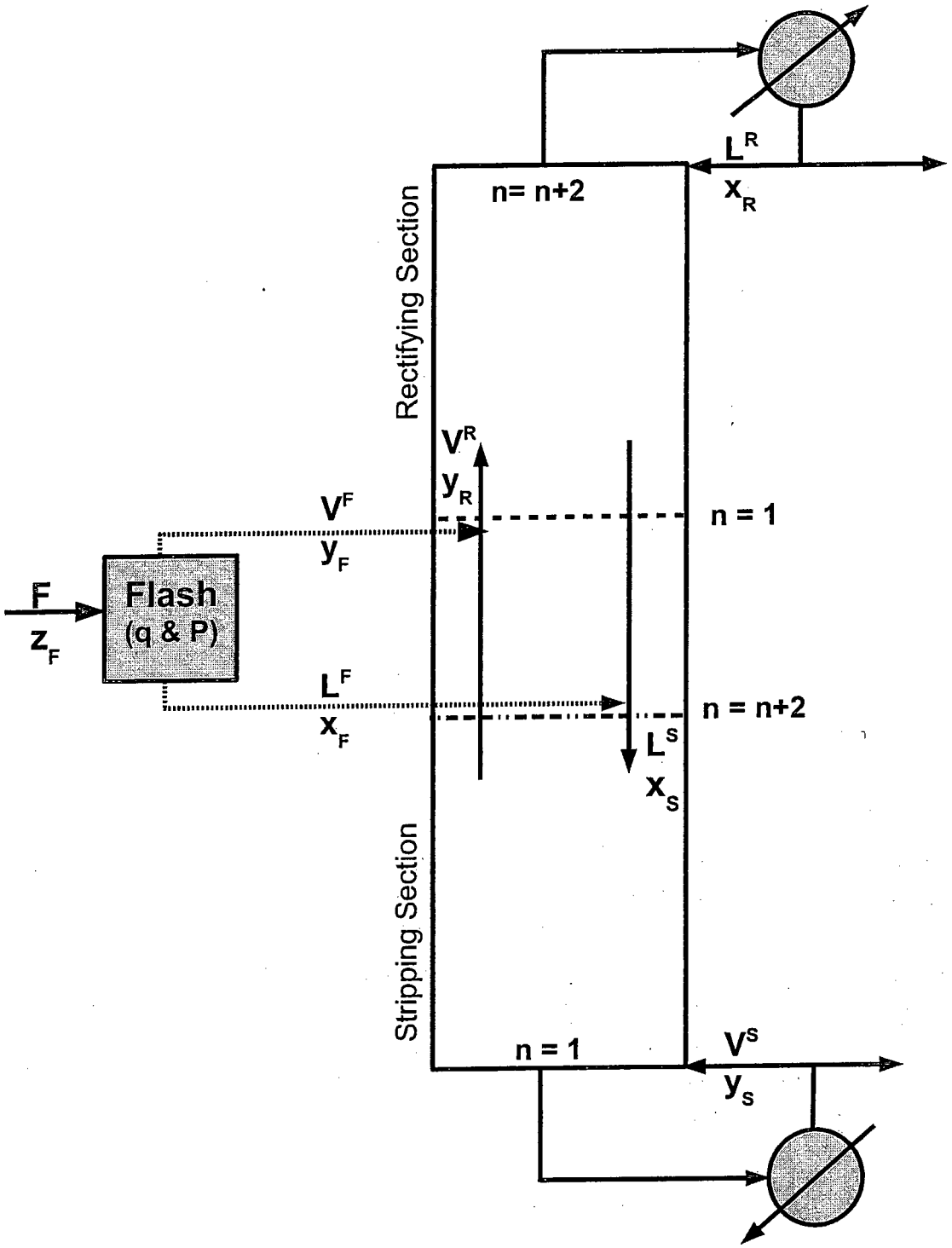

Figure 4.2: Collocation Structure for **Models 2 & 3**

Table 4.2: Explanation of Boundary Conditions used in **Models 2 & 3**

Rectifying Section		
Profile	*Position*	*Boundary condition*
x_k	$n+2$	$x\|^R_{k,n+2} = y\|^R_{k,n+2}$
y_k	1	$y\|^R_{k,1} \cdot V\|^R_1 = y^F_k \cdot V^F + y\|^S_{k,n+2} \cdot V\|^S_{n+2}$
L	$n+2$	$L\|^R_{n+2} \cdot (1+Re) = V\|^R_{n+2}$
V	1	$V\|^R_1 = V^F + V\|^S_{n+2}$
Stripping Section		
Profile	*Position*	Boundary_condition
x_k	$n+2$	$x\|^S_{k,n+2} \cdot L\|^S_{n+2} = L^F \cdot x^F_k + x\|^R_{k,1} \cdot L\|^R_1$
y_k	1	$x\|^S_{k,1} = y\|^S_{k,1}$
L	$n+2$	$L\|^S_{n+2} = L^F + L\|^R_1$
V	1	$V\|^S_1 \cdot (1+Rb) = Rb \cdot L\|^S_1$

Trying to minimize the feed discontinuity inherent in a collocation system, is an interesting problem. For a binary system with an optimal position, there should be no resulting feed discontinuity. This is shown in Figure 4.3. In the figure, point A represents the entering feed composition. If the feed is flashed, point C is fully defined. However neither of these points provide any information as how to find the associated column composition, as indicated by point B.

If the feed is optimally placed as is shown in Figure 4.3, the 'stepping over' from the rectifying to stripping operating line occurs exactly at the flashed feed composition (point C). This results in a smooth composition profile in both phases. For a ternary or multicomponent system, the best continuity possible using this approach will be a smooth composition profile for *either* the light *or* heavy key. This has been proven for the heavy key in later results (Figures 5.21 and 5.30).

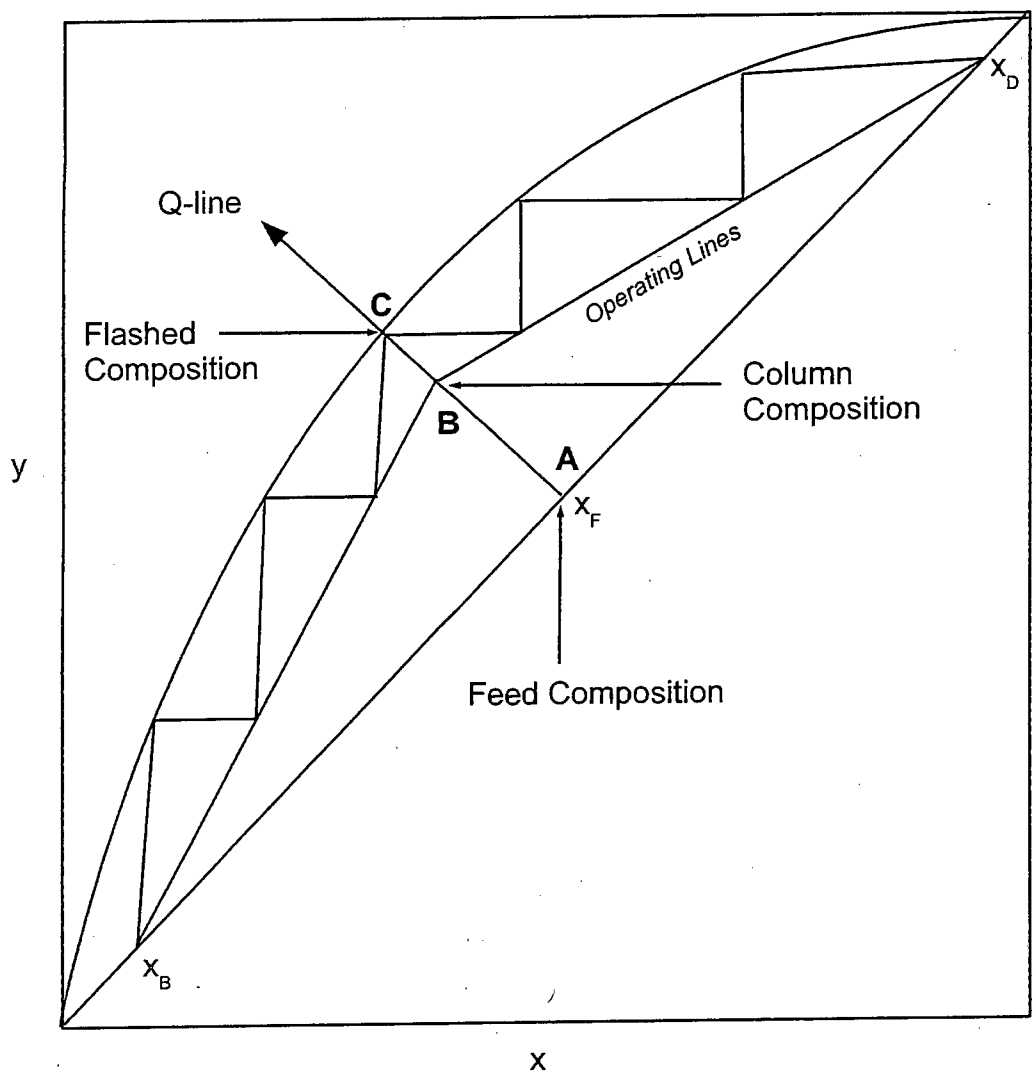

Figure 4.3: McCabe -Thiele diagram for a packed binary system indicating optimal feed placement and equivalent 'stages'

Chapter 5

Results and Discussion

The first three sections in this chapter present and discuss results for each of the individual models developed in Chapters 3 and 4. The final section uses Models 2 & 3 to generate *feasible regions* using *separation surface* plots.

5.1 Model 1: A Learning Curve

The primary objective of developing the first set of models (Models 1.A, 1.B & 1.C) was a two-fold learning exercise. The *first stage* was to establish a clear understanding of 'how rate-based distillation works'. This is easier when a simple model is considered. Part of this understanding was structured into a methodology for finding *and* classifying a pinch. A binary analysis is presented in Section 5.1.1, an extension to a multicomponent system is straightforward.

The *second stage* in the learning exercise was to confirm how effective collocation is with respect to a standard integrator i.e. LSODE. A useful extension of this goal was a comparison between the different types of collocation coding available. This involved experimenting with the two standard collocation codes i.e COLSYS and ABW routines. The results from all the comparisons are presented and discussed in Section 5.1.2.

After meeting the above objectives, it became apparent that there was something crucial missing from the above framework. The most standard distillation calculations of minimum flows and minimum height, had not yet been addressed. These calculations present a problem when considering how the degrees of freedom were previously defined in Chapter 4, Section 4.1. The problem is defined and resolved, and the results are shown and discussed in Section 5.1.3.

5.1.1 Finding a Solution: *Operating or Azeotropic Pinch?*

A pinch can be generally defined as a section of a distillation column where the composition (and consequently temperature) is constant. When designing a distillation column, pinches are a common occurrence. In order to eliminate them, it is important to know why they occur in the first place. For example, are they operational or azeotropic?

An operational pinch is more commonly due to minimum internal column flows, often a result of the introduction of a feed or side stream. According to the Underwood method [15], operational pinches are defined as class 2 separations and typically have wide boiling points. For a class 2 separation, one or more of the components appear in only one of the products. If neither the distillate nor bottoms product contains all feed components, two pinches occur away from the feed position. If a heavy component does not appear in the distillate then there is a pinch between the feed and rectifying section. The opposite is true for disappearance of a light component in the bottoms. Therefore, operational pinches are known to occur half-way up or down a column, when both stripping and rectifying sections are considered.

An azeotropic pinch is a result of the properties of the vapor-liquid equilibrium (VLE). Should the equilibrium line cross the $y = x$ line, an azeotrope is present in the VLE. This is easy to see in a binary system, but needs to be analytically checked in a multicomponent system due to the existence of multiple equilibrium lines. *Pinch identification* in general is easy to implement within multicomponent distillation code i.e. check for $x_k = y_k$ at points other than the total condenser. *Pinch classification* requires an analysis of the residual of $y_k - y_k^*$.

To structure the approach used in developing a general methodology for distillation column solution and pinch classification, Figure 5.1 was included. The diagram is representative of a binary azeotropic system and is closely modeled by Model 1.B. The following solution steps are suggested:

1. **Define the feed:** Although this may be obvious, the feed composition must be chosen such that it lies within the VLE. If this is not the case, absorption will result instead of distillation as shown in Figure 5.2. If the reflux ratio is increased, the separation factor increases. This is seen in Figure 5.2, where the higher reflux ratio corresponds to a longer operating line. The separation factor is the difference in composition between the column endpoints. In Model 1.B, the feed had a vapor fraction of 1 and known composition. The corresponding values of the liquid composition at that point (i.e. *leaving* the rectifier), must lie within the VLE somewhere on the line delimited by the points A and B as indicated in Figure 5.1.

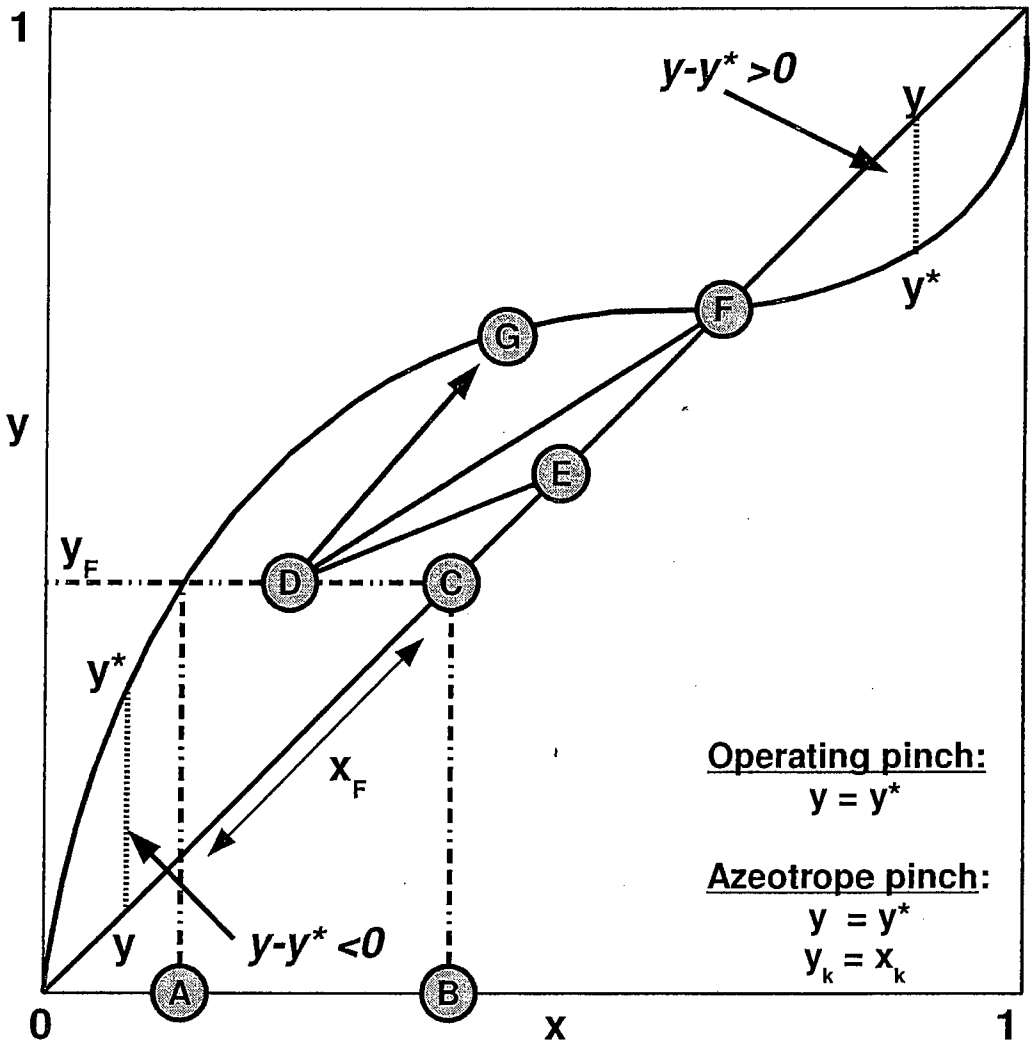

Figure 5.1: Solution development: Identifying and characterizing a pinch

2. **Define the direction of mass transfer correctly:** Mass transfer is usually defined as being from the vapor to the liquid phase i.e. $N = K_{og}a \cdot S \cdot (y - y^*)$. When using an ODE integrator, the direction of mass transfer is fixed as the sign of $(y - y^*)$ cannot change. At most, it will approach zero. However with a collocation approach, the DE is replaced with a set of AE's. Therefore the sign of $(y-y^*)$ can change resulting in *reverse distillation*[1].

   This is apparent if the rectifying profile is decreasing with increasing height. An example of reverse distillation is shown in Figure 5.3. It is almost always a consequence of an azeotrope. Boiling point temperature inversion results as the azeotrope has the lowest temperature. However, the temperature increases down the column, therefore the operating line moves downward. From Figure 5.1, reverse distillation occurs when the feed is located in the upper VLE i.e. beyond the point F.

   Reverse distillation can be controlled within a collocation code by forcing the flux of the component with an azeotrope to zero, if the azeotrope is crossed. This is preferable to interfering with the equilibrium values i.e. an alternative to forcing $N = 0$ would be to force $y - y^* = 0$. These are not equivalent as the latter changes the shape of the equilibrium curves, which results in unstable code. By forcing the flux term to zero, the equilibrium lines are still calculated, but mass transfer is assumed to stop at the azeotrope instead of reversing itself and changing sign.

3. **Gradually increase the reflux ratio:** Once a starting point has been correctly chosen, such as point D in Figure 5.1, the reflux ratio can be systematically increased. This increases the slope of the rectifying operating line. Point E represents normal distillation solution, whereas a further increase in the reflux ratio will result in point F, which is an azeotropic pinch point. If the reflux ratio is increased further in an attempt to by-pass the pinch, the collocation code will not converge as point G lies on the equilibrium line and subsequently can never be achieved.

4. **Check for operating pinch:** A check should be programmed into the code which notifies the user when a pinch occurs. A pinch could occur on either side of the operating line i.e. at the $y = x$ line or at the equilibrium line. Therefore there need to be two separate pinch checks. The first and more obvious would be $x_k = y_k$ at any point other than the total condenser or reboiler. The second check would be a notification to the user when the change in composition over a large section of packing[2] is $< 1\%$.

[1] Technically, reverse mass *transfer* occurs and this only becomes reverse *distillation* if the feed is defined such that it lies within the VLE i.e. a two-phase mixture. This was the case in this example.

[2] The section of packing should be large relative to the total height i.e. 10% of the total height

Table 5.1: Summary of the variables used in each figure representing alternative solutions to **Model 1.B** as part of a solution methodology development (presented in Section 5.1.1)

Solution	**Figure**	**Height** (cm)	**Reflux Ratio**	$K_{og}a \cdot S$ $\left(\frac{gmol.hr}{cm}\right)$	**Feed** y_{pentane}
Absorption	Figure (5.2)	200	0.9 1.9	-10	0.3
Reverse distillation	Figure (5.3)	200	1.9	10	0.7
Operating pinch	Figure (5.4)	1000	0.9	10	0.3
Azeotrope pinch	Figure (5.5)	200	2.9	10	0.3

Once a pinch has been found, it is by default an operating pinch unless it can be proved to be azeotropic. An azeotropic pinch can be confirmed by testing for coincidence of the operating and equilibrium lines i.e. $x_k = y_k$ **and** $y_k = y_k^*$? An example of an operating pinch *at the feed* is subsequently shown in Figure 5.4. This would have been found using the second check.

5. **Check for azeotropic pinch:** Finally the pinch may satisfy both conditions $x_k = y_k$ and $y_k = y_k^*$, in which case a azeotropic pinch results. This is shown in Figure 5.5. Note that for a multicomponent system, the above conditions must be true for all components in the system.

The data used to find the solutions in the above development, is listed in Table 5.1 along with the appropriate figure references. While the methodology is presented for a binary system, it can be applied to a multicomponent system using purely analytical techniques, as the graphical approach becomes confusing beyond three components.

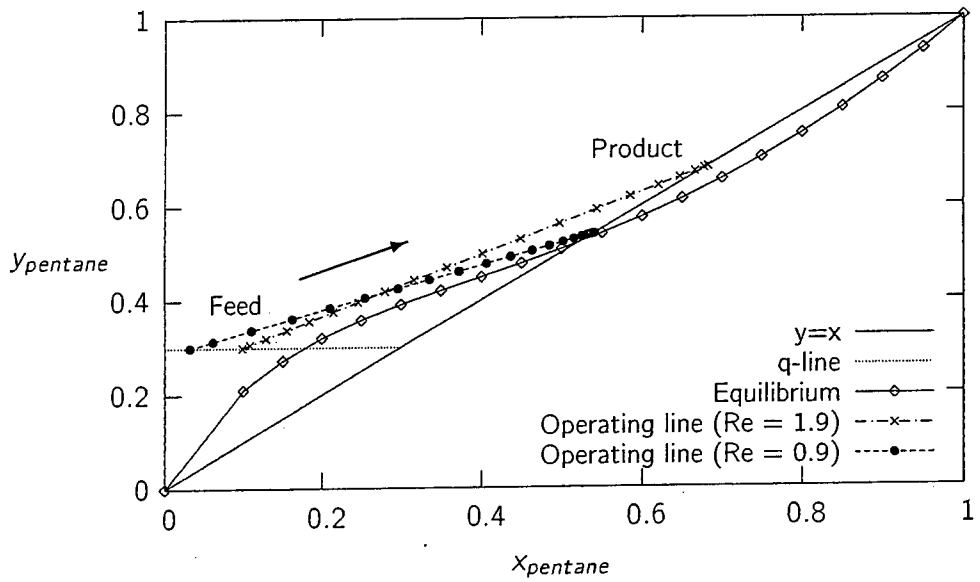

Figure 5.2: *Developing a pinch methodology:* Converging to an absorption solution and investigating the effect of a reflux ratio on the absorption solution for **Model 1.B**

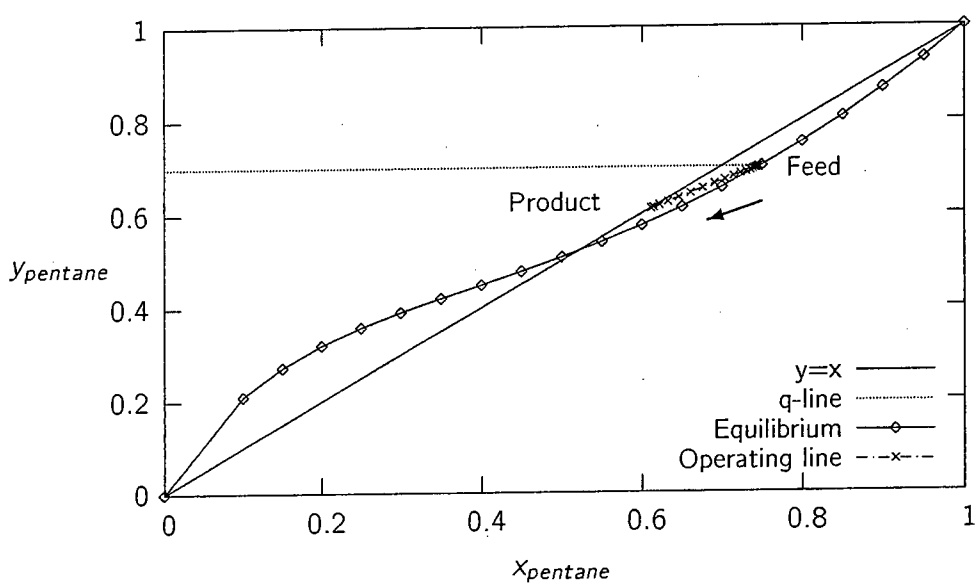

Figure 5.3: *Developing a pinch methodology:* Converging to a reverse distillation solution for **Model 1.B**

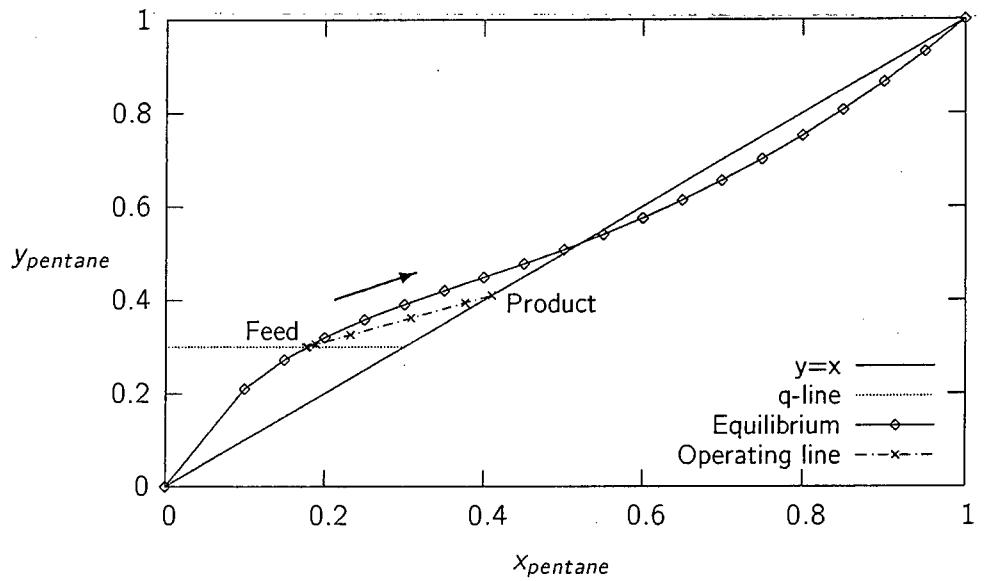

Figure 5.4: *Developing a pinch methodology:* Converging to an operating pinch at the feed for **Model 1.B**

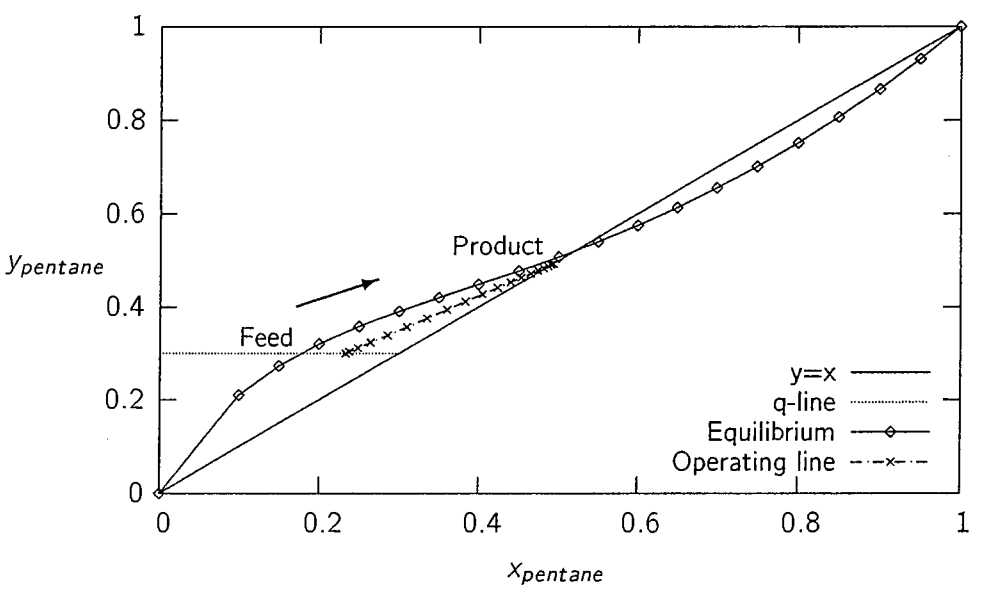

Figure 5.5: *Developing a pinch methodology:* Converging to an azeotropic pinch at the distillate for **Model 1.B**

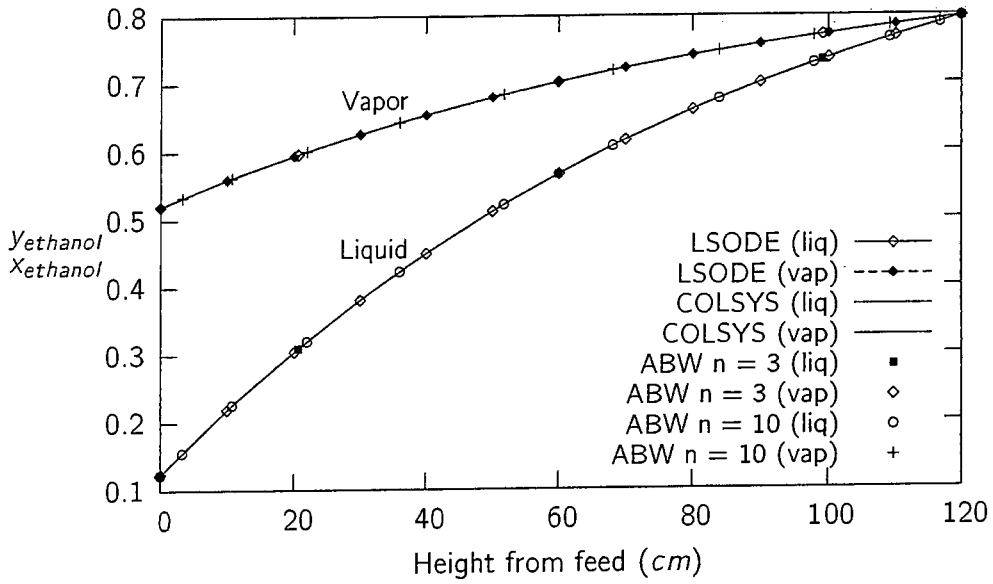

Figure 5.6: Comparing numerical routines: Liquid and vapor compositions for **Model 1.A**

5.1.2 Comparison Between Numerical Routines

Three numerical methods were used to solve each model as shown in Table C.1 on page 156. The two collocation methods were ABW routines and COLSYS. These were compared to each other as well as to the results obtained using the shooting method with LSODE. More specifics regarding these models and their differences are given in Appendix C on page 155. The most important point with regard to the LSODE method, is that an additional solver is required to find the split boundary values. A basic bisection shooting method was tested and found to be very unstable. It was replaced with an alternative shooting method using least squares optimization: LMDIF in MINPACK. All the subsequent results presented here refer to LSODE with the latter solver.

The accuracies of each method were compared by plotting the resulting profiles for each model with a uniform tolerance of 10^{-8}. These are shown in Figures 5.6, 5.7 and 5.8 for Models 1.A, B and C respectively. All profiles are in close agreement.

Model 1.A had a linear set of equilibrium relationships and differential equations. It also unintentionally had an azeotrope. Therefore, irrespective of the number of points used in the ABW routine, the results all lie on same line. This is shown in Figure 5.6. As an aside, these models are all of small experimental-scale columns with very low flowrates (as seen in Table 3.1). Hence the heights are small.

The azeotrope in Model 1.B is visible in Figure 5.7 as the composition profiles tend toward it.

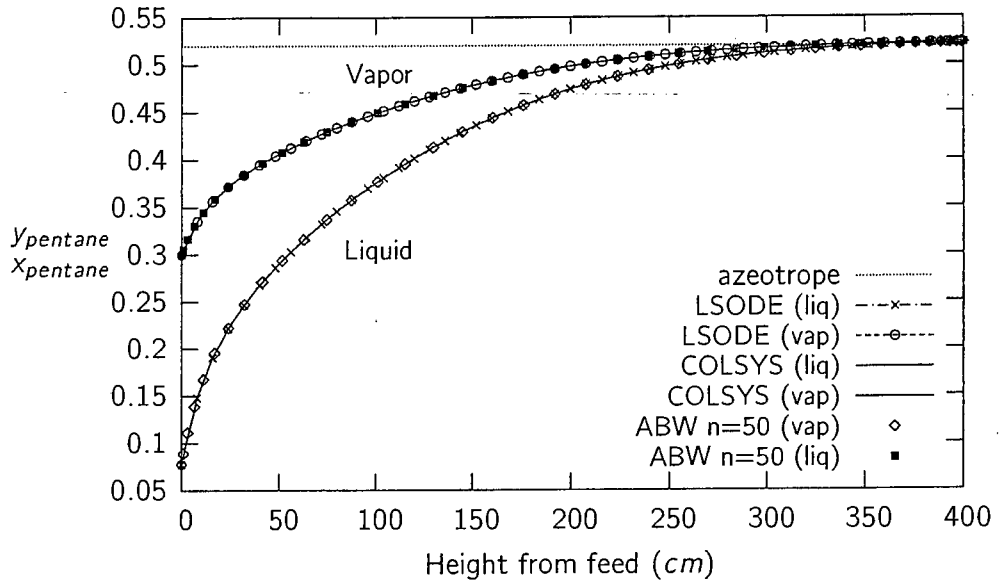

Figure 5.7: Comparing numerical routines: Liquid and vapor compositions for **Model 1.B**

An excessive number of collocation points were used in the ABW routines. The purpose was to test for instability, which is sometimes thought to be present when too many collocation points are used. If this was the case, oscillations would have occurred. Because this did not happen, the resulting collocation model of this system is stable. Finally for Model 1.C, only one of the four component profiles are shown in Figure 5.8, although all had comparable accuracy. In conclusion, all numerical methods produced exact answers, validating the further use of ABW routines.

5.1.3 Minimum Flows and Height

In the literature review, an analysis of the degrees of freedom in a distillation system was given (see Chapter 2, Section 2.2.2). Using this information, a standard approach for defining the degrees of freedom in all the models in this work was outlined in Chapter 4, Section 4.1. In brief, the internal flows, height and feed position and condition were defined. Consequently, the product specifications were not fixed i.e. the code solved for them, but they varied for each system. This was the procedure followed in the first part of this chapter, and will be consistently followed throughout the remainder. This is the best way to solve distillation problems.

The problem should now be apparent. When considering the minimum height, it is defined in terms of a fixed separation i.e. what is the shortest column which can still achieve a certain distillate purity? The same is true for defining minimum flows. Therefore to *directly* calculate either the minimum flows or height, the degrees of freedom will have to be re-worked.

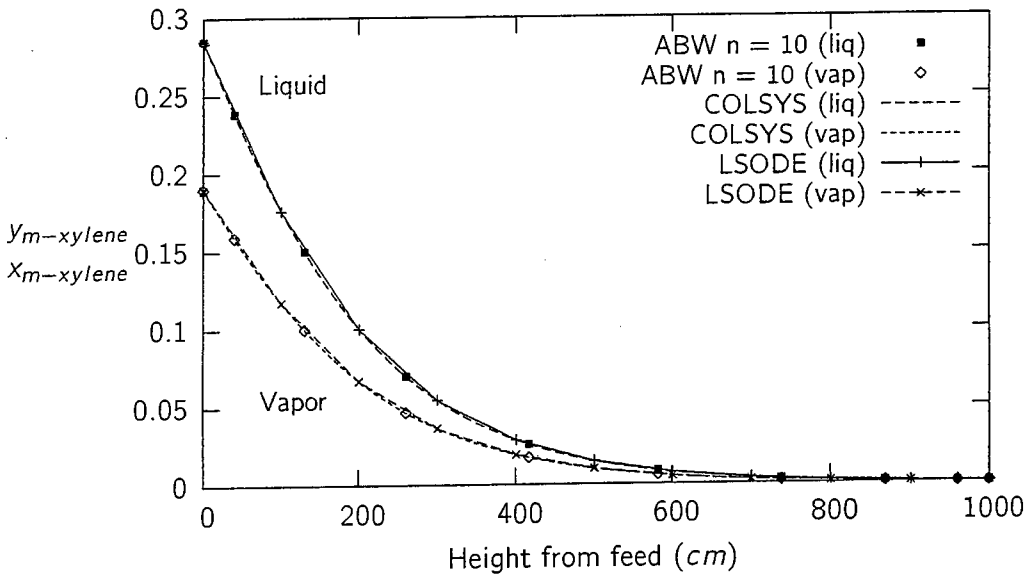

Figure 5.8: Comparing numerical routines: Liquid and vapor compositions for m-xylene for **Model 1.C**

This is the appropriate place to point out that the choice of degrees of freedom made in Chapter 4, Section 4.1 was not incorrect. It simply implies that if the choice of degrees of freedom are not changed, the minimum flows and height cannot be calculated directly. However because they are intrinsic system parameters, they will still be found on the surface of a hyperplane (i.e. 4 dimensions), consisting of all the specifications.

To elaborate, in order to achieve the thesis objective, namely to create a robust and accurate low order model which can be used in an optimization routine, the separation feasibility must be calculated. This calculation will be quick because of the low order collocation model. The separation feasibility will be presented in the form of a surface plot where the separation feasibility (i.e. product purity) will be plotted against all possible combinations of the 4 specified degrees of freedom i.e x_D versus Re and Rb, or x_D versus Re and $Height$ etc.

Hopefully the direction of the argument is becoming apparent, as if the separation feasibility (x_D) is plotted against $Height$ and Re, a horizontal plane intersecting the separation feasibility axis at the required product purity (i.e $x_D < 0.01$) can be defined. The lowest value of Re for which the surface intersects this plane (at a sufficiently large height), is subsequently the minimum reflux for that specific product purity.

To conclude this argument, there will always be a minimum height or minimum column flows for a feasible product specification. Depending on how the degrees of freedom are defined, these minimums can either be directly or indirectly found. In this case, indirectly. From the perspective of determining minimum flows and height, this could seem like the more inefficient choice for degrees of freedom specification. However, one of the criterion for choosing the degrees of freedom was the ease of model convergence. From personal experience[3], when designing a column using an industrial package, the combination of *Re*, *Rb* and *Height* are usually the most successful specifications for convergence i.e. an initial value problem not a split BVP.

For Models 2 & 3, the surface plots as mentioned above, will be used to illustrate the separation feasibility and indirectly determine the minimum flows and height. The models discussed in this section are very basic and do not merit such a detailed analysis. Therefore, the minimum flows and height have been calculated *directly* by specifying an arbitrary product purity (at the azeotrope if there is one), and allowing *Re* (or *Height*) to 'float' until the specification is just met. This is undertaken at either an infinite *Height* or *Re*, depending on which minimum is being determined. 'Infinity' is a much used over-exaggeration in the literature, usually a factor of 10 times N^{min} or R^{min} has been used in this work. Even smaller ratios are quoted in the standard reference text [15].

Therefore contrary to the above argument, the degrees of freedom were temporarily re-worked for illustrative purposes only. Previously, the free or 'floating' variable was the product specification. This has been replaced by either *Re* or *Height* as shown in Table 5.2.

Table 5.2 lists the minimum height and flows calculations used for each model. The results are also presented in a graphical form. The key graphical feature defining a minimum height is the coincidence of the operating line with the $y = x$ line. Similarly for minimum flows, the operating lines must pinch with the q-line at the equilibrium curve. The usefulness of pseudo McCabe -Thiele diagrams, as shown in Figures 5.13 and 5.14, is apparent. The graphical technique which is indispensable in binary systems, can be successfully translated into a multicomponent system by normalizing the axes with respect to the light and heavy keys.

Hopefully the importance of a product specification is now clear with regards to determining minimum heights and flows. From any of the graphs, this has the effect of tying down the upper end-points of the operating lines. The lower end-point is constrained by the feed condition; this applies as only a rectifying section was modeled. If these ends were not tied down, as the reflux ratio or height was systematically decreased, the length of the operating line would also shrink, thereby defeating the purpose of the analysis.

[3] admittedly limited

Table 5.2: Minimum flows and height for **Model 1**(Note: Degrees of freedom have changed)

Parameter	**Model 1A**	**Model 1B**	**Model 1C**
Minimum Flows Calculation			
Reflux Ratio	0.8	1.9	1.2
Height (cm)	1000	1000	3000
Product Specification	$x_{ethanol,D} = 0.78$	$x_{pentane,D} = 0.52$	$x_{m-xylene,D} < 10^{-4}$
$K_{og}a \cdot S$ $(\frac{gmol.hr}{cm})$	10	10	1
Figure	Figure 5.10	Figure 5.12	Figure 5.14
Free Variable	Reflux ratio		
Minimum Height Calculation			
Reflux ratio	20	20	20
Height (cm)	50	150	280
Product specification	$x_{ethanol,D} = 0.78$	$x_{pentane,D} = 0.52$	$x_{m-xylene,D} < 10^{-4}$
$K_{og}a \cdot S$ $(\frac{gmol.hr}{cm})$	10	10	1
Figure	Figure 5.9	Figure 5.11	Figure 5.13
Free Variable	Packed height		

In other words once the reflux ratio is sufficiently large, the height must be reduced to a its minimum value. However, this 'minimum' has little meaning unless a product specification is given. For example, the height could be reduced such that $x_D = 0.95$. The height could be further decreased, resulting a further reduction in x_D, as the rectifying operating line shrinks. If this procedure is adopted, the code will find the minimum height where convergence is just possible, and this will correspond to a very small separation as a result of the shrinking operating line. Therefore the concept of minimum height (and flows) is void unless it is used in reference to a fixed product purity i.e. a fixed operating line length.

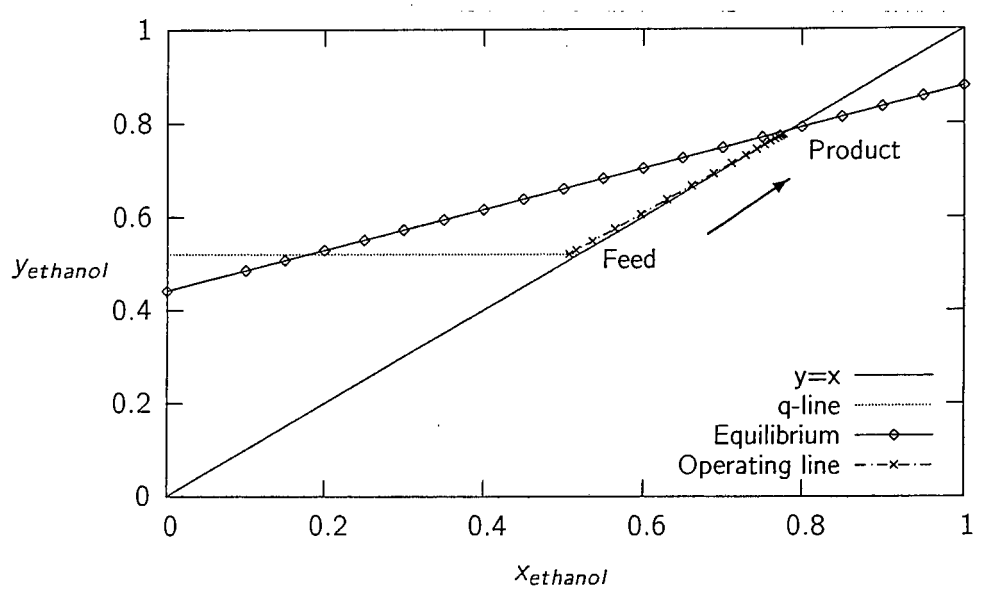

Figure 5.9: Finding the minimum height for **Model 1.A**

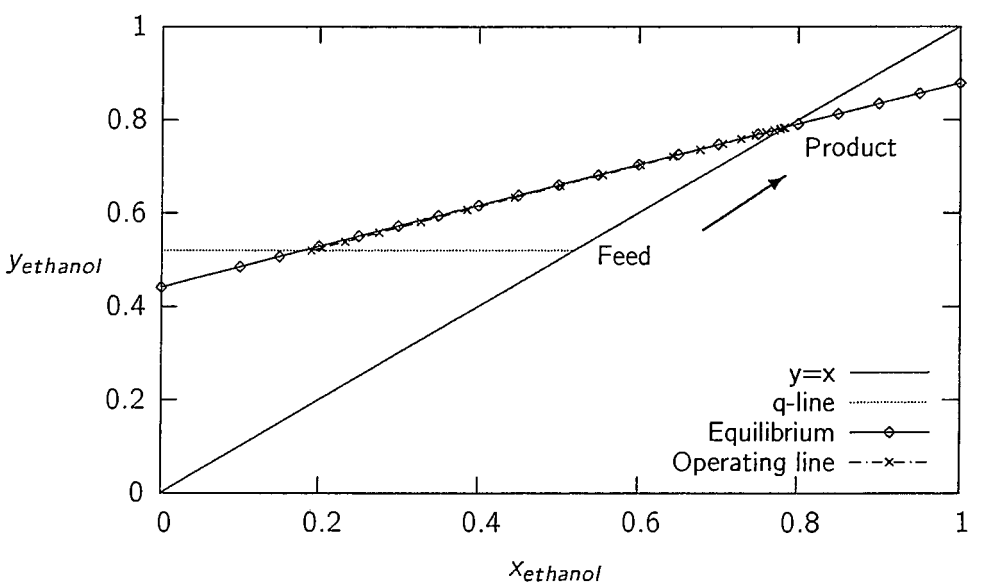

Figure 5.10: Finding the minimum flows for **Model 1.A**

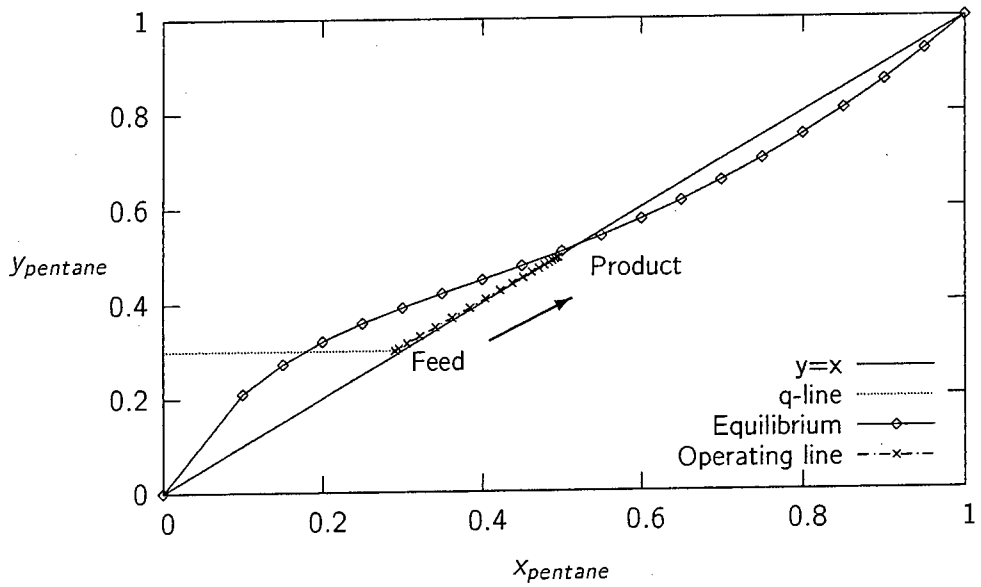

Figure 5.11: Finding the minimum height for **Model 1.B**

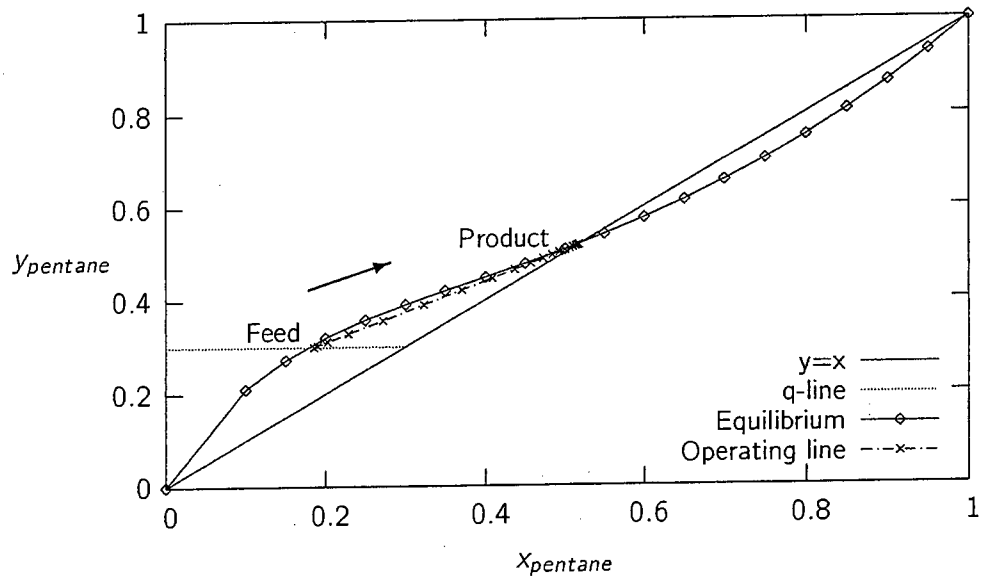

Figure 5.12: Finding the minimum flows for **Model 1.B**

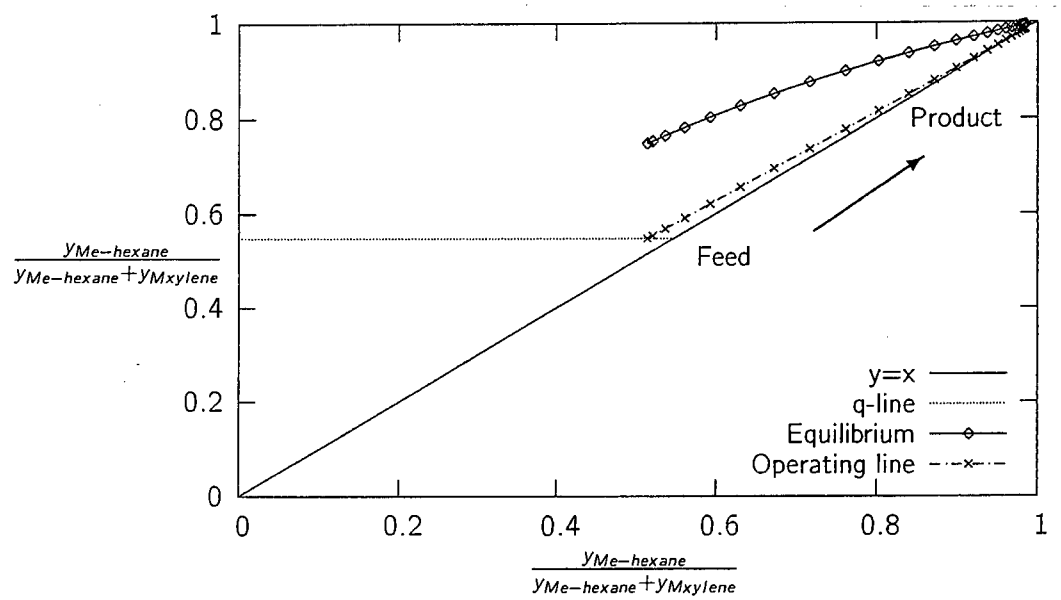

Figure 5.13: Finding the minimum height for **Model 1.C**

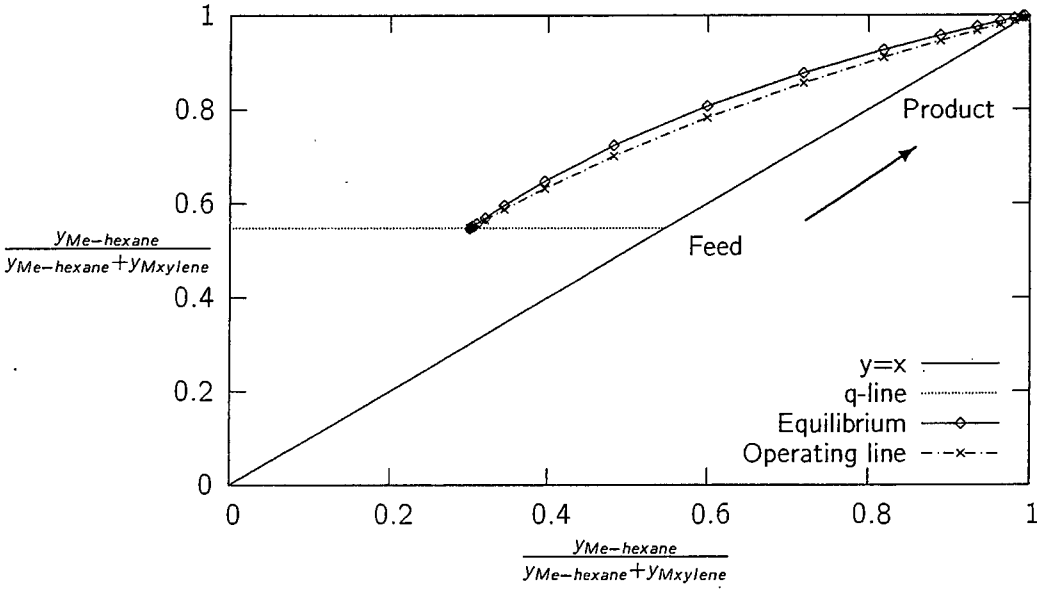

Figure 5.14: Finding the minimum flows for **Model 1.C**

5.2 Model 2: Increasing the Complexity

Model 2 has an increased level of complexity, namely an energy balance. As explained in Chapter 3, the energy balance increases the number of variables requiring solution. In Model 1 there were $2C$ variables per collocation point. Model 2 has $3C + 3$ variables per collocation point, where C is the total number of components. The four available degrees of freedom however remain the same. To recap Section 4.1, they are the **reflux** and **reboil** ratios, the column **height** and the **feed position**. The feed composition and quality is assumed to be constant, as shown in Table 3.3 on page 66.

A solution to the model has been presented in Section 5.2.1 with the relevant profiles. Because of the increased level of complexity in Model 2, initially finding a feasible solution from which to work is non-trivial. The resulting solution is important for two reasons. Firstly, the same resulting values for the degrees of freedom will be inputted in Model 3. This allows for a comparison between the models, which in turn will be useful when investigating the separation feasibility. Secondly, it will provide an initial feasible starting point in the solution space. Subsequent iteration will generate the separation surfaces in Section 5.4.

As done previously for Model 1, a discussion on minimum flows and height is included in Section 5.2.2. This includes an analysis of the degrees of freedom. Collocation accuracy is briefly reported in Section 5.2.3.

5.2.1 Finding a Starting Point Solution

To start generating the necessary data for optimization of the separation sequence, an initial feasible solution is required. The initial guesses required to find this solution, used previous results. This was done for the majority of the profiles. Besides providing a starting point for further iterations, this solution is useful for gaining understanding of the specific physical system. The degrees of freedom and their associated values used to find the solution presented in the following figures, are included in Table 5.3. Table 5.4 presents a summary of the different figures used to draw attention to certain aspects of the model solution.

5.2.1.1 Ternary Diagrams

For a ternary system, there are three possible variations of ternary diagrams. These are presented in Figures D.1, 5.15 and D.2, where the overall mass balance is shown as a straight line intersecting the end-points of the rectifying and stripping profiles. The overall mass balance represents the composition at the distillate, feed and bottom streams of the column.

Table 5.3: Degrees of freedom and their assigned values for **Model 2**:
Finding a feasible solution: (Section 5.2.1)

Degree of Freedom	**Value**
Reflux Ratio	1
Reboil Ratio	2.4
Feed Position	50% of the Column Height
Total Packed Height (m)	10
Experimental Parameter	**Value**
$K_{og}a \cdot S \left(\frac{kmol.min}{m}\right)$	180 (Model 2)
$a_p \left(\frac{m^2}{m^3}\right)$	300 (Model 3)

Table 5.4: Summary of the purpose, type and location of figures used in **Model 2**:
Finding a feasible solution: (Section 5.2.1)

Purpose	**Type of Plot**	**Figure**
Use of an alternative graphical technique for gaining a different perspective compared to that of a pseudo McCabe - Thiele diagram	Liquid Phase Ternary Diagram: *Methanol & Ethanol*	Fig D.1
	Liquid Phase Ternary Diagram: *Water & Methanol*	Fig 5.15
	Liquid Phase Ternary Diagram: *Water & Ethanol*	Fig D.2
Familiar binary system graphical technique which has been modified for multicomponent systems	Pseudo McCabe-Thiele Diagram: *Methanol & Water*	Fig 5.16
	Pseudo McCabe-Thiele Diagram: *Ethanol & Water*	Fig 5.17
Demonstrate the variation in flows with height as a result of the energy balance	Internal Flow Profiles: *Vapor and Liquid*	Fig 5.18
Useful for identifying a pinch	Temperature Profile: *Liquid*	Fig 5.19
Interesting to compare normal profiles with ternary and pseudo McCabe - Thiele diagrams	Liquid Composition Profiles	Fig 5.20
	Vapor Composition Profiles	Fig D.3
Classification of pinches found in above graphs	Equilibrium Profiles: *Vapor*	Fig 5.21

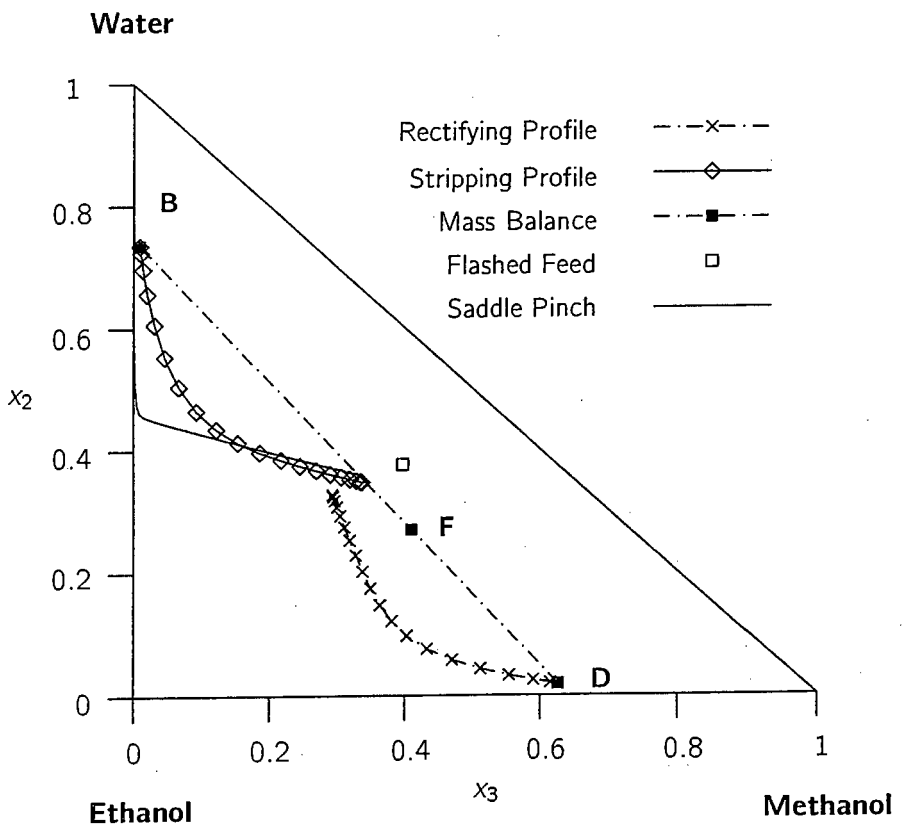

Figure 5.15: Liquid phase ternary plot of Water versus Methanol for **Model 2**: *Finding a feasible solution:* (Section 5.2.1)

The order is subsequently always point D, followed by point F and finally point B. If this line is not straight, the mass balance (and therefore the model), has not converged correctly. An additional point has been included in these diagrams, which represents the composition of the flashed feed.

The standard methodology when using ternary diagrams requires that a distillate and bottoms composition be specified such that the overall mass balance is satisfied. The mole fractions on successive stages above the bottoms stream and below the distillate are computed. Because the product compositions are specified at both ends, this is referred to as a *boundary value design procedure*. The feed location is found from the intersection of the two profiles and is a dependent variable. The number of stages required such that the profiles intersect, is found by adding the stages in each column section [9].

The mathematical structure of the collocation models is a *split boundary value problem.* The user inputs a reflux and reboil ratio, feed position and height. The code solves the system of equations which are constrained at the column endpoints by the reboiler and condenser boundary conditions, as shown in Table 4.2 on page 81. However from a degrees of freedom perspective, the system is being solved as an initial boundary problem as the feed and height is specified. This is the same as supplying the start point and the length of integration. Therefore there is a subtle difference between the *mathematical structure* (split boundary value problem), and the *degrees of freedom or physical structure* (initial value problem). With regards to ternary diagrams, the standard approach as discussed previously calculates inwards from the endpoint compositions toward the feed. This is opposite to that of Models 2 & 3, which move from the feed outwards.

In standard distillation texts [9], the rectifying and stripping profiles intersect. However there is a distinct discontinuity at the feed in all the figures shown in Table 5.4. This is expected due to the use of two separate collocation sections below and above the feed, and the resulting manner in which they were connected as described in Chapter 4, Section 4.2. To summarize, the feed vapor content was added to the rectifying vapor stream and the feed liquid content was added to the stripping liquid stream. This was done assuming adiabatic conditions, and can be regarded as a discrete mixing stage with no height or separation.

Therefore if the composition of the stripping operating line below the feed tray, is combined with the feed concentration, the starting point for the rectifying operating line is defined. The discontinuities are an intrinsic part of these models and will be evident throughout all the results. As discussed in Chapter 2, Section 2.10.1, there are several documented attempts to smooth out these discontinuities using a variety of interpolation routines [28, 19, 8]. However, this is not necessarily the correct approach as the feed discontinuity is a *physical feature* of the system.

The flashed feed composition has been included in the ternary diagrams for illustrative purposes. The end points of the stripping and rectifying operating lines, as well as the flashed feed composition, *must be collinear*. Although not drawn in, this can be clearly seen in all the ternary diagrams. This collinearity is a necessary condition as a result of the adiabatic mixing feed stage boundary condition.

Ternary diagrams are useful for identifying system pinches as detailed in Chapter 2, Section 2.3.4. In Figure D.2, it is conceivable that methanol may approach a saddle pinch at the lower end of the column. If the separation was pushed further by increasing the height or reflux and reboil ratios, the stripping operating line as represented in Figure D.2, would coincide with the $y = x$ line. Using the rectifying profile, methanol appears to be approaching a pinch shortly above the feed, as future parallelism is likely with the $y = x$ line. If this observation is shown to be correct and a pinch does develop with an increase in column height, the resulting pinch is most likely operational. The operational pinch would be a consequence of the introduction of the feed.

From Figure 5.15, there is a possibility of a water saddle pinch developing in the stripping section. This will become more prominent if the separation is increased. For example, the height was doubled while retaining the remaining input parameters in Table 5.4. The resulting stripping section profile is plotted in Figure 5.15 as line without points. A saddle pinch is clearly evident as predicted. The overall mass balance is represented by the line joining the bottoms, feed and distillate composition points as indicated in the ternary diagrams. This line will pivot around the feed composition as represented by point F, for different solutions to the distillation problem i.e. alternate degrees of freedom. A type of distillation boundary is subsequently conceivable.

To summarize, the system is not currently pinching. However, it is anticipated that future pinches will become apparent if the separation factor is increased. While ternary diagrams may identify the pinch, they cannot categorize them. The node pinches may be operational, azeotropic or both. Using the analysis presented in Section 5.1.1, the pinches will be investigated further in a later part of this section.

5.2.1.2 Pseudo McCabe-Thiele Diagrams

While there a several possible combinations for pseudo McCabe - Thiele diagrams, only two have been included here. The first is the light key methanol normalized with respect to the heavy key water, and is shown in Figure 5.16. It is from this diagram that the optimal feed position can be inferred. The second pseudo McCabe-Thiele diagram uses the intermediate key ethanol normalized with respect to water. This diagram has been included in Figure 5.17, as the operating lines are strongly curved. Although this is known to occur when using pseudo McCabe-Thiele diagrams (see Section 2.3.1), it is nonetheless interesting to see in practice. The reason is for this behavior is that the intermediate key ethanol has been represented. Ethanol consequently switches mass transfer direction throughout the column i .e. stripping versus absorption. The oscillatory behavior counter-balances the uniform increase or decrease of the key components through the column. In both diagrams the q-lines have been normalized according to the axes used. As with the ternary diagrams, there is an obvious and expected feed discontinuity.

The position of the q-line is fixed as the feed composition and quality is both known and assumed to be invariant[4]. The optimal feed location is subsequently found by positioning the operating lines such that the stepping over the rectifying line onto the stripping line happens as close to the q-line as is possible. The operating lines should not extend excessively beyond the feed position for optimal feed placement. If this happens, the solution continues to be found from stepping off the rectifying operating line *below the feed tray*, or vice versa for the stripping operating line, unless there is a feed pinch.

The correct feed position has subsequently been identified. While this is immediately obvious in Figure 5.16, it is not as clear in Figure 5.17. This is expected as the optimal feed position can only be inferred from the pseudo McCabe-Thiele diagram which uses the light key i.e. Figure 5.16. The separation is almost perfect as the operating lines extend into the corners of the VLE diagram. In Figure 5.17 there is a larger feed discontinuity and a strongly curved stripping operating line.

In Figures 5.16 and 5.17, the upper and lower end-points of the operating profiles intersect with the $y = x$ line. This is expected due to the total condenser and reboiler. These endpoints correspond to the node pinches identified in the ternary diagrams.

As with the ternary diagrams, the pseudo McCabe - Thiele analysis cannot definitively categorize the pinches. To do so, the relationship between the interface and bulk vapor composition must be analyzed in conjunction with the liquid and vapor composition profiles i.e. $x = y$ and $y = y^*$?

[4]It can easily be changed, but to simplify matters it was assumed fixed throughout.

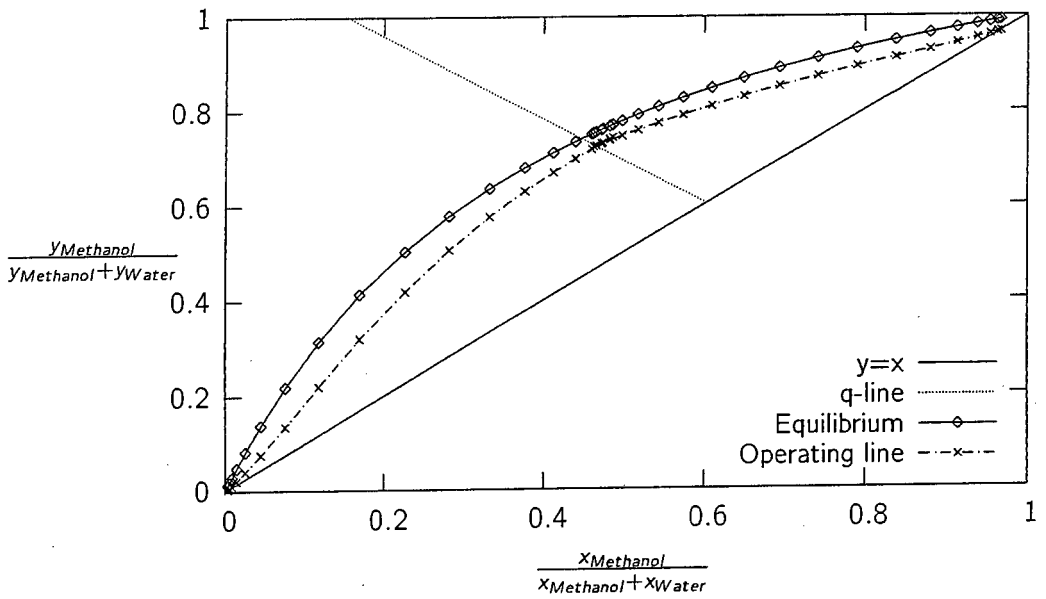

Figure 5.16: Pseudo McCabe-Thiele plot of Methanol with respect to Water for **Model 2**: *Finding a feasible solution:* (Section 5.2.1)

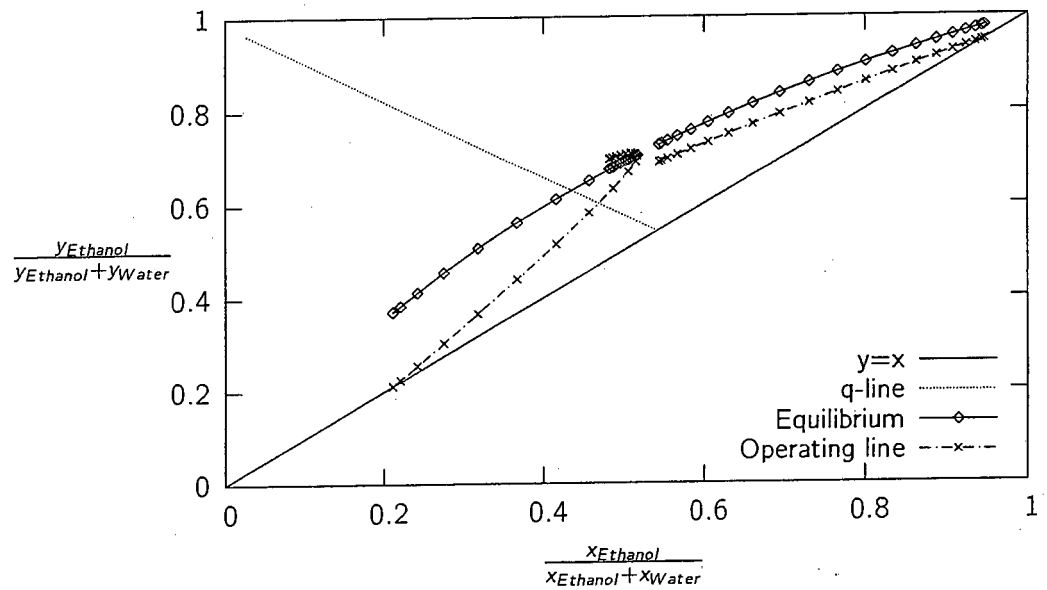

Figure 5.17: Pseudo McCabe-Thiele plot of Ethanol with respect to Water for **Model 2**: *Finding a feasible solution:* (Section 5.2.1)

5.2.1.3 General Profiles

Before the above analysis was performed, the internal flow and temperature profiles were included in Figures 5.18 and 5.19 respectively. As anticipated, the vapor and liquid flows change through the column as a consequence of the energy balance. The rectifying section is of interest as between the height of 10m and 8m, both the liquid and vapor flows decrease with a decrease in height. This loss of mass down the column is counter-intuitive, but nonetheless expected. Mass transfer was defined from the vapor to the liquid phase. This increases the liquid flow rate and decreases the vapor flow rate. But because of the counter-current flow, liquid moves down the column as the vapor moves upward. Therefore this also decreases the liquid flow, resulting in an overall loss of mass.

Because of the manner in which the feed tray was integrated into the column (i.e. an adiabatic mixing stage), it is important to place the feed such that the feed temperature is as close as possible to the column temperature. The feed temperature has been shown as a solid point in Figure 5.19.

From Figure 5.19, there is a discrepancy between the feed temperature and the temperature profiles. The feed position is optimal with respect to the pseudo McCabe-Thiele diagram for the key components as shown in Figure 5.16. Alternatively, the internal flows can be changed[5] such that the temperature discrepancy is minimized as shown in Figure D.4. However the corresponding pseudo McCabe-Thiele diagram in Figure D.5, indicates subsequent non-optimal feed location. This is an interesting result, as according to the second law of Thermodynamics[6], the smallest column should result when there is the greatest similarity between the column and feed temperature at the feed position. However it should be emphasized that the internal flows were used to change the temperature i.e. the physical position was fixed at 50 % of the height. Trying to match the temperatures by only adjusting the feed location was not possible. This might explain the contradictory result.

While the compositions have been displayed using ternary and pseudo McCabe-Thiele diagrams, the simpler representation of composition as a function of height, was included for liquid and vapor phases (Figures 5.20 and D.3 respectively). The feed discontinuity is obvious. The feed composition has been included in these figures as a solid point. If this composition value is added to the end point composition value of one of the profiles above or below the feed, the starting point composition value of the remaining profile is found. The equilibrium y^* values were included in Figure 5.21.

[5]The reflux ratio was doubled; the remaining values were the same as in Table 5.3

[6]The rate of internal generation of entropy within a system is always > 0

The ethanol composition profile is of interest. Reverse mass transfer is apparent as the equilibrium values cross over with the bulk values several times down the column, thereby changing the direction of the flux. For example at the top of the column $y_{etoh} > y^*_{etoh}$, indicating stripping. This switches to absorption, back to stripping and again to absorption at the bottom of the column. The reverse mass transfer does not indicate an azeotrope as $x_k \neq y_k$ for $k = 1...C$.

In Figure 5.21, the methanol bulk and equilibrium values are very close in value. This appears to indicate a pinch. However if this was true, there would be no change in the methanol profiles. As can be seen from both Figures 5.21 and 5.20, this is not the case. Firstly, the equilibrium and bulk values are not exact. They differ in the second decimal place. More importantly, the temperature is still changing in that column section. The variation in temperature affects the equilibrium values. Therefore, all equilibrium values are changing throughout the column. The changing methanol composition drags the methanol bulk composition values with them.

To summarize, the apparent methanol pinch Figure 5.21 is contradictory as the methanol composition profile are still changing. This is attributed to the effect of the changing temperature on the equilibrium values. While the equilibrium and bulk values are close, the overall effect is a steady adjustment of both in the direction of the temperature change.

It might be helpful to point out that these types of diagrams are often misleading. Because the equilibrium and bulk values of methanol are close, the flux of that species is zero. Therefore the flow rate of methanol is constant. However, because the rate of mass transfer between the remaining species is non-zero, the flow rates of ethanol and water in each phase, are still changing. Therefore the composition changes, as seen in Figure 5.21. To reiterate, the flow rate of methanol is constant, yet the composition in the stream is changing due to variations in the ethanol and water flow rates, which are have non-zero fluxes. This type of behavior should be further investigated by including more sophisticated mass transfer effects i.e. interaction coefficients in Maxwell-Stefan mass transfer.

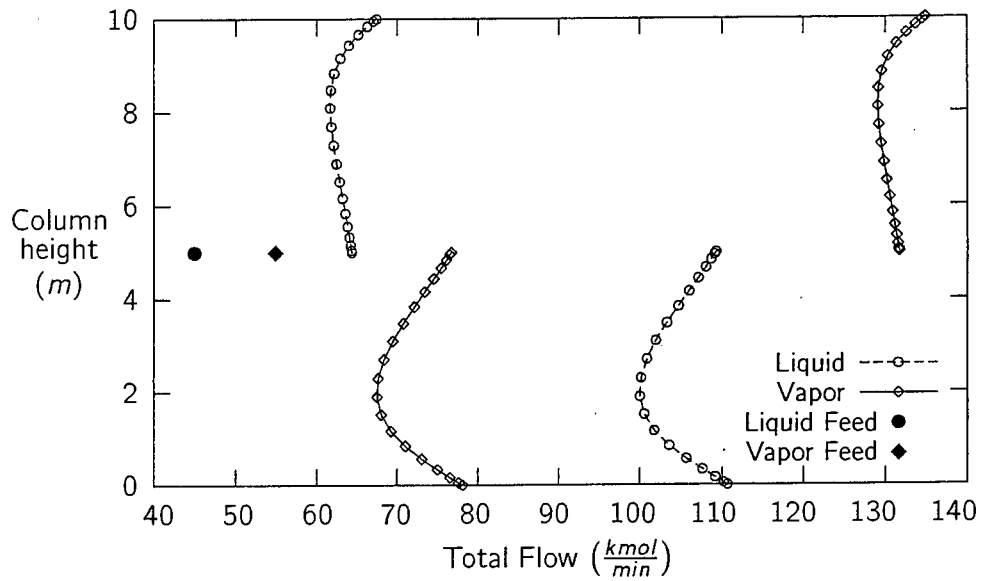

Figure 5.18: Liquid and vapor flows in column for **Model 2**:
Finding a feasible solution: (Section 5.2.1)

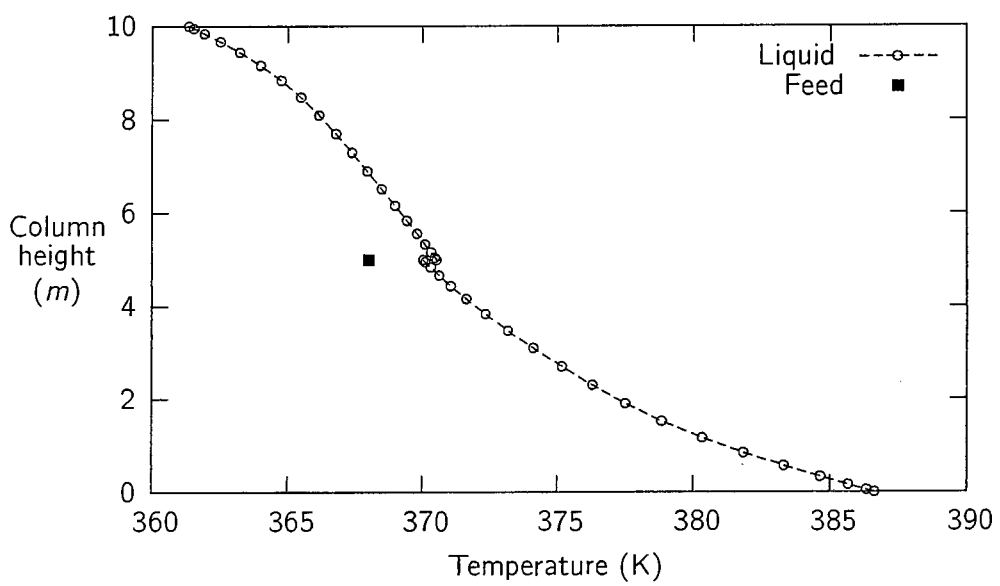

Figure 5.19: Vapor and Liquid Temperature plot for **Model 2**:
Finding a feasible solution: (Section 5.2.1)

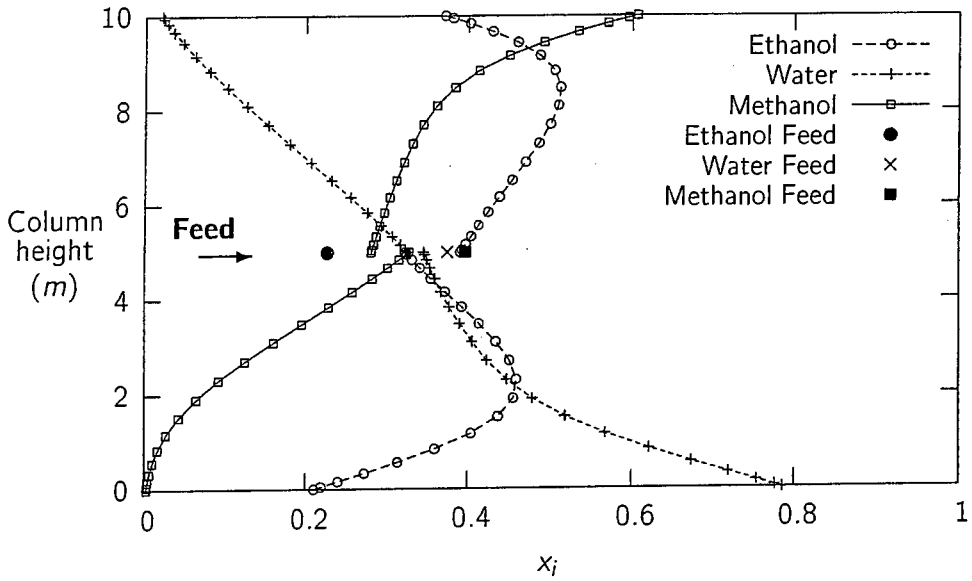

Figure 5.20: Liquid composition profiles for **Model 2**:
Finding a feasible solution: (Section 5.2.1)

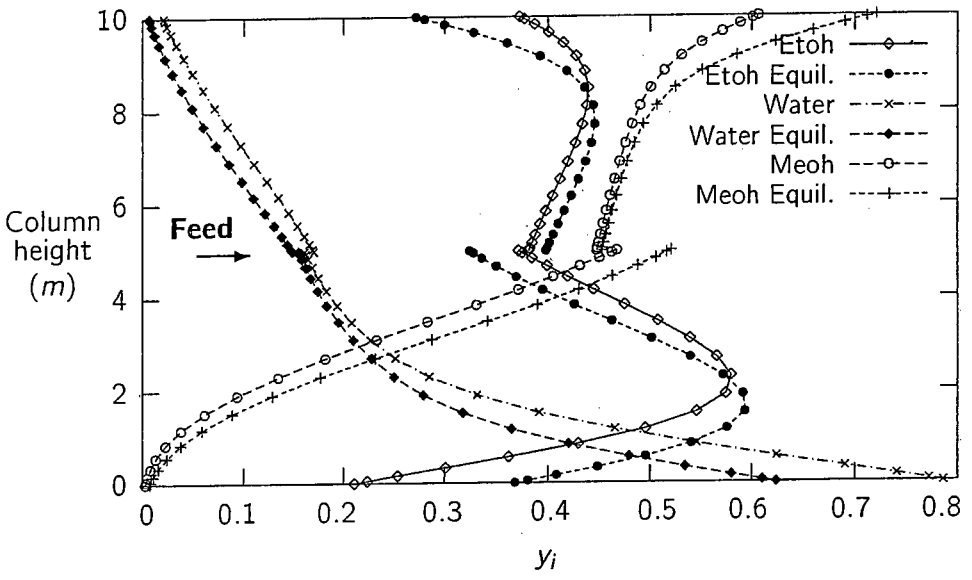

Figure 5.21: Equilibrium and Operating y_i profiles showing an azeotrope for **Model 2**:
Finding a feasible solution: (Section 5.2.1)

5.2.2 Discussing Minimum Flows and Heights

The issues regarding the degrees of freedom have been extensively discussed both in Chapter 4, Section 4.1 and in Section 5.1.3. To find the minimum flows and height a re-definition of the degrees of freedom is necessary. Previously the internal flows and section heights were specified. Now, a product specification is required instead.

While it is possible to constrain both extremes of the rectifying and stripping operating lines, only the lower end-point of the stripping operating line was fixed. The reason for this was to keep the changes in the code to a minimum, while still demonstrating the principle. In this case, the bottoms composition of methanol was specified as being $x_{methanol,B} \leqslant 0.05$. Therefore the only true minimum flow is Rb^{min}, at a bottoms composition of $x_{methanol,B} \leqslant 0.05$. The resulting Re^{min} is dependent on the composition of $x_{methanol,B} \leqslant 0.05$ as well as the feed location. This is due to the distillate composition being unspecified i.e 'floats'. All the specifications and degrees of freedom are shown in Table 5.5.

The minimum flows are shown in Figure 5.22. The stripping and rectifying operating lines and the q-line pinch at the equilibrium line. The solution for the minimum height is shown in Figure 5.23. The stripping profile tends to the $y = x$ line as expected. A complete coincidence of these lines does not occur as the reflux and reboil ratios are not at infinity. All results and specifications for the degrees of freedom are shown in Table 5.5.

Although in both sets of results the feed position is optimal, the *feed position is irrelevant at both minimum flows and height*. Under minimum height conditions, the separation envelope has completely opened up and the coincidence of the operating lines with the $y = x$ lines negates any influence of feed position. At minimum flows, the pinch at the q-line renders the feed position irrelevant, as the pinch composition is constant across the feed tray and q-line.

Table 5.5: Minimum flows and height for **Model 2** (Note: Degrees of freedom have changed)

Calculation	**Model 2**
Minimum Flows Calculation	
Reflux Ratio	0.5 (R^{min} at Feed location of 50% and $x_{methanol,B} = 0.05$)
Reboil Ratio	1.4 (R^{min} at $x_{methanol,B} = 0.05$)
Height (m)	23
Feed location	50% of the Column Height
Product Specification	$x_{methanol,B} = 0.05$
Figure	Figure 5.22
Free Variable	Reflux ratio
Minimum Height Calculation	
Reflux Ratio	5
Reboil Ratio	15
Height (m)	7.5
Feed location	65% of the Column Height
Product specification	$x_{methanol,B} = 0.05$
Figure	Figure 5.23
Free Variable	Packed height

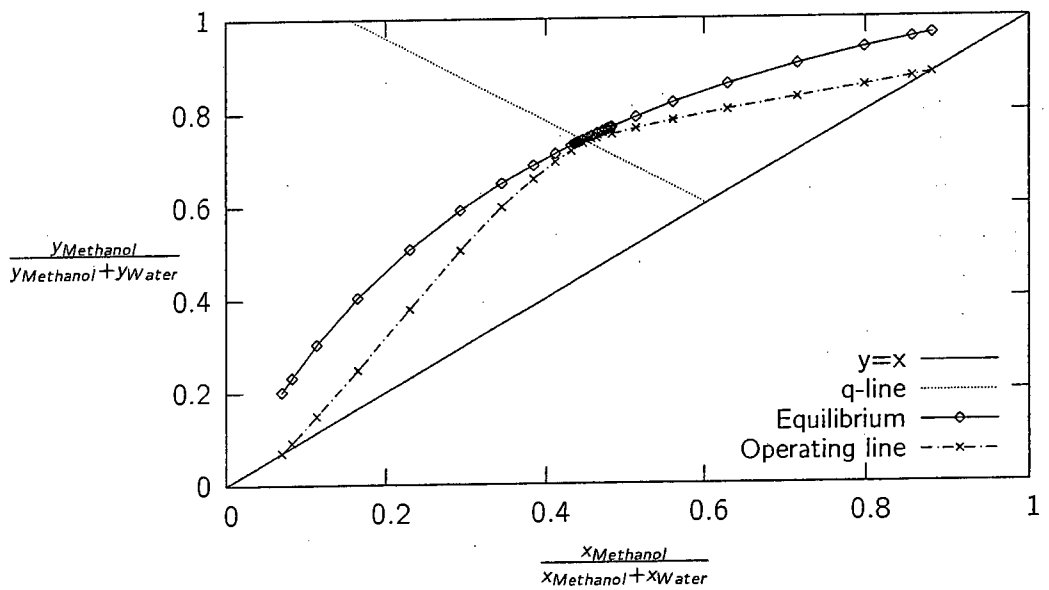

Figure 5.22: Pseudo McCabe-Thiele plot of Methanol with respect to Water for **Model 2**: *Finding the minimum flows for a fixed bottoms composition of Methanol* (Section 5.2.2)

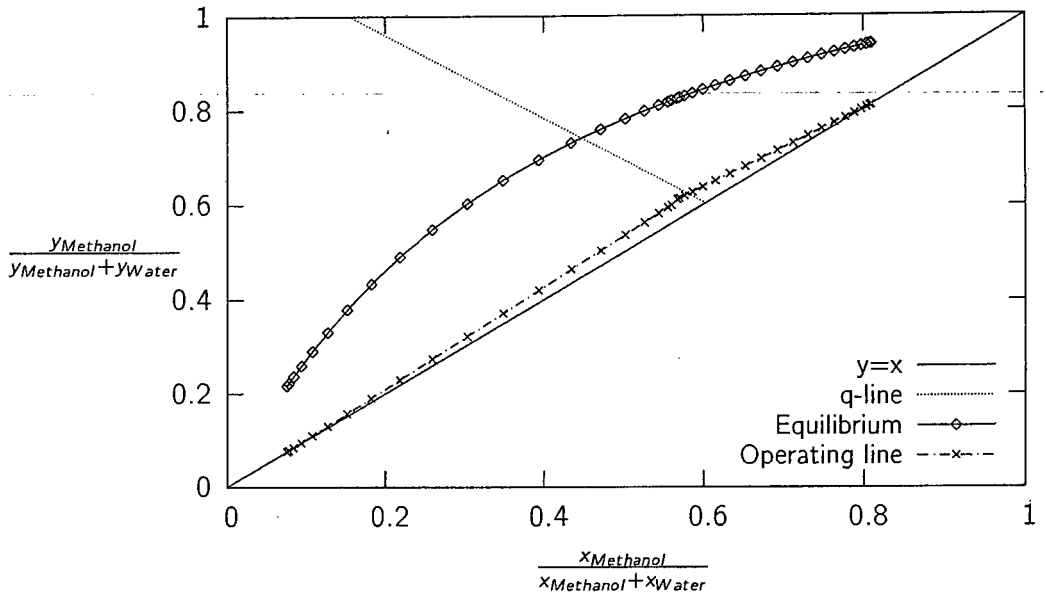

Figure 5.23: Pseudo McCabe-Thiele plot of Methanol with respect to Water for **Model 2**: *Finding the minimum height for a fixed bottoms composition of Methanol* (Section 5.2.2)

5.2.3 Collocation Accuracy

Because distillation profiles are smooth, OC works sufficiently well without having to resort to OCFE. Throughout the above analysis of Model 2, an average of 15 collocation points were used per profile. It may be interesting to see what the lower limit on this is. From the liquid composition plot in Figure 5.20, the methanol profile in the stripping section is the steepest. For this reason, the effect of a varying number of collocation points was investigated using that profile. The results are shown in Figure 5.24. The solid line represents the solution with a large number of collocation points and can be considered to be the most accurate. The accuracy is retained with 12 collocation points. For 6 collocation points, the accuracy is acceptable in the top half of the profile i.e. at a height > 3m. When the gradient becomes steeper, the accuracy deteriorates noticeably. This is a key feature of collocation. The same is true for 4 collocation points with an even more pronounced loss of accuracy in the steeper section as expected.

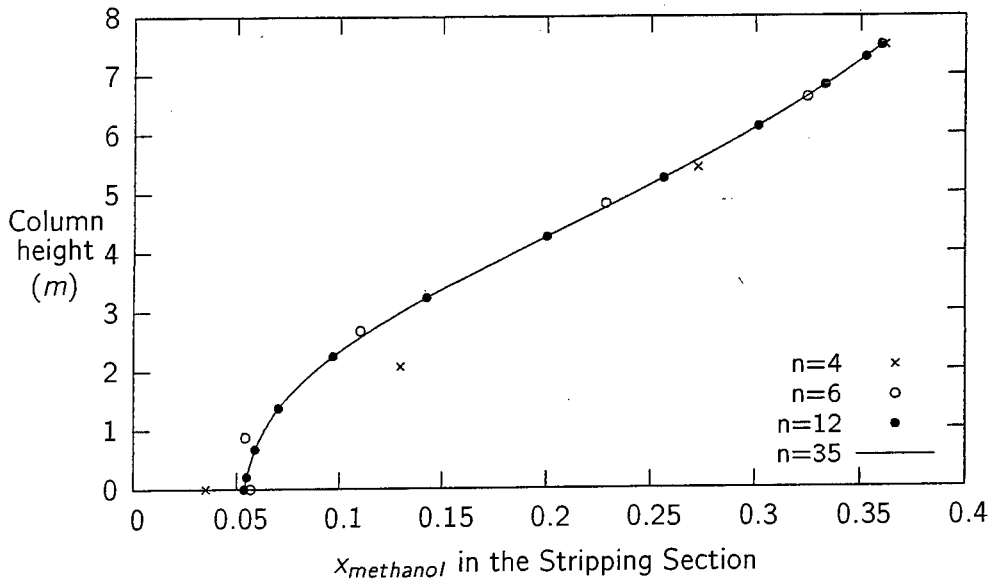

Figure 5.24: Effect of the number of collocation points on the profile accuracy: *Methanol in the stripping section*

5.3 Model 3: Increasing the Complexity Further

Model 3 increases the complexity by including sophisticated mass transfer effects with two interfacial compositions i.e. liquid and vapor. The previous assumption of an ideal thermal phase is also relaxed. This is shown in Figure 3.1. Therefore there are now $5C + 5$ variables, whereas previously in Model 2 there were $3C + 3$ variables per collocation point, where C is the number of components. As always, the degrees of freedom have not changed. To summarize, they are the reflux and reboil ratio, the height and the feed position. The feed composition and quality is assumed to be constant as shown in Table 3.3 on page 66.

The same procedure used for Model 2 in Section 5.2 is followed. Initially a feasible solution is required. This solution was obtained with the same values for the degrees of freedom as used in Model 2, Section 5.2.1. The subsequent results for Model 3 are presented and discussed in Section 5.3.1. Some specific comparisons are drawn between these results and those of Model 2 in Section 5.2.

The minimum flows and height analysis follows in Section 5.3.2, with a modified definition for the degrees of freedom. Several assumptions were made regarding the mass transfer, which will affect the model realism. This is discussed in Section 5.3.3. Finally the comparisons drawn between Model 2 and Model 3 in Section 5.3.4, motivate the choice of model for investigating the separation feasibility in the final section of this chapter, Section 5.4. Generally the proceeding

Table 5.6: Summary of the purpose, type and location of figures used in **Model 3**: *Finding a feasible solution:* (Section 5.3.1)

Purpose	**Type of Plot**	**Figure**
Use of an alternative graphical technique for gaining a different perspective compared to that of a pseudo McCabe - Thiele diagram	Liquid Phase Ternary Diagram: *Methanol & Ethanol*	Fig E.1
	Liquid Phase Ternary Diagram: *Water & Methanol*	Fig 5.25
	Liquid Phase Ternary Diagram: *Water & Ethanol*	Fig E.2
Familiar binary system graphical technique which has been modified for multicomponent systems	Pseudo McCabe-Thiele Diagram: *Methanol & Water*	Fig 5.26
	Pseudo McCabe-Thiele Diagram: *Ethanol & Water*	Fig E.3
Demonstrate the variation in flows with height as a result of the energy balance	Internal Flow Profiles: *Vapor and Liquid*	Fig 5.27
Useful for identifying a pinch	Temperature Profiles: *Vapor and Liquid*	Fig 5.28
Interesting to compare normal profiles with ternary and pseudo McCabe - Thiele diagrams	Liquid Composition Profiles	Fig 5.29
	Vapor Composition Profiles	Fig E.4
Classification of pinches found in above graphs	Equilibrium Profiles: *Vapor only*	Fig 5.30

discussion will be shorter, as the same argument as outlined in Section 5.2 applies. Because of the larger problem size, fewer collocation points per profile were used (usually 12 points per profile as opposed to 15 previously). This had a negligible effect on the model stability.

5.3.1 Finding a Starting Point Solution

To start generating the necessary data for optimization of the separation sequence, an initial feasible solution is required. Besides providing a starting point for further iterations, this solution is useful for gaining understanding of the specific physical system. The degrees of freedom and their associated values used to find the solution presented in the following figures, are the same as used in Model 2 and can be referenced in Table 5.3 on page 99. Table 5.6 presents a summary of the different figures used to draw attention to certain aspects of the model solution. As explained in Section 5.2.1, a feed discontinuity is expected due to the collocation sections used.

Although the problem order has increased significantly from Model 2 to Model 3, the main difference between the two models is the mass transfer. Therefore, the results listed in Table 5.6 should be similar to those listed in Table 5.4.

5.3.1.1 Ternary Diagrams

As stated before, for a ternary system there are three possible variations of ternary diagrams. These are shown in Figures E.1, 5.25 and E.2. The overall mass balance is included as a straight line. Pinches are usually evident when using ternary diagrams. As is standard, node pinches occur at the end points of all the operating profiles. The corresponding ternary diagrams for Model 2 are Figures D.1, 5.15 and D.2. When comparing the two sets, it is apparent that the separation in Model 2 is slightly superior. The possibility of saddle pinches arising is more pronounced in Model 2 and can be seen in Figure D.2, where the stripping profile tends toward the 45 degree line. This could be indicative of a future methanol pinch if the separation is pushed further.

The improved separation can be attributed to the effects of mass transfer. In Model 2 an overall mass transfer coefficient $K_{og}a \cdot S$ was estimated. If this value was increased, the separation improved. Likewise in Model 3, the estimated value for the specific packing surface ($a_p = 300$) has an effect on the separation. If this value is increased, the separation improves. This is intuitive as if the area available for mass transfer increases, and the rate remains constant, the overall amount of mass transfer must increase and hence the separation. Both of these experimental parameters and their values are listed in Table 5.3.

5.3.1.2 Pseudo McCabe-Thiele Diagrams

Two pseudo McCabe - Thiele diagrams have been plotted. The first and most important one is the light key methanol normalized with respect to the heavy key water, and is shown in Figure 5.26. The feed is optimally placed. The second pseudo McCabe - Thiele diagram uses ethanol normalized with respect to water in Figure E.3.

As noted before, the separation is slightly improved in Model 2 in comparison to Model 3. This is not obvious in the first set of pseudo McCabe-Thiele diagrams using methanol normalized with respect to water (Figures 5.16 and 5.26). In these diagrams the separation is almost perfect. Instead the differences are more visible in the second set of pseudo McCabe-Thiele diagrams, which use ethanol normalized with respect to water (Figures 5.17 and E.3). The minor deterioration in separation is evident due to the shorter stripping operating line in Model 3.

However, it must be emphasized that the aim is not to generate identical solutions for both models. This will never be possible due to the different mass transfer used i.e. $K_{og}a \cdot S$ is a constant in Model 2, whereas $D_{i,j}$ varies with height in Model 3. It is sufficient to note that there are evident similarities between the two models. This information will be used later when generating the separation surfaces.

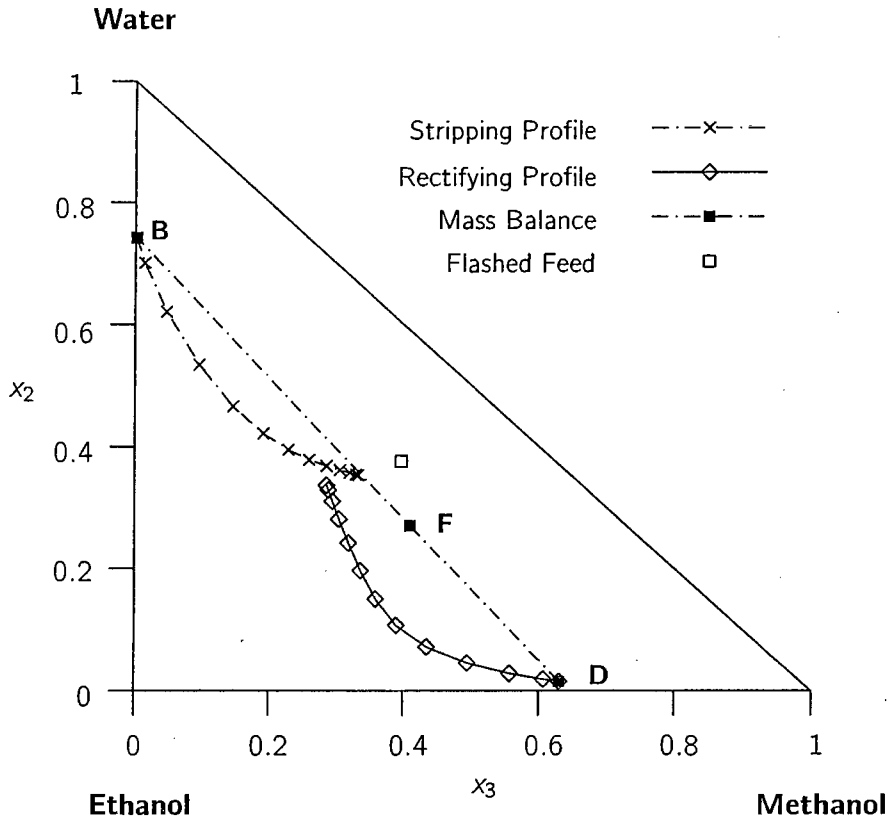

Figure 5.25: Liquid phase ternary plot of Water versus Methanol for **Model 3**: *Finding a feasible solution:* (Section 5.3.1)

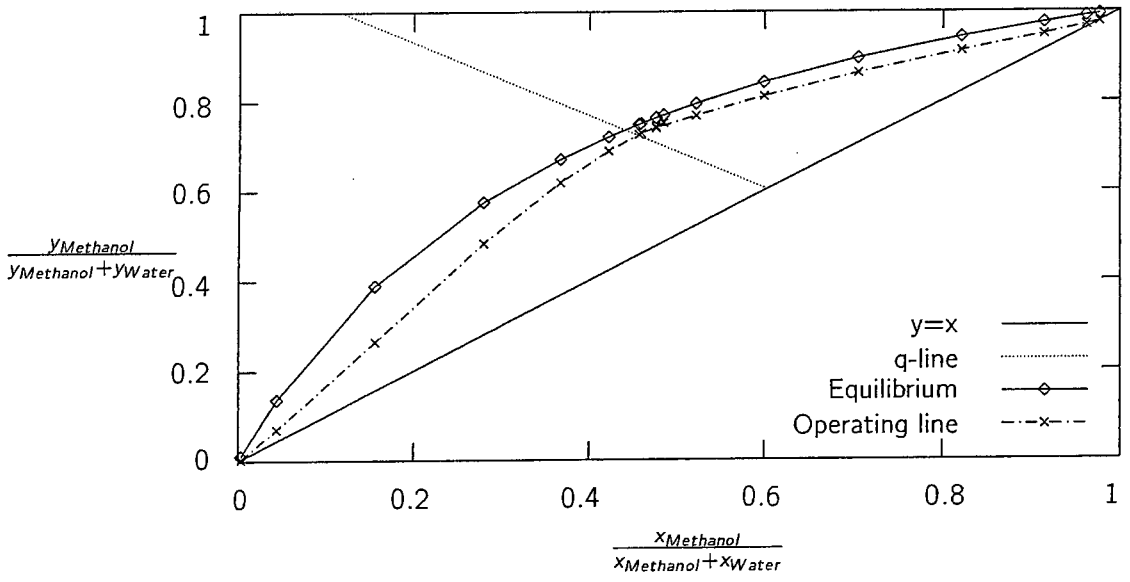

Figure 5.26: Pseudo McCabe-Thiele plot of Methanol with respect to Water for **Model 3**: *Finding a feasible solution* (Section 5.3.1)

5.3.1.3 General Profiles

Figure 5.27 shows the variation of internal flows with column height. It is very similar to the corresponding Model 2 plot shown in Figure 5.18. The temperature profiles as seen in Figure 5.28 show very little variation between the interface, liquid and vapor phase temperatures. The heat transfer is subsequently very fast. The value of the heat transfer coefficient h would affect the rate of transfer, although the movement of mass is more likely to be the dominating effect. A lateral boundary condition was applied at each collocation point in the form of the adiabatic bootstrap as shown in equation (3.34). The temperature decreases up the column as is expected.

Finally, the standard composition plots for the liquid and vapor bulk phase as well as the liquid interface composition, are shown in Figures 5.29, E.4 and 5.30. These are similar to those of Model 2. Reverse mass transfer of ethanol occurs as seen previously in Model 2.

Overall, Model 2 and Model 3 have very similar profiles. There is a slight discrepancy in the separation factor, which is higher in Model 2. This can be lowered by decreasing the value of the overall vapor phase mass transfer coefficient. These consistent results allow for Model 2 and Model 3 to be used inter-changeably.

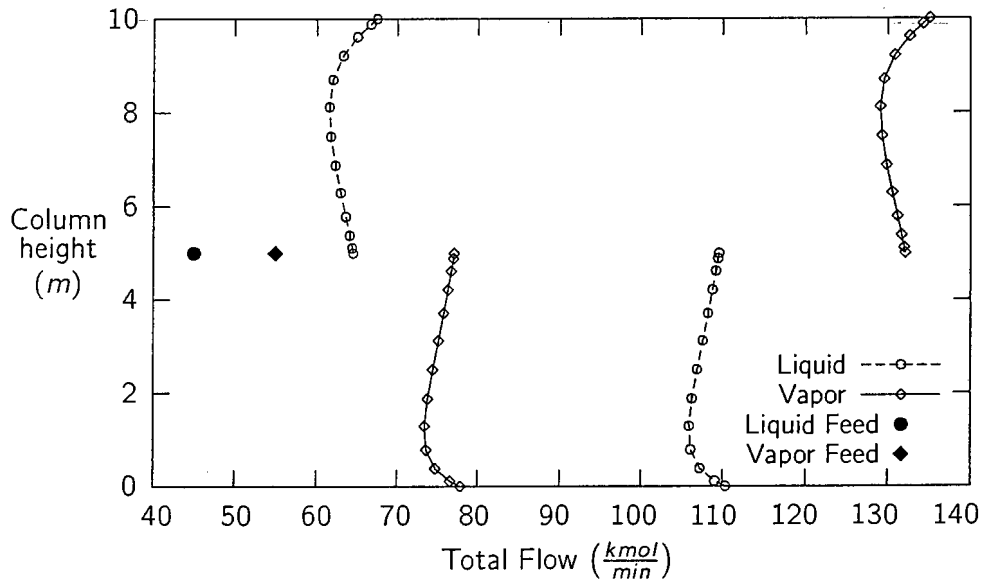

Figure 5.27: Liquid and vapor flows in column for **Model 3**:
Finding a feasible solution: (Section 5.3.1)

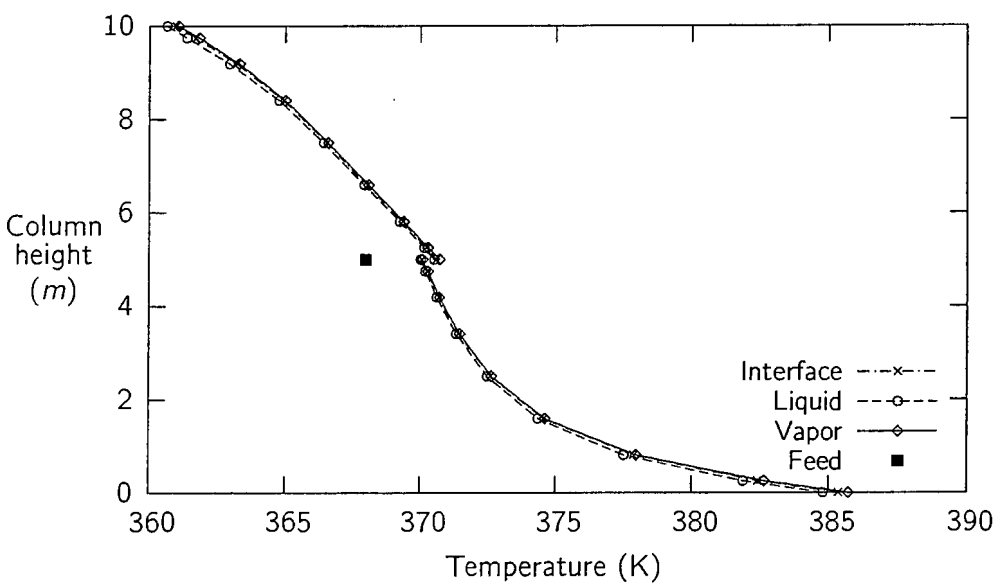

Figure 5.28: Vapor and Liquid Temperature plot for **Model 3**:
Finding a feasible solution: (Section 5.3.1)

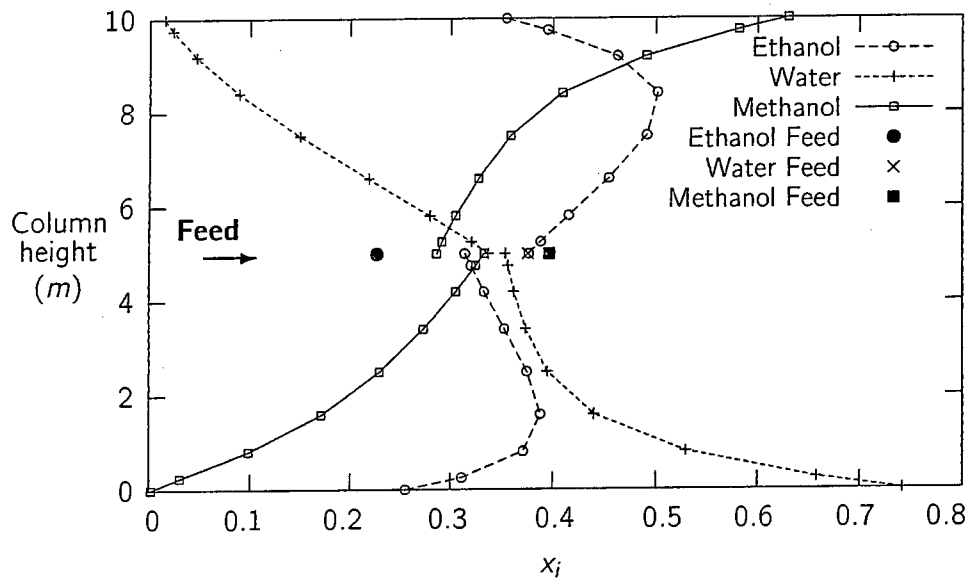

Figure 5.29: Liquid composition profiles for **Model 3**:
Finding a feasible solution: (Section 5.3.1)

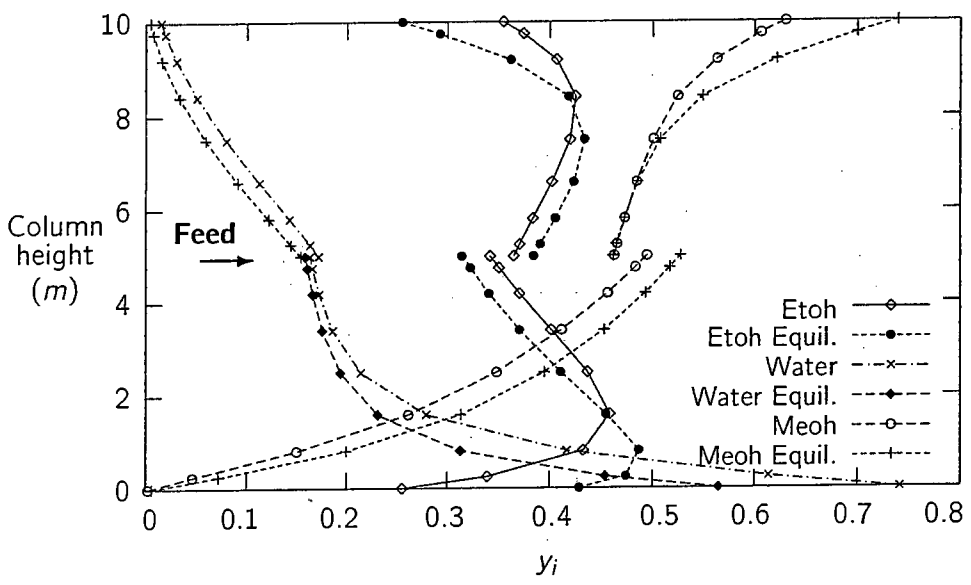

Figure 5.30: Equilibrium and Operating y_i profiles showing an azeotrope for **Model 3**:
Finding a feasible solution: (Section 5.3.1)

Table 5.7: Minimum flows and height for **Model 3** (Note: Degrees of freedom have changed)

Calculation	**Model 3**
Minimum Flows Calculation	
Reflux Ratio	0.5
Reboil Ratio	1.4
Height (m)	23
Feed location	50% of the Column Height
Product specifications	$x_{methanol,B} < 0.05$ and $x_{water,D} < 0.005$
Figure	Figure E.6
Free Variable	Reflux ratio
Minimum Height Calculation	
Reflux Ratio	9
Reboil Ratio	9
Height (m)	6
Feed location	50% of the Column Height
Product specifications	$x_{methanol,B} < 0.05$ and $x_{water,D} < 0.005$
Figures	Figure E.5 & E.7
Free Variable	Packed height

5.3.2 Discussing Minimum Flows and Height

For the minimum height and flows calculation, it was decided to change the degrees of freedom to include a specification for purities in *both* the distillate and bottoms. The purity of the heavy key in the distillate and light key in the bottoms, was chosen to be minimized. The resulting degrees of freedom and their values are shown in Table 5.7, as well as the code results. For minimum flows, the pseudo McCabe-Thiele plot of methanol normalized with respect to water is included in Figure E.6. For minimum height, both pseudo McCabe-Thiele plots of methanol and ethanol normalized with respect to water, are included in Figures E.5 and E.7. Complete coincidence of the operating lines with $y = x$ lines has not occurred, as the reflux and reboil ratios are not at infinity.

5.3.3 Model Realism

The model has some impediments to being fully realistic, one of which are the assumptions surrounding the mass transfer. Although the system is definitely non-ideal, this work assumed that the VLE was ideal. This meant that the thermodynamic correction factors as shown in equation (3.51) on page 70 are unity. In general, these correction factors account for non-ideal behavior. If non-ideal VLE was assumed, these correction factors will be large, particularly in the liquid phase. This in turn would affect the calculations for the mass transfer coefficients. However, the overall aim of this work was not to use rigorous non-ideal VLE, instead the *focus* was on *developing a feasible region*.

5.3.4 Comparing Model 2 & Model 3

Model 3 is 60 % larger than Model 2. It is subsequently less stable and has longer computational times. Both models have similiar profiles with the differences being attributed to the mass transfer definitions used. From an experimental perspective Model 2 may be more useful as the mass transfer can be grouped into a single constant $(K_{og}a \cdot S)$. Because the model results are similiar, the following separation feasibility analysis was primarily perfomed using Model 2. This model will be used to find the *broad* separation feasibility boundaries. Model 3 could then be used to *focus* on smaller regions of interest.

5.4 Investigating the Separation Feasibility

The overall objective of this work was to provide a rigorous low order model which can be used to assess separation feasibility. Initially the approach is defined using an argument based on a degrees of freedom analysis in Section 5.4.1. Two separation surfaces are introduced in this section. The following Section 5.4.2 completes the analysis started previously, by presenting all possible surface plots. Some noteworthy characteristics of the surfaces are identified and explained.

Model 2 was used in the first two sections for the reasons discussed in Section 5.3.4. Therefore the same analysis was not repeated for Model 3. Instead, a closer look at the interpolation routine and data generation routine was taken. Two surface plots for using Model 3 and the alternative interpolation routines are presented in Section 5.4.3. This penultimate section provides good continuity for the future work, as suggested in Section 5.4.4.

5.4.1 Analyzing the Separation Feasibility: *Defining the Approach*

The overall purpose of this dissertation is to develop a low order OC model, which can be used to optimize separation feasibility. The optimization will require the use of a flowsheet simulator superstructure, which repeatedly calls the low order model. This superstructure and any optimization, is definitely beyond the scope of this work. However, it should still be shown how the OC model will provide data necessary for optimization. To do this, an algorithm must be defined.

A good suggestion for developing a separation feasibility algorithm is shown in Figure 5.31. An objective function is chosen, for example a product purity, recovery or even the column height. Then a product specification is decided on as degree of freedom i.e. $x_{methanol,B} < 0.05$. The remaining three degrees of freedom are the feed position and the reboil and reflux ratios (note that the feed is fully defined and unchanging). This is mathematically shown as:

$$Objective\ function = f(Re, Rb, x_{k,B}, Feed\ position) \tag{5.1}$$

The way this would work is that a range of feasible operating conditions would be found by solving for the height and the remaining product specifications. This *Feasible Region (FR)* corresponding to a predetermined separation specification, can subsequently be optimized using MINLP.

While the above suggestion is very sensible, the reader should refer back to Section 4.1 where an argument for a different choice of degrees of freedom was given. In retrospect the code could have been better designed to allow for more flexibility in the choice of degrees of freedom. As it currently stands, the height cannot directly be solved for. However, this can be worked around

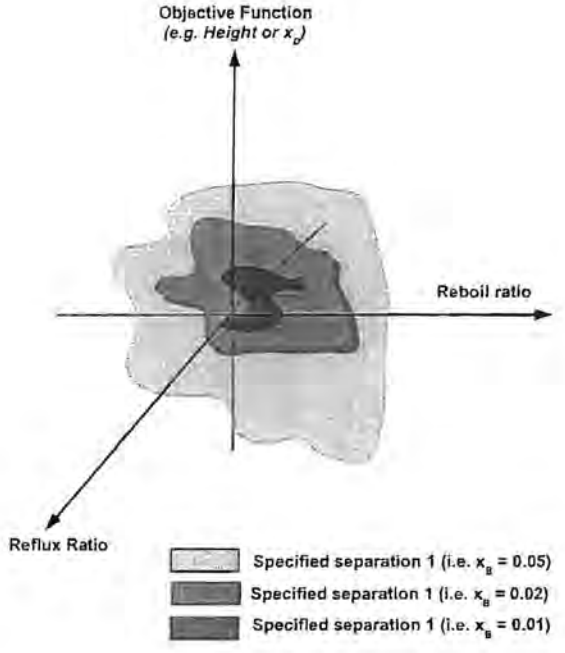

Figure 5.31: Postulated separation feasibility analysis where the feed position is assumed to have been specified

with a bit of thought. Instead of the objective function suggested in equation (5.1), the below function will be used:

$$Objective\ function = f(Re, Rb, Height, Feed\ position) \tag{5.2}$$

The above equation represents the *easiest* and *most stable* method for finding the separation feasibility. Further, *there will always be a solution* and it is this characteristic which distinguishes this choice of objective function above any other.

It will be shown that the FR can still be found for a specified separation as required by MINLP. The way to do this is use the specified separation as the objective variable. For example, if the desired separation is a minimum purity of methanol in the bottoms of 0.05, the objective function is chosen as the methanol purity in the bottoms. This does not affect the four available degrees of freedom. Out of these four, the feed position is fixed. This leaves three degrees of freedom, which can be neatly represented on a three-dimensional map. An example of such a solution is shown in Figure 5.32.

To find the FR, a plane must be drawn perpendicular to the objective function axis at the value of the desired specification. This too has been shown in Figures 5.32 at a value of $x_{methanol,B} = 0.1$. The section of the surface which lies below this plane is representative of the FR. The FR can be projected onto a grid as shown in Figure 5.33. The graphical approach has been used here, but it probably more straightforward to perform a data search and extract the information. The resulting matrix will be in three dimensions, i.e. combinations of height, reflux and reboil ratio which result in the desired separation specification. This data is then ready for optimization.

Of course, purity is not the only possible objective function. Recovery is another good option as shown in Figure 5.34. In this case, a maximum recovery of 5% of water to the distillate is the required separation, and shorter columns have been used. The associated FR has been included in Figure 5.35. This particular result validates the approach taken here as two minima are easily identifiable from Figure 5.34. If the first objective function as shown in equation (5.1) had been used instead, these minima would not have been identified.

There are consequently numerous different routes that could be followed when solving a distillation problem. However, the resulting solution will *always* have satisfied *all the degrees of freedom*. Hence, through data manipulation it is *always* possible to find certain combinations irrespective of how the solution was initially approached. To summarize, the distillation solution is solved using the necessary four degrees of freedom. For graphical purposes, two cutting planes are taken, thereby eliminating the variation in those degrees of freedom.

The obvious alternative to the above-mentioned technique is to guess a height at each point, specify the separation, solve the problem and check if it converged. Besides having an aversion to guessing variables when coding, this approach is cumbersome and time-consuming, which of course defeats the original objective of the OC model.

5.4.2 Analyzing the Separation Feasibility: *Completing the Analysis*

As mentioned previously, there are four degrees of freedom which can be varied. However, only three of these can be graphically represented using surface maps. The four degrees of freedom as shown in equation (5.2), can be combined in four sets (assuming that only three can be represented at any one time). These four possible combinations are listed below with the relevant figure references. In most cases two plots are used per combination, as both purities and recoveries are used as objective functions. The value of the remaining degree of freedom is indicated in the figure caption:

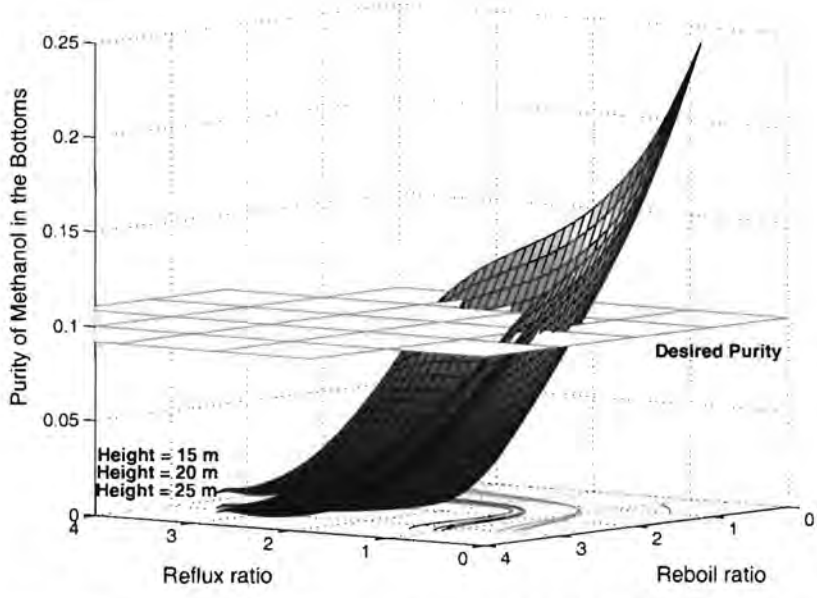

Figure 5.32: Investigating the Separation Feasibility for **Model 2**: Purity of Methanol in the bottoms as a function of the *reflux ratio*, *reboil ratio* and the *height*. The feed position is 0.5 and the desired purity < 0.1

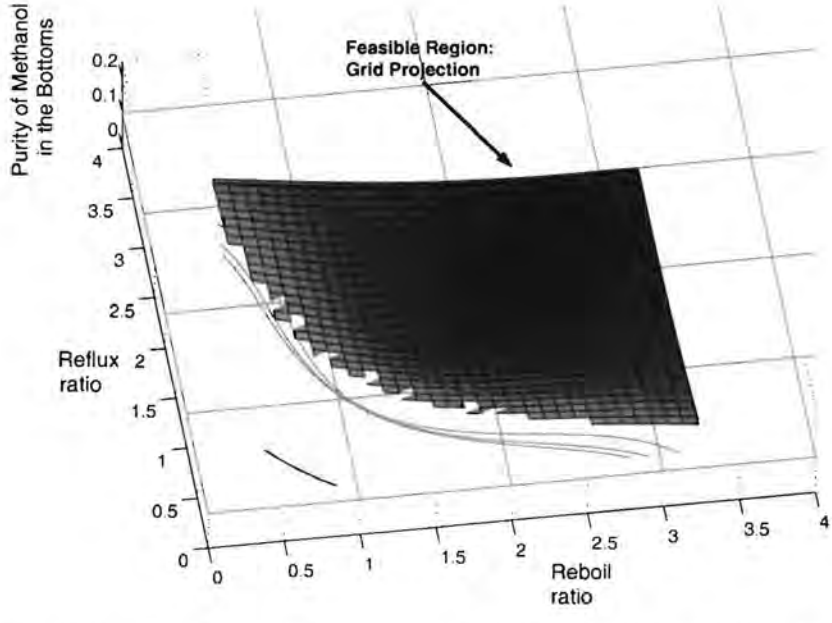

Figure 5.33: Highlighting the Feasible Region for **Model 2**: Purity of Methanol in the bottoms as a function of the *reflux* and *reboil ratios*. The feed position is 0.5 and the desired purity < 0.1

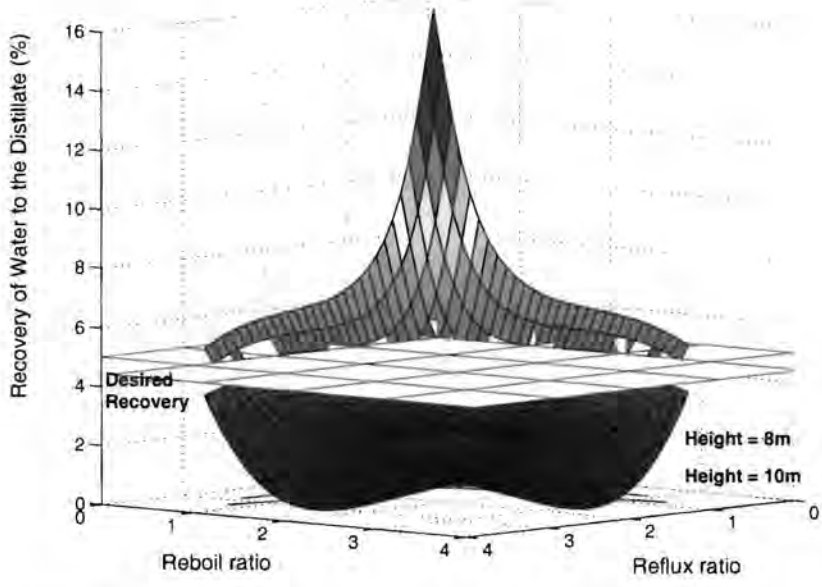

Figure 5.34: Investigating the Separation Feasibility for **Model 2**: Recovery of Water to the distillate as a function of the *reflux* and *reboil ratios* and the *height*. The feed position is 0.5 with a desired recovery $< 5\%$

Height-Reboil-Reflux: Figures 5.32, 5.33, 5.34 & 5.35

Height-Reboil-Feed position: Figure F.1 & 5.37

Height-Reflux-Feed position: Figure F.2 & 5.38

Reboil-Ratio-Feed position: Figure F.3

From a mathematical perspective, the surfaces shown in the figures extend to all eight quadrants. However only the section lying in the first quadrant is physically meaningful. These surfaces are not designed to be at optimal operating conditions (although the optimal is usually apparent). They are included primarily to suggest how the OC model could be used within an optimization routine. In the subsequent surface maps, the grid projection of the FR has not been shown.

The surfaces which have been constructed using the OC model are a good indication of the impressive robustness (and speed) of the data generation. For example, if the effect of height and reflux and reboil ratios on the purity of methanol in the distillate is desired, the the collocation code can be incrementally looped with a very small index. The small index prevents later inaccuracies when interpolating the results. Further, the collocation code remains the same size (i.e. the order is unchanged), despite an increasing height. This is even more useful when pinches are concerned as the code does not crash or slow down.

If a standard integrator such as LSODE was used, pinches constantly reduce the step size, thereby increasing the code run-time and problem order. In severe cases, the code will crash. Using collocation, this does not happen due to the robust mathematical techniques described in length in Chapter 2. The major advantage of rapid and robust data generation is that optimization becomes a simpler problem. Further advantages of collocation when using a MINLP optimizing superstructure are outlined in Section 2.1.1.

A few observations regarding the separation feasibility surfaces will shortly be made. However it is probably not necessary to discuss them all in detail. Two objective functions were broadly assigned; a recovery or purity of any component in either the bottoms or distillate streams.

Returning to Figure 5.33, the feasible region for the purity of methanol in the bottoms is shown as a function of the reflux and reboil ratio and height. The darker region at the coordinates corresponding to higher reflux and reboil ratios, indicates the lowest purity as expected. However from the associated surface plot in Figure 5.32, there appears to be some minor indentation in the surfaces at the lower purity values.

A similar and more pronounced effect is observed in Figure 5.34, where the recovery of water to the distillate is expressed as a function of reflux and reboil ratio. In this case, there is a definite symmetrical indentation in the surfaces. Therefore, the lowest recovery is not at the highest reboil and reflux ratios, but at an intermediate value. This observation justified the inclusion of the feasible region for this plot in Figure 5.35. From this figure, two darker 'eyes' are visible in the grid[7], indicating local minimums. This is an interesting observation, requiring further explanation.

What appears to be happening for example at a fixed reflux ratio of 3, is that the recovery decreases until it reaches a minimum at a reboil ratio of 2. As the reboil ratio increases beyond this point, the recovery increases indicating a deteriorating separation. This behavior was further seen in Model 3. The data is included in Table 5.8. As a final check, the same behavior was noted in the ChemSep equivalent of Model 3. The collaborating data is shown in Table F.1. From one perspective, the counter-intuitive drop in the methanol purity in the bottoms can be explained using the below equation:

$$\frac{D}{B} = \frac{Rb + 1 - q}{Re + q} \tag{5.3}$$

[7] This may not be clear as a result of the color definition on the printer used.

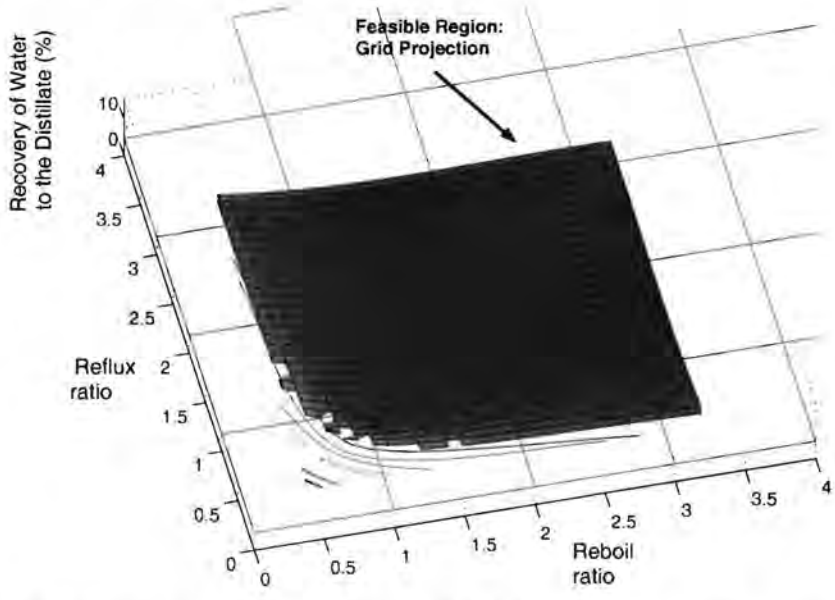

Figure 5.35: Highlighting the Feasible Region for **Model 2**: Recovery of Water to the distiбllate as a function of the *reflux* and *reboil ratio*. The feed position is 0.5 and the desired purity < 5%

In the above set of results, the liquid feed fraction q and reboil ratio Rb, are fixed. Therefore as the reflux ratio *increases*, the distillate flow rate *decreases* and the bottoms flow rate *increases*. The relative ratio of the bottoms to distillate flow is reported in Table 5.8 and F.1. As can be seen, the overall effect of an increase in reflux ratio is a drop in the ratio $\frac{D}{B}$. Hence more mass leaves in the bottoms stream. This would negatively affect the purity of methanol in the bottoms, as indeed is seen.

Table 5.8: Solutions for **Model 3** with constant reboil ratio indicating a counter-intuitive increase in methanol purity in the bottoms with increasing reflux ratio

Ratios		**Methanol Purity**		**Separation Ratios**		**Methanol Recovery**
Reflux	**Reboil**	**Bottoms**	**Distillate**	$\frac{d_{Methanol}}{b_{Methanol}}$	$\frac{D}{B}$	**Distillate**
1.0	2.4	0.002	0.607	395	2.08	99.8 %
2.0	2.4	0.009	0.694	79.6	1.37	97.3 %
2.5	2.4	0.022	0.727	32.9	1.18	95.3 %
3.0	2.4	0.037	0.754	20.4	1.04	92.6 %
3.5	2.4	0.054	0.774	14.3	0.92	89.3 %
4.0	2.4	0.073	0.788	10.8	0.83	85.6 %

Figure 5.36 attempts to predict what would happen if the reflux ratio was systematically increased while assuming an optimal feed position, and constant reboil ratio and column height. If the reboil ratio is constant, the gradient of the stripping operating line is fixed. The starting point for the stripping operating line at the feed, is found from the intersection of the rectifying operating line with the q-line. This is true as both operating lines must intersect across the q-line. If the reflux ratio is high, the gradient of the rectifying operating line is steep. The subsequent intersection of the operating lines at the q-line occurs at point A in Figure 5.36. From equation 5.3, a larger amount of material leaves in the bottoms resulting in an increase in x_D i.e a worsening bottoms purity of methanol. The stripping operating line is unable to extend further down into the bottom VLE corner as it is constrained by the intersection with the q-line and rectifying operating line at point A.

If the reflux ratio is *decreased*, the gradient of the rectifying operating line flattens until the intersection of the operating lines happens at point C in Figure 5.36. This lower reflux ratio corresponds to more material leaving in the distillate, and hence the distillate purity drops. Therefore in summary, as the reflux ratio increases, the purity of methanol in the distillate increases. The purity of methanol in the bottoms will decrease. However, the separation factor as represented by $\frac{d_i}{b_i}$ in Tables 5.8 and F.1, is expected to *increase* with an increase in reflux ratio. The reasoning is that x_B will increase more slowly than the increase in x_D. Therefore, the overall ratio should indicate an overall increase in separation.

However, all but the last point is seen in the results. While the compositions x_D and x_B move in the correct directions with an increase in the reflux ratio, the separation factor *decreases* with an increase in reflux ratio. This must be attributed to a non-optimal feed position. In which case, the analysis is distorted as the operating lines extend beyond the q-line.

The above discussed behavior is a characteristic of surface plots as a function of reflux and reboil ratio. The remaining surface plots follow expected behavior, and for this reason are mostly placed in Appendix F.

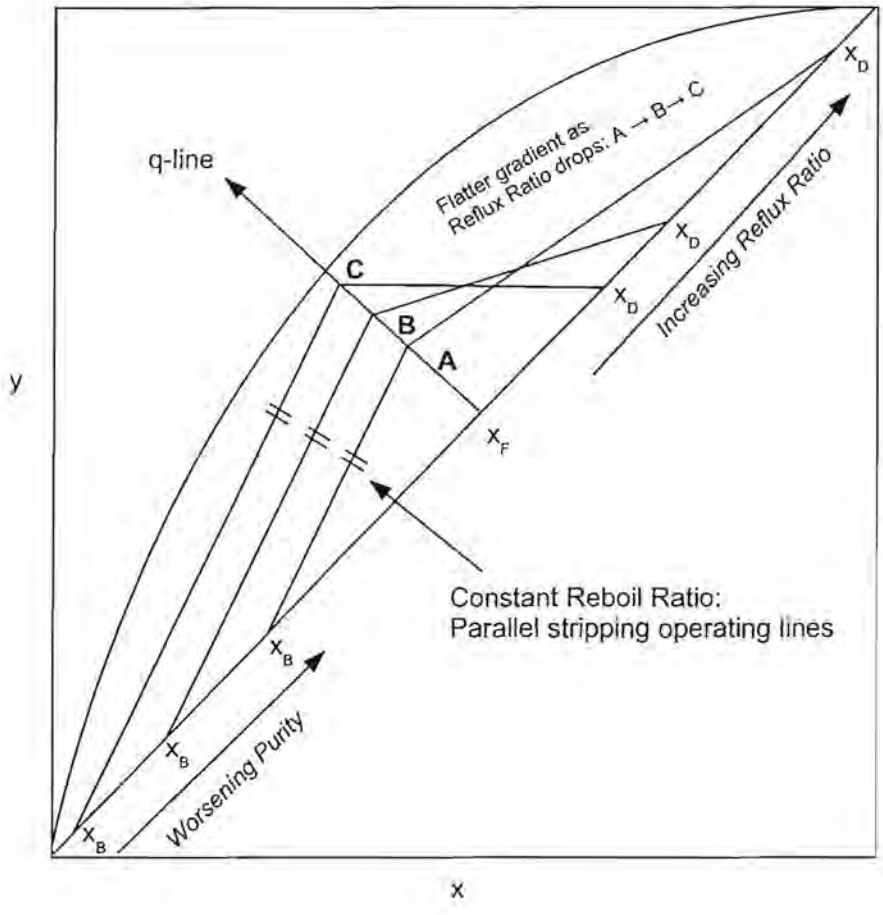

Figure 5.36: McCabe-Thiele diagram illustrating a deterioration in separation with an increase in reflux ratio at a constant reboil ratio

Generally it is expected that the separation would improve with a simultaneous increase in reflux or reboil ratio and height. If the desired split is between the ethanol and water, an improved separation would be evident if either:

1. The methanol or ethanol purity in the bottoms decreased
2. The water purity in the bottoms increased
3. The ethanol or methanol recovery to the distillate increased
4. The water recovery to the distillate decreased

The first point is true in Figures 5.32, 5.37 and F.3. The second point applies in Figure F.2. Likewise, the third point is upheld in Figure F.1, where the recovery of ethanol to the distillate increases. The fourth point holds true in Figures 5.34 and 5.35. An increase in methanol purity in the distillate with reflux ratio and height is consistent with point 1 and is shown in Figure 5.38. Therefore the results are consistent and indicate the separation factor improves with an increase in height, reflux and reboil ratio.

In the majority of the figures, the feed position does not appear to have a significant effect on the separation factor. However, the feed location may create pinches which would not be visible due to the solution strategy used. All the surfaces are relatively smooth, without any sharp kinks. This is typical of distillation solutions. Finally, it also should be noted that the separation feasibility is a true function of four parameters and not three, which have been used here. Therefore, there may be interaction effects which have not been identified. This would become more of an MINLP problem.

5.4.3 Interpolation and Data Generation

The argument presented for the degrees of freedom used and the subsequent method for determining the feasible region (FR) was presented at length in Sections 5.4.1 & 5.4.2. It will consequently not be repeated here. Instead, a closer look at how the surfaces used to find the FR were calculated. The overall aim of this dissertation is to develop a model which has a low order and subsequent fast computational time. Therefore when deriving the surfaces, it would be counter-productive to calculate each and every point. Instead an interpolation routine is used on fewer points. Interpolation has associated problems however, for example if the data is collinear, degeneracy results depending on the interpolation routine. Triangulation of data is not possible in such cases. For this reason, an alternative data generation and interpolation methodology was used for Model 3 in comparison to the simpler approach used in Model 2. Figure 5.39 should be consulted in conjunction with the following discussion.

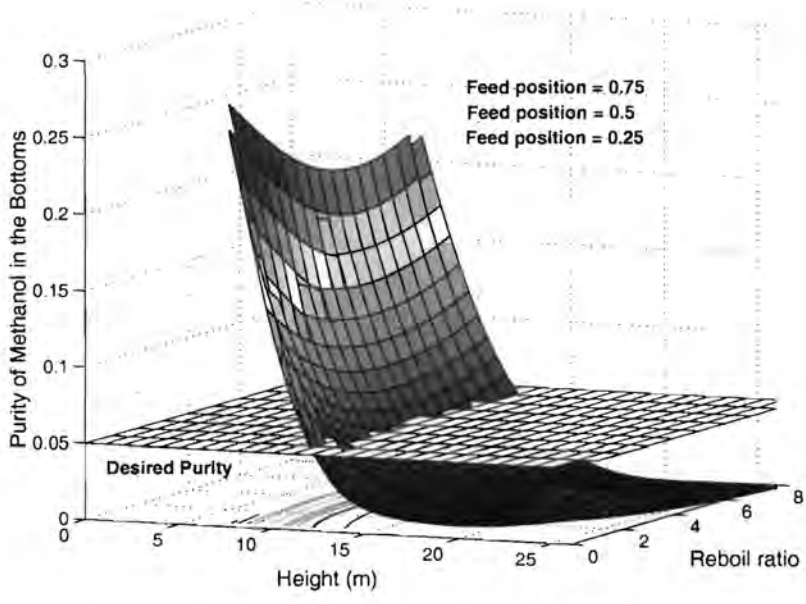

Figure 5.37: Investigating the Separation Feasibility for **Model 2**: Purity of Methanol in the bottoms as a function of the *reboil ratio*, *feed position* and the *height*. The reflux ratio is 2 and the desired purity < 0.05

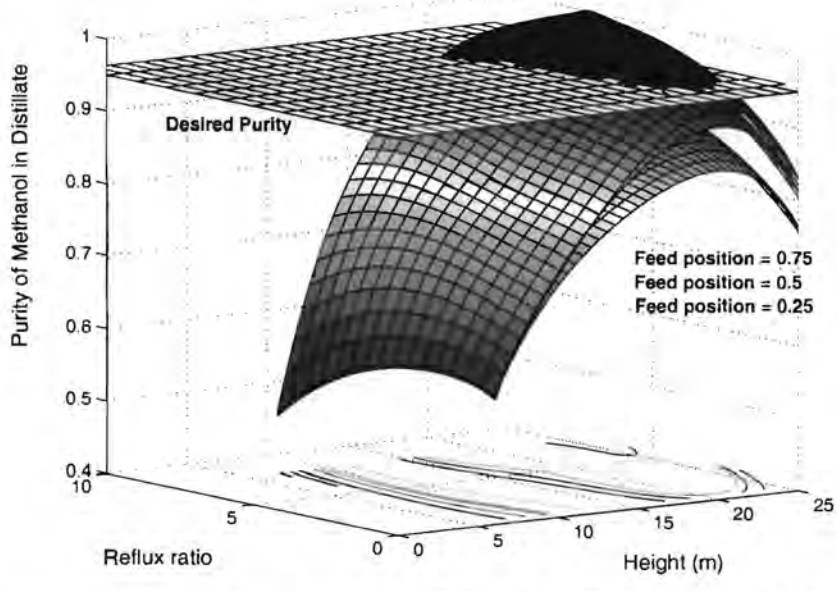

Figure 5.38: Investigating the Separation Feasibility for **Model 2**: Purity of Methanol in the distillate as a function of the *reflux ratio*, *feed position* and the *height*. The reboil ratio is 1 and the desired purity $> 95\%$

5.4.3.1 Model 2

The surface maps shown in Sections 5.4.1 & 5.4.2 were found by systematically simultaneously looping two of the four degrees of freedom (i.e. inner loop). This procedure was repeated for different values of the third degree of freedom (i.e. outer loop). A mesh grid was created from the two degrees of freedom, which had been regularly incremented in the inner loop. An intrinsic MATLAB interpolation routine was used to generate the surface data. While this is the easiest means of deriving an interpolated surface from non-symmetrical data, it may not be the most realistic. Therefore, a different approach was tested on a smaller range of data from Model 3.

5.4.3.2 Model 3

Although the data generation and subsequent optimization of the distillation model is beyond the scope of this work, some thought was nonetheless given to this problem. The main concern is that data should not be regularly incremented as there may be subsequent bias in the interpolation routine. This may be the case if the interpolation routine uses gradient information. If the data points are regularly spaced, the gradient information may be incorrect. Further the interpolation routine previously used extrapolates the data, which may not be desirable. Figure 5.39 presents a summary of the two different approaches used to generate and interpolate the data as used in Models 2 and 3.

For Model 2, the degrees of freedom were regularly incremented. This was replaced in Model 3 with a randomized adjustment of the inner loop variables. The subroutine used to generate the random numbers was also randomly re-seeded at the beginning of each loop. The resulting data was appropriately scattered with a normal distribution. Before the triangulation routine could be used, random fuzz was added to the data set to prevent degeneracy of collinear data. The Delaunay triangulation routine returns a set of triangles such that no data points are contained in any triangle's circumcircle. This data is subsequently placed into a grid and the surface is interpolated using the grid points. The interpolation routine can be either linear or cubic, both of which have similar results. Figure 5.40 is a surface plot found using a cubic routine. It describes the purity of methanol in the bottoms as a function of reflux and reboil ratios and height. The surface is constrained to a smaller range, and there is no extrapolation as seen previously.

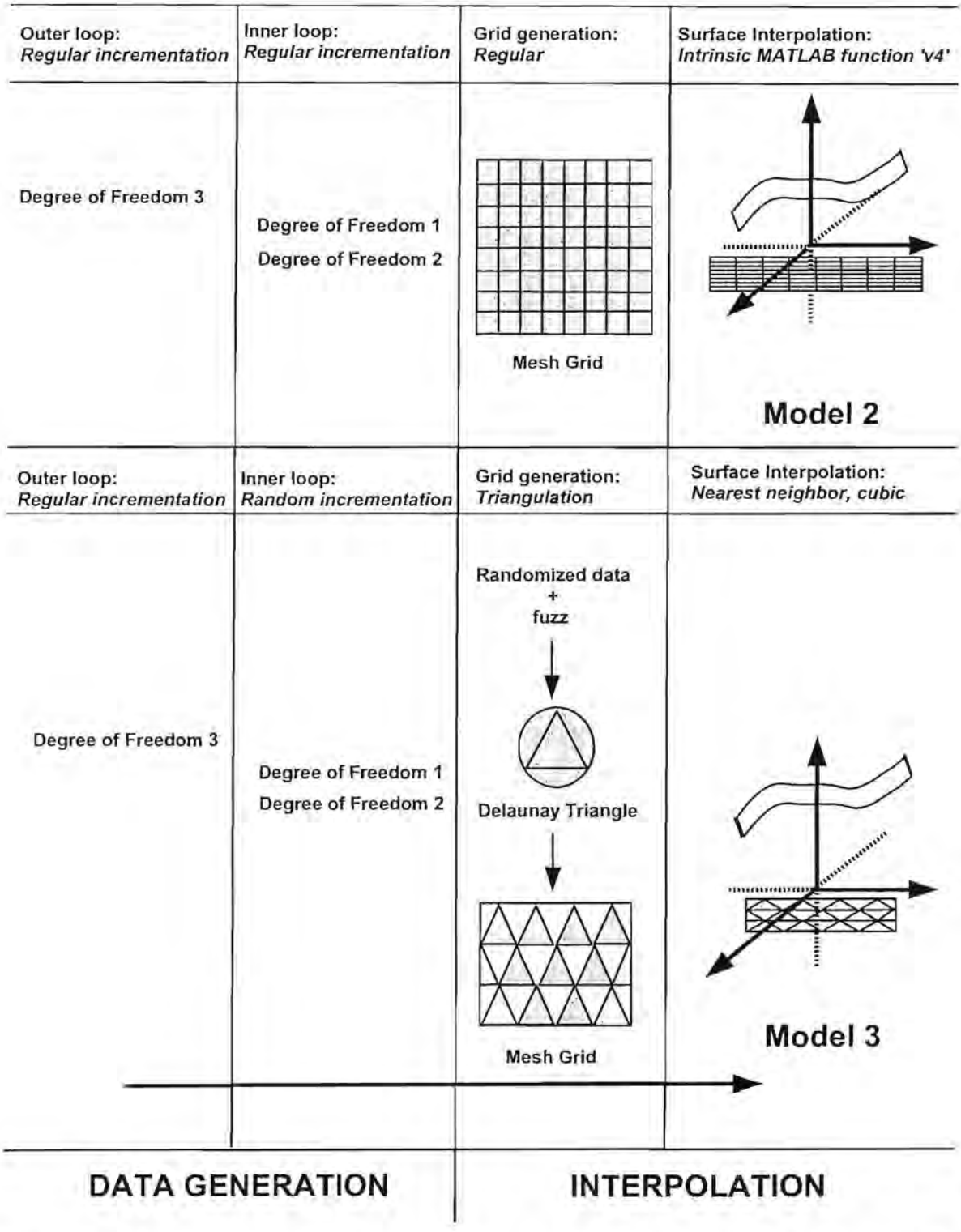

Figure 5.39: Schematic summarizing the two different approaches taken for Data Generation and Interpolation for **Models 2 & 3**

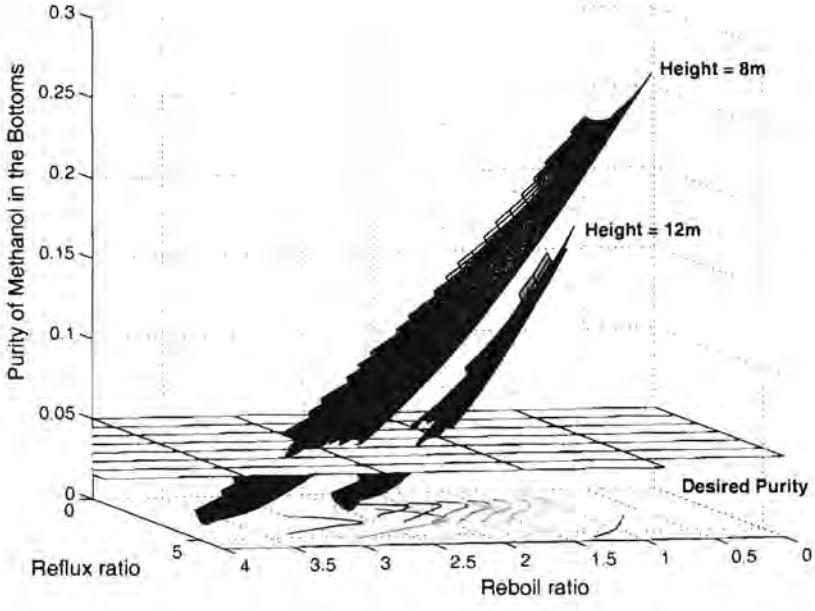

Figure 5.40: Using alternative data generation and interpolation routines for **Model 3**: Purity of Methanol in the bottoms as a function of the *reflux ratio*, *reboil ratio* and the *height*. The feed position is 0.5

An alternative representation of the same data can be seen in Figure 5.41 where the interpolation routine was replaced with a 'nearest neighbor' method. This method has discontinuities in the zero-th derivative and is an interesting alternative means of representing the data. Both of these plots show the same behavior noted in Section 5.4.2. For example, at a fixed reboil ratio of 2.4, the purity of methanol in the bottoms goes through a minimum at an intermediate value for the reflux ratio. Beyond that point, the purity increases with an increase in reflux ratio, indicating a deterioration in separation. This is consistent with the argument presented in Section 5.4.2.

In summary, this more complicated means of data generation and interpolation is not likely necessary, but is nonetheless interesting. However if the available data was scarce, or the system did not have smooth profiles, then the above method is preferable.

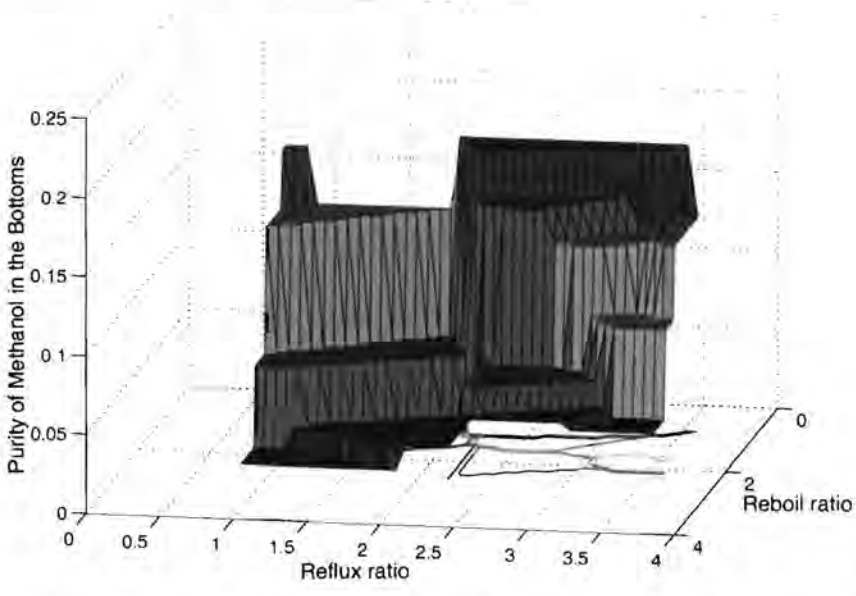

Figure 5.41: Using alternative data generation and interpolation routines for **Model 3**: Purity of Methanol in the bottoms as a function of the *reflux and reboil ratios*. The feed position is 0.5 and the height is $10m$

5.4.4 Future Work

The separation surfaces shown in the above sections, provide a rudimentary approach to finding an optimal solution. It is suggested that future work would involve the use of a NLP optimizer. An objective function could be defined in terms of the reflux and reboil ratios and section heights. This objective function would be minimized with respect to a product specification i.e. $x_{methanol,B} = 0.05$. If software such as GAMS was used, this would be a straightforward task. The most difficult aspect thereof would be constructing a link between GAMS and the FORTRAN model. GAMS would need to call the FORTRAN model as part of the optimization routine. An interface to the FORTRAN model would also be required for varying the degrees of freedom.

Chapter 6

Conclusions

The aim was to develop a low order model which could be used as a building block within a MINLP flow sheet for analyzing separation feasibility. From a broad perspective, this work had three aspects. The first was a detailed understanding of collocation mathematics, and the second, an understanding of distillation theory. Because of the vague project description, the second aspect had to be broad to achieve the correct final distillation system (i.e. Model 3). Some of the pertinent issues included the *differences between*:

- Staged or Packed Columns,
- Equilibrium or Nonequilibrium Stages,
- Rates or Efficiencies,
- Overall Liquid or Vapor Films

and *consequences of*:

- McCabe-Thiele Theory applied to Packed Columns,
- Assumptions such as CMO, Constant Relative Volatility, Ideal Solutions etc.,
- Energy Balance Assumptions on the Bootstrap.

Both aspects were non-trivial. The first was mathematically orientated, and the second used chemical engineering design theory. The final and most difficult aspect was embedding collocation into a distillation problem such that a feasible region (FR) could be defined for MINLP optimization. This required an analysis of the degrees of freedom. It was the most technical aspect, requiring coding using different computer languages. Following the standard approach, this chapter is separated into three sections to emphasize the model progression. A fourth and final section ties up the general aims stated in Chapter 1.

6.1 Model 1

Model 1 was a learning curve. It was important to understand the basic distillation and collocation theory before attempting the more complex models. A methodology was developed to *both* identify and characterize a system pinch. It was successfully implemented using Model 1.B. The minimum flows and height were determined, while carefully considering the degrees of freedom. From a technical perspective, different numerical routines were tested and found to have similar accuracy. Therefore the further use of the ABW collocation routines was validated.

6.2 Model 2

Model 2 was a more complex version of Model 1 as an energy balance was included. Mass transfer was simplified using an overall vapor phase coefficient, while heat transfer was assumed ideal. An initial starting point solution was fully defined. The results were consistent with the collocation structure with an expected feed tray discontinuity. The minimum flows and height analysis was performed, with the necessary discussion on the degrees of freedom.

Conclusions drawn regarding collocation in general included:

- The packed height could be stretched or shrunk without changing the number of collocation points. The accuracy was unaffected provided sufficient collocation points were initially used. The continuity of the column height, as well as the constant problem size, are useful characteristics for future MINLP optimization.
- The feed position was absorbed into the model as a continuous variable. This is beneficial when using MINLP optimization.
- Similarly with respect to the packed height, adjusting the feed position did not affect the number of collocation points.

Conclusions drawn regarding previous literature-based use of collocation included:

- There is little understanding in the literature regarding the structure of a collocation model. The feed discontinuity is an expected result and should not be smoothed out using interpolation as has generally been done in the past.
- Collocation is fundamentally incorrect when applied to equilibrium-based staged distillation columns.

6.3 Model 3

Model 3 was a more complex version of Model 2 with rigorous mass and energy transfer. The same analysis as used for Model 2 was repeated for Model 3. As expected, the resulting profiles for an initial starting point solution were similar to those of Model 2. The slightly improved separation in Model 2 was attributed to the experimental value of the mass transfer coefficient. Similarly to Model 2, a minimum flows and height analysis was performed, although an alternative degrees of freedom definition was used. In conclusion, Model 3 provides a more rigorous solution than that of Model 2 at the expense of a 60% larger problem size. The similarity between the results is provides good model validation.

6.4 Final Comments: *Building Blocks and Separation Feasibility*

As stated in Chapter 1, the reduced order model must effectively determine the separation feasibility for it to have application as a building block within an MINLP structure. Further, the model must have demonstrated a significant order reduction.

In the final section of Chapter 5, a methodology was proposed and implemented for defining and finding the FR through interpolation of the model results. The FR is a data set for use in MINLP optimization. Because of the similarity between Model 2 & 3 results, the bulk of the separation surfaces were generated using the more robust Model 2. Instead of a repetitive analysis of the separation feasibility surfaces, a closer look at the data generation and interpolation routine was taken using Model 3. Suggestions for future work included the use of a more sophisticated MINLP optimization technique. Therefore, both Models 2 & 3 were able to determine the separation feasibility as a function of any combination of three of the following four degrees of freedom:

1. Packed Height
2. Reflux Ratio
3. Reboil Ratio
4. Feed Position

Models 2 & 3 used on average 12 collocation points per profile. ChemSep uses in excess of 5 times as many points. Hence, a conservative order reduction of $\frac{1}{5}^{th}$ of the full order model has been shown. Models 2 & 3 *conclusively* meets the above separation feasibility *and* order reduction criteria. This will allow for the eventual placement in an optimization flow sheet superstructure, as shown in Figure 6.1.

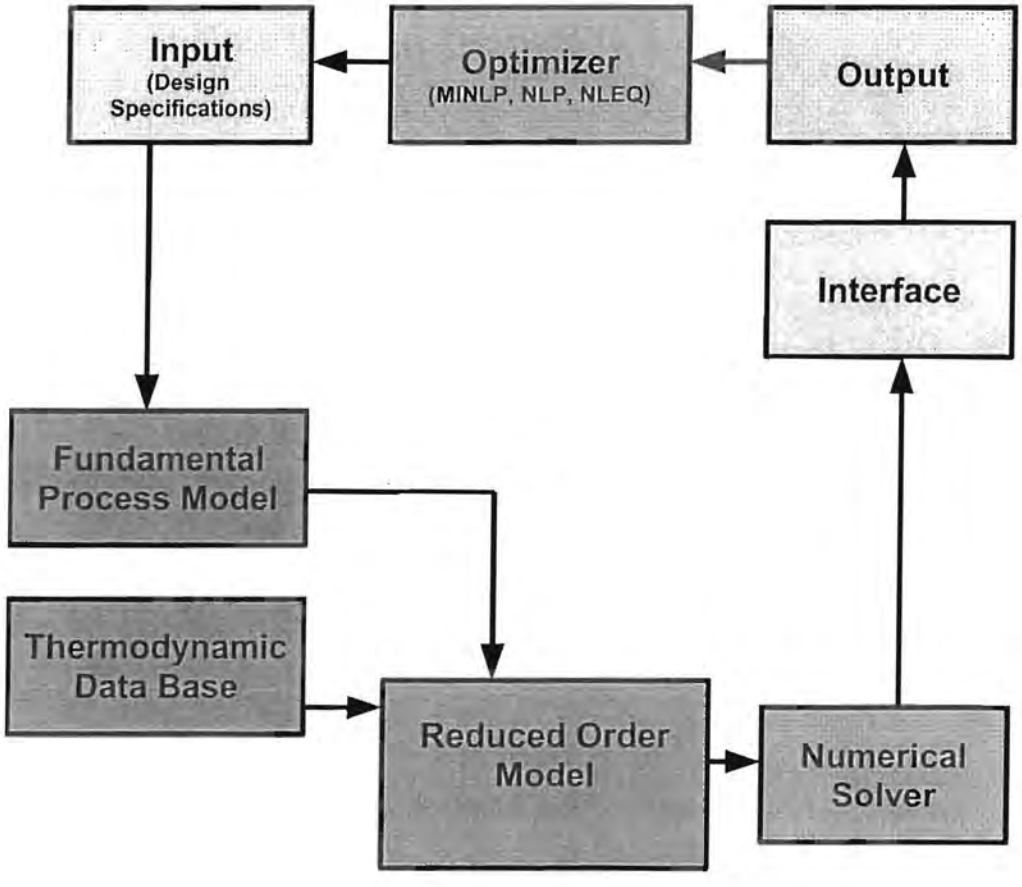

Figure 6.1: Super-structure: Suggested Optimization Architecture

Nomenclature

A_{ij} Entry in the AOC matrix

a Interface area

B Bottoms

C Total number of components

c Concentration

c_p Heat capacity

D Distillate

(D) Diffusivity Matrix

E Energy Balance Equation

F Feed

(F) Functional vector form of model equations

f Fugacity

g Vector containing variables of model equations

H Enthalpy

J Flux

K Equilibrium coefficient

k Component index for mass transfer coefficient

Kog_a Overall vapor phase mass transfer coefficient

L Liquid flow rate

l Column height (total)

M Mass Balance equation

MS Maxwell-Stefan

MW Molecular weight

mix Mixture

n Collocation point

N Rate of mass transfer

P Pressure

Q Equilibrium equation

q Liquid feed fraction

R Rate Balance equation

$\mathbb{R}$ Reciprocal mass transfer function

Rb Reboil ratio

Re Reflux ratio

S Summation equation

S Surface area

T Temperature

V Vapor flow rate

x Liquid mole fraction

y Vapor mole fraction

z_k Mole fraction (either phase)

z Height

Superscripts:

B Bottoms

D Distillate

F Feed

I Interface

L Liquid flow rate

liq Liquid

R Rectifying section

Ref Reference

S Stripping section

V Vapor flow rate

Vap Vaporization

vap Vapor

Subscripts:

B Bottoms

C Total number of components

Con Condenser

D Distillate

i Counter

j Counter

k Component

n Total number of collocation points

R Reboiler

t Total

Greek Letters:

α Relative volatility

ϵ Rate of energy transfer

Γ Thermodynamic factor

κ Mass transfer coefficient

λ Thermal conductivity

Φ Thiele modulus

ρ Density

Bibliography

[1] T. Y. Algusane, P. Proios, Michael C. G., and E. N. Pistikopoulos. A framework for the synthesis of reactive absorption columns. *Chemical Engineering and Processing*, 45(4):276–290, April 2006.

[2] M. H. Bauer and J. Stichlmair. Design and economic optimization of azeotropic distillation processes using mixed-integer nonlinear programming. *Computers & Chemical Engineering*, 22(9):1271–1286, 1998.

[3] L.T. Biegler, I.E. Grossman, and A.W. Westerberg. *Systematic Methods of Chemical Process Design*. Prentice Hall International Series, 1997.

[4] G. F. Carey and B. A. Finlayson. Orthogonal collocation on finite elements. *Chemical Engineering Science*, 30(5-6):587–596, 1975.

[5] R. Carta, G. Tola, A. Servida, and M. Morbidelli. Performance of collocation models for simulating transient multistage separation units. *Computers & Chemical Engineering*, 19(11):1141–1151, November 1995a.

[6] Y.S. Cho and B. Joseph. Reduced-order steady-state and dynamic models for separation processes. Part 1. Development of model reduction procedure. *AIChE*, 29:261–269, 1983a.

[7] Y.S. Cho and B. Joseph. Reduced-order steady-state and dynamic models for separation processes. Part 2. Application to nonlinear multicomponent systems. *AIChE*, 29:270–276, 1983b.

[8] Y.S. Cho and B. Joseph. Reduced-order models for separation columns-III. Application to columns with multiple feeds and sidestreams. *Computers and Chemical Engineering*, 8:81–90, 1983c.

[9] M.F. Doherty and Malone. *Conceptual Design of Distillation Systems*. McGraw-Hill Inc. New York, 2001.

[10] B.A. Finlayson. *Nonlinear Analysis in Chemical Engineering*. McGraw-Hill Inc. USA, 1980.

[11] L. Gardini, A. Servida, M. Morbidelli, and S. Carra. Use of orthogonal collocation on finite elements with moving boundaries for fixed bed catalytic reactor simulation. *Computers & Chemical Engineering*, 9(1):1–17, 1985.

[12] M. Heath. *Scientifc Computing: An Introductory Survey*. McGraw - Hill, New York, 2002.

[13] R.S. Huss and A.W. Westerberg. Collocation methods for distillation design. 1. Model description and testing. *Ind. Eng. Chem. Res.*, 35:1603–1610, 1996a.

[14] R.S. Huss and A.W. Westerberg. Collocation methods for distillation design. 2. Applications for distillation. *Ind. Eng. Chem. Res.*, 35:1611–1623, 1996b.

[15] Seader J.D. and Henley E. *Separation Process Principles*. Wiley and Sons, 1998.

[16] K. Kaczmarski, M. Mazzotti, G. Storti, and M. Morbidielli. Modelling fixed-bed absorption columns through orthogonal collocations on moving finite elements. *Computers and Chemical Engineering*, 21:641–660, 1995.

[17] S. Karacan, Y. Cabbar, M. Alpbaz, and H. Hapoglu. The steady-state and dynamic analysis of packed distillation column based on partial differential approach. *Chemical Engineering and Processing*, 37(5):379–388, September 1998.

[18] P. Lory. Mathermatical Models in Process Engineering. *Nonlinear Analysis, Theory, Methods and Applications*, 30:4965–4972, 1997.

[19] J. C. Pinto and E. C. Biscaia. Order reduction strategies for models of staged separation systems. *Computers & Chemical Engineering*, 12(8):821–831, August 1988.

[20] R.G. Rice and D.D. Do. *Applied Mathematics and Modelling for Chemical Engineers*. Wiley and Sons, 1995.

[21] P. Seferlis and J. Grievink. Optimal design and sensitivity analysis of reactive distillation units using collocation models. *Ind. Eng. Chem. Res.*, 40:1673–1685, 2001.

[22] P. Seferlis and A. N. Hrymak. Adaptive collocation on finite elements models for the optimization of multistage distillation units. *Chemical Engineering Science*, 49(9):1369–1382, May 1994a.

[23] P. Seferlis and A. N. Hrymak. Optimization of Distillation Units Using Collocation Models. *AICHE*, 40:813–825, 1994b.

[24] R.K. Sinnot. *Chemical Engineering Design*, volume 6. Elsevier, third edition edition, 2004.

[25] R.K. Srivastava and B. Joseph. Simulation of packed-bed separation processes using orthogonal collocation. *Computers and Chemical Engineering*, 8:43–50, 1984.

[26] R.K. Srivastava and B. Joseph. Reduced-order models for separation columns-V. Selection of collocation points. *Computers and Chemical Engineering*, 6:601–613, 1985a.

[27] R.K. Srivastava and B. Joseph. Reduced-order models for separation columns-VI. Columns with steep and flat composition profiles. *Computers and Chemical Engineering*, 11:165–176, 1985b.

[28] R.K. Srivastava and B. Joseph. Reduced-order models for separation columns-IV. Treatment of columns with multiple feeds and sidestreams via spline fitting. *Computers and Chemical Engineering*, 11:1519–164, 1986.

[29] W.E. Stewart. Additional comments on the article "solution of boundary-value problems by orthogonal collocation". *Chemical Engineering Science*, 51(15):3887–3887, August 1996.

[30] W.E. Stewart, K. L. Levien, and M. Morari. Simulation of fractionation by orthogonal collocation. *Chemical Engineering Science*, 40(3):409–421, 1985.

[31] C.L.E. Swartz and W.E. Stewart. Finite-element steady state simulation of multiphase distillation. *AIChE*, 33:1977–1987, 1987.

[32] R. Taylor and H. Kooijman. *The ChemSep Book*. Books on Demand, 2000.

[33] R Taylor and R. Krishna. *Multicomponent Mass Transfer*. John Wiley and Sons, 1993.

[34] D. Tieu, W. R. Cluett, and A. Penlidis. A comparison of collocation methods for solving dynamic optimization problems. *Computers & Chemical Engineering*, 19(4):375–381, April 1995.

[35] G. Tommasi and P. Rice. Dynamics of packed tower distillation. *Ind. Eng. Chem. Process. Des. Develop*, 9:234–243, 1970.

[36] J. V. Villadsen and W. E. Stewart. Solution of boundary-value problems by orthogonal collocation. *Chemical Engineering Science*, 50(24):3981–3996, December 1995.

[37] J.V. Villadsen and M.L. Michelsen. *Solution of differential equation models by polynomial approximation*. Prentice-Hall, Englewood Cliffs, New Jersy, 1978.

[38] R.M. Wajge, J.M. Wilson, J.F. Pekny, and G.V. Reklaitis. Investigation of numerical solution approaches to multicomponent batch distillation in packed beds. *Ind. Eng. Chem. Res*, 36:1738–1746, 1997.

[39] K.T. Wong and R. Luus. Model Reduction of High-Order Multistage Systems by the Method of Orthogonal Collocation. *Canadian Journal of Chemical Engineering*, 58:382–388, 1980.

[40] L. Zhang and A. A. Linninger. Temperature collocation algorithm for fast and robust distillation design. *Ind. Eng. Chem. Res.*, 43:3163–3182, 2004.

[41] L. Zhang and A. A. Linninger. Towards Computer-Aided Separation Synthesis. *AIChE*, 52:1392–1406, 2006.

Appendix A

Transfer Derivations using Structured Packings

This chapter completes the derivations for the rate expressions in Section 3.3.1.3. For clarity a separate nomenclature list is included at the end of this chapter. It only refers to nomenclature used in this section.

A.1 Mass Transfer

A nonequilibrium model cannot proceed without knowledge of the internals. Equipment design details are needed in order to calculate the mass transfer coefficients. Correlations exist for the Bravo method of structured packings. The geometry of the structured packing is shown in Figure A.1. The model assumes that the surface is completely wetted and that the interfacial area density is equal to the specific packing surface. The equations used to determine the mass transfer coefficients for the vapor and liquid phases are listed below in the same order as used in the code.

The *equivalent diameter* of the channel d_{eq} is given by:

$$d_{eq} = B \cdot h_c \left(\frac{1}{B + 2S} + \frac{1}{2S} \right) \tag{A.1}$$

In equation (A.1), B is the channel base, S is the channel side and h_c is the height of the triangle as shown in Figure A.1. The *wetted perimeter* P is calculated next:

$$P = \frac{4S + B}{B \cdot h_c} \tag{A.2}$$

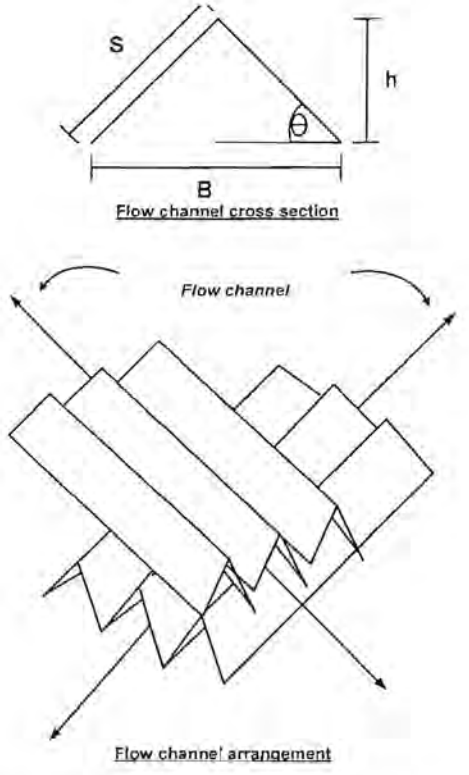

Figure A.1: Geometry of structured packings [33]

The *superficial vapor velocity* u^V can be calculated from the vapor flow rate and is a function of packed column height z:

$$u^V(z) = \frac{V(z) \cdot MW^V}{A_t \cdot \rho_t^V(z)} \tag{A.3}$$

The *effective velocity* of vapor through the channel u^{Ve} is:

$$u^{Ve}(z) = \frac{u^V(z)}{\epsilon \cdot \sin\theta} \tag{A.4}$$

In equation (A.4), ϵ is the void fraction and θ is the angle of the channel with respect to the horizon. The *superficial liquid velocity* u^L can be calculated from the liquid flow rate:

$$u^L(z) = \frac{L(z) \cdot MW^L}{A_t \cdot \rho_t^L(z)} \tag{A.5}$$

The *effective velocity* of liquid u^{Le} is based on the relationship for laminar flow in a falling film:

$$u^{Le}(z) = \frac{3\Omega(z)}{2\rho_t^L(z)} \left(\frac{\rho_t^L(z)^2 \cdot g}{3\mu^L(z) \cdot \Omega(z)} \right)^{0.333} \tag{A.6}$$

In equation (A.4), Ω is the liquid flow rate per length of perimeter:

$$\Omega(z) = \frac{\rho_t^L(z) \cdot u^L(z)}{P \cdot A_t} \tag{A.7}$$

In equation (A.7), A_t is the cross-sectional area of the column. The penetration model is used to predict the *liquid phase mass transfer coefficient*:

$$\kappa_{i,j}^L(z) = 2\left(\frac{D_{i,j}^L(z)}{\pi \cdot t_e}\right)^{0.5} \tag{A.8}$$

If the exposure time t_e assumed to be the time required for the liquid to flow between corrugations, the following equation is derived [33]:

$$\kappa_{i,j}^L(z) = 2\left(\frac{D_{i,j}^L(z) \cdot u^{Le}(z)}{\pi \cdot S}\right)^{0.5} \tag{A.9}$$

The vapor phase *Reynolds number* is:

$$Re^V(z) = d_{eq} \cdot \rho_t^V(z) \frac{\left(u^{Ve}(z) + u^{Le}(z)\right)}{\mu^V(z)} \tag{A.10}$$

The vapor phase *Schmidt number* is:

$$Sc^V(z) = \frac{\mu^V(z)}{\rho_t^V(z) \cdot D^V(z)} \tag{A.11}$$

The *Sherwood number* can subsequently be determined using:

$$Sh^V = 0.0338 \cdot Re^V(z)^{0.8} \cdot Sc^V(z)^{0.333} \tag{A.12}$$

Finally, the *vapor phase mass transfer coefficient* can be determined as:

$$\kappa_{i,j}^V(z) = \frac{Sh^V(z) \cdot D_{i,j}^V(z)}{d_{eq}} \tag{A.13}$$

When determining the mass transfer coefficients using equations (A.9) and (A.11), the liquid and vapor diffusivities, $D_{i,j}^V$ and $D_{i,j}^L$ are required. The Fuller *et al* equation was used for *vapor diffusivities* as it is easy to apply and gives reliable results [24]:

$$D_{i,j}^V(z) = \frac{1.013 \times 10^{-7} \cdot T(z)^{1.75} \cdot \left(\frac{1}{MW_i} + \frac{1}{MW_j}\right)^{0.5}}{P\left[\left(\sum_i v_{element}\right)^{\frac{1}{3}} + \left(\sum_j v_{element}\right)^{\frac{1}{3}}\right]^2} \tag{A.14}$$

In the above equation, $\sum_i v_{element}$ is the summation of the special diffusion volume coefficients for component i. In other words the component is broken down into its constituent elements and the diffusion volume coefficients for each element are summed. These constants are referenced in [24].

The Wilke-Chang equation was used for *liquid diffusivities*. It gives satisfactory predictions for the diffusivity of organic compounds in water but not for water in organic solvents. Although the systems modeled contained water and organics, there is likely to be some error as the water will alternate from being the solvent to being the solute depending on the concentration in the column. Nonetheless, the relation was still acceptable [24]:

$$D_{i,j}^{L}(z) = \frac{1.173 \times 10^{-13} \cdot (\phi \cdot MW)^{0.5} \cdot T(z)}{\mu^{L}(z) \cdot V_m^{0.6}} \tag{A.15}$$

In the above equation, ϕ is an association factor for the solvent, MW is the molecular mass of the solvent, μ is the solvent viscosity, T is the temperature and V_m is the molar volume of the solute at its boiling point.

A.2 Energy Transfer

A semi-theoretical correlation by Billet and Schultes [15] was used for the *vapor phase heat transfer coefficient*. It is applicable to both structured and random packings. The vapor phase heat transfer coefficients are estimated using the Chilton-Colburn analogy between energy and mass transfer:

$$h^{V}(z) = \kappa^{V}(z) \cdot \rho^{V}(z) \cdot c_p^{V} \cdot N_{Le}(z)^{\frac{2}{3}} \tag{A.16}$$

$$N_{Le}(z) = \left(\frac{N_{Sc}(z)}{N_{Pr}(z)} \right) \tag{A.17}$$

The Prandtl and Schmidt numbers as shown in equations (A.18) and (A.19) respectively, are needed when using equation (A.17):

$$N_{Pr}(z) = \frac{c_p \cdot \mu(z)}{\kappa(z)} \tag{A.18}$$

$$N_{Sc}(z) = \frac{\mu(z)}{\rho(z) \cdot D_{A,B}(z)} \tag{A.19}$$

For the *liquid-phase heat transfer coefficient*, the penetration model was used:

$$h^{L}(z) = \kappa^{L}(z) \cdot \rho^{L}(z) \cdot c_p^{L} \cdot N_{Le}(z)^{\frac{1}{2}} \tag{A.20}$$

Table A.1: Column internals data used to determine the transfer coefficients in **Model 3**

Specific packing surface	$a_p = 300 \left[\frac{m^2}{m^3}\right]$
Crimp height	$h = 6.4$ [mm]
Channel base	$B = 12.7$ [mm]
Channel side	$S = 8.9$ [mm]
Void fraction	$\epsilon = 0.9$
Channel flow angle	$\theta = 60$
Column diameter	1 [m]

A.3 Column Internals Data

Table A.1 contains the data used when calculating the mass and heat transfer coefficients as detailed in the previous section. The data was taken from a case study for lack of a better idea [33].

Nomenclature

A_t Cross sectional area

B Channel base

c_p Heat capacity

D Diffusion coefficient

d_{eq} Equivalent diameter

g Gravitational constant

h Heat transfer coefficient

h_c Crimp height

MW Molecular weight

N_{Le} Lewis number

N_{Sc} Schmidt number

N_{Pr} Prandtl number

P Wetted perimeter

Re Reynolds number

S Channel side

S_c Schmidt number

S_h Sherwood number

T Temperature

t_e Exposure time

u Superficial velocity

u^{Le} Effective liquid velocity

u^{Ve} Effective vapor velocity

V Vapor flow rate

z Packed column height

Superscript:

L Liquid

V Vapor

Superscript:

i Component

j Component

t Total

Greek Letters:

ϵ Void fraction

κ Mass transfer coefficient

μ Viscosity

Ω Liquid flow rate per length of perimeter

ϕ Association factor for the solvent

ρ Density

θ Channel flow angle

Appendix B

Physical Properties Used

Table B.1: Correlations used to determine the physical properties in **Model 3**

Property	*Equation*	*Source*
Liquid Density	$\rho_k^L = \left(\frac{A}{B^{1+\left(1-\left(\frac{T^L}{C}\right)\right)^D}}\right) \cdot MW_k$	[32]
Vapor Density	$\rho_k^V = \left(\frac{P}{R \cdot T^V}\right) \cdot MW_k$	Ideal gas law
Mixture Density Liquid	$\rho_{mix}^L = \sum_{k=1}^{C} \left(x_k \cdot \rho_k^L\right)$	[24]
Mixture Density Vapor	$\rho_{mix}^V = \sum_{k=1}^{C} \left(y_k \cdot \rho_k^V\right)$	[24]
Vapor Heat Capacity	$A + B \cdot T^V + C \cdot (T^V)^2 + D \cdot (T^V)^3$	[32]
Liquid Heat Capacity	$c_{p,compound} = \sum_{i=1}^{N^o Element} c_{p,i}$	[24]
Partial Vapor Pressure	$P_k = e^{\left(A - \frac{B}{T^V + C}\right)}$	[24]
Liquid Viscosity	$\left(A + \frac{B}{T^L} + C \cdot log(T^L) + D \cdot (T^L)^E\right)$	[32]
Vapor Viscosity	$A \cdot \left(\frac{(T^V)^B}{1 + \frac{C}{T^V} + \frac{D}{(T^L)^2}}\right)$	[32]
Liquid Thermal Conductivity	$\lambda^L = 3.56 \times 10^{-5} \cdot C_P^L \cdot \left(\frac{(\rho^L)^4}{MW}\right)^{\frac{1}{3}}$	[24]
Vapor Thermal Conductivity	$A \cdot \left(\frac{(T^V)^B}{1 + \frac{C}{T^V} + \frac{D}{(T^V)^2}}\right)$	[32]

Appendix C

More on the Technical Aspects of Collocation Programming

C.1 Numerical Methods Used

Table C.1 lists the numerical methods used to develop and solve the models. To clarify, when given a set of differential equations (DE's) which require solving, there are several approaches available. Rigorous collocation requires reformulation of the DE's into collocation equations using the ABW routines. These resulting nonlinear equations require solving. In which case a robust nonlinear equation solver such as HYBRD is a good choice.

If it is preferred to integrate the DE's numerically as they stand, LSODE is a useful tool. However, because of the structure of LSODE, it requires an additional solver to converge a split boundary problem. The simplest and most inefficient method would be a shooting method. A more sophisticated technique is a least square minimization algorithm such as LMDIF.
From the above explanation, COLSYS is a useful collocation tool as it both formulates the collocation equations and solves them.

C.2 Developing the Collocation Equations

There are two numerical methods commonly used for solving a collocation model: COLSYS (Section C.2.1) and ABW Routines (Section C.2.2). COLSYS accepts the differential equations (DE's) in their standard form. ABW routines are more rigorous and require the reformulation of the DE's into 'true' collocation format.

Table C.1: Numerical Methods used to develop and solve the models

Model	Equations Developed Using:	Equations Solved Using:
Model 1.A, B & C	ABW Routines	HYBRD
	COLSYS	COLSYS
	LSODE	Levenberg-Marquardt Search
	LSODE	Shooting method
Model 2	ABW Routines	HYBRD
Model 3	ABW Routines	HYBRD

C.2.1 COLSYS

COLSYS was developed for the solution of boundary value problems using collocation and piecewise polynomials or B-splines [22]. This method requires the evaluation of the approximation error for each element. However, the actual solution is usually not known and an approximation must be supplied. COLSYS calculates the optimal distribution of element length, rather than the optimal location of each break point. Physical meaning can be given to the break points by locating them at points where discontinuities in the flow rates are introduced [30]. The residuals of the equations at non-collocation points can provide an estimate of the approximation error. Several different approaches have been used e.g. polynomial interpolation to approximate residuals within each element [22]. If COLSYS is implemented correctly[1], accuracy can be increased and model order reduced.

C.2.2 ABW Routines

ABW routines are rigorous and require a sometimes lengthy collocation equation development. However the longer time required to set-up the equations is recovered when de-bugging the code[2]. In order to convert the DE's into an set of algebraic collocation equations, several routines need to be used [37]:

JCOBI vector: For finding the collocation roots

AOC matrix: For evaluating first order DE's

BOC matrix: For evaluating second order DE's

WOC vector: For evaluating integrals

Lagrange Interpolation Subroutine: For generating a smooth solution

[1] Not necessarily a trivial task

[2] While the COLSYS interface is more convenient, it also presents serious problems when attempting to de-bug.

The nomenclature used in the next two sections describing the JCOBI and INTRP subroutines is the same as that used in Chapter 2.6 on page 19, and can be referenced in associated the nomenclature list on page 31. Any additional terms introduced below will be explained in context to avoid confusion.

C.2.2.1 Jacobi Subroutine

The recurrence relation is used to determine the Jacobi polynomial $P_n(x_k)$ as defined by equation (2.31) in the Chapter 2. It has been re-included below:

$$P_n^{(\alpha,\beta)}(x) = \sum_{i=0}^{n} (-1)^{n-i} \cdot \gamma_i \cdot x^i \tag{C.1}$$

When using the JCOBI subroutine, the polynomial $P_n^{(\alpha,\beta)}(x)$ is rescaled. The derivations are more eloquently explained in the reference texts ([20] is particularly clear although [37] is more rigorous), and therefore only the final rescaled polynomial is presented here:

$$p_n(x) = \frac{P_n^{(\alpha,\beta)}(x)}{\gamma_{n,n}} \tag{C.2}$$

The above equation is not very helpful from a programmatic perspective. Therefore, $p_n(x)$ and the first derivative thereof $p_n'(x)$, can be calculated from the below recursive formulae:

$$p_n(x) = (x - g_n) \cdot p_{n-1} - h_n \cdot p_{n-2} \tag{C.3}$$

$$p_n'(x) = p_{n-1}' + (x - g_n) \cdot p_{n-1}' - h_n \cdot p_{n-2}' \tag{C.4}$$

where g_n and h_n are functions of n, α and β. The detailed derivation is in [37]. The subroutine JCOBI is used to calculate the zeros of scaled polynomial $p_n(x)$, as well as the first three derivatives of the node polynomial:

$$p_{(n=n+2)}(x) = (x)^{(n=0)} \cdot p_n(x) \cdot (x-1)^{(n=1)} \tag{C.5}$$

The subroutine therefore calculates the AOC and BOC matrices as required. Because no integral expressions were evaluated, there was no need to calculate the WOC matrix using RADAU.

C.2.2.2 Lagrange Subroutine

Lagrange interpolation is discussed in Section 2.6.3 on page 23. Linear operations on Lagrangian polynomials require derivation as $l_i(x)$ is not easily differentiated or integrated. The full derivation for the relationship between the Lagrange polynomials and the node polynomials can be found in [37]. In short, the building block relation given in equation (2.38) on page 23 is extended for computational purposes through an extensive derivation. The final outcome as used in the subroutine INTRP is:

$$l_i(x) = \prod_{\substack{j=1 \\ j \neq i}}^{n+1} \frac{(x - x_j)}{(x_i - x_j)} = \frac{p_{(n+1)}(x)}{(x - x_i) \cdot p'_{(n+1)}(x_i)} \tag{C.6}$$

C.2.2.3 Example of a Collocation Equation Set

Unlike staged systems where the same tray index is given to streams leaving a stage, collocation liquid and vapor variables have the same 'tray' index at each collocation point i.e. instead of x_j and y_j, $x(z)$ and $y(z)$ are used where z is the height variable. The equations representing Model 3 have been written out exhaustively in collocation format. Model 3 was chosen as it was the most complex.. The inner equations representing the film balance are shown in equations (C.17) to (C.27). The outer equations representing the bulk phase balance are listed below in equations (C.7) to (C.16). Both equation sets are looped for $i, j = 1, ...NT$ where NT is the total number of collocation points[3]. Where matrices are used (i.e. $A_{i,j}$), nested loops are necessary. Note that the equations have been written out for three components:

[3]Inclusive of the endpoints

The outer equations i.e. the bulk phase balance:

$$\textbf{(M)}: \sum_{j=1}^{j=NT} A_{i,j} \cdot (L_i \cdot x_{1,i}) + N_{1,i} \cdot Height = 0 \quad (C.7)$$

$$\textbf{(M)}: \sum_{j=1}^{j=NT} A_{i,j} \cdot (L_i \cdot x_{2,i}) + N_{2,i} \cdot Height = 0 \quad (C.8)$$

$$\textbf{(M)}: \sum_{j=1}^{j=NT} A_{i,j} \cdot (L_i \cdot x_{3,i}) + N_{3,i} \cdot Height = 0 \quad (C.9)$$

$$\textbf{(M)}: \sum_{j=1}^{j=NT} A_{i,j} \cdot L_i + N^L_{total,i} \cdot Height = 0 \quad (C.10)$$

$$\textbf{(M)}: \sum_{j=1}^{j=NT} A_{i,j} \cdot (V_i \cdot y_{1,i}) + N_{1,i} \cdot Height = 0 \quad (C.11)$$

$$\textbf{(M)}: \sum_{j=1}^{j=NT} A_{i,j} \cdot (V_i \cdot y_{2,i}) + N_{2,i} \cdot Height = 0 \quad (C.12)$$

$$\textbf{(M)}: \sum_{j=1}^{j=NT} A_{i,j} \cdot (V_i \cdot y_{3,i}) + N_{3,i} \cdot Height = 0 \quad (C.13)$$

$$\textbf{(M)}: \sum_{j=1}^{j=NT} A_{i,j} \cdot V_i + N^V_{total,i} \cdot Height = 0 \quad (C.14)$$

$$\textbf{(E)}: \sum_{j=1}^{j=NT} A_{i,j} \cdot \left(V_i \cdot \left(\sum_{k=1}^{k=3} H^V_k \cdot y_{k,i}\right)\right) + \epsilon^{V,I}_i \cdot Height = 0 \quad (C.15)$$

$$\textbf{(E)}: \sum_{i=1}^{i=NT} A_{i,i} \cdot \left(L_i \cdot \left(\sum_{k=1}^{k=3} H^L_k \cdot x_{k,i}\right)\right) + \epsilon^{L,I}_i \cdot Height = 0 \quad (C.16)$$

In the above set of equations, the variable *Height* was used instead of the usual z, as the entire column height is meant i.e. not a 'stage' as what is understood by using z. The nomenclature used in the above and below sets of equations can be referenced on page 141.

Appendix D

Results: Model 2

D.1 Starting Point Solution: Ternary Diagrams

The inner equations i.e. the film balance:

$$\mathbf{(R)}: h_i^V \cdot a \cdot (T_i^V - T_i^I) + \sum_{k=1}^{k=C} N_{k,i} \cdot (H_{k,i}^V - H_{k,i}^L) - h_i^L \cdot a \cdot (T_i^I - T_i^L) = 0 \quad \text{(C.17)}$$

$$\mathbf{(R)}: N_{1,i} - c_{total,i}^L \cdot \kappa_{11,i}^L \cdot a \cdot (x_{1,i}^I - x_{1,i}) - x_{1,i} \cdot N_{total,i}^L = 0 \quad \text{(C.18)}$$

$$\mathbf{(R)}: N_{2,i} - c_{total,i}^L \cdot \kappa_{22,i}^L \cdot a \cdot (x_{2,i}^I - x_{2,i}) - x_{2,i} \cdot N_{total,i}^L = 0 \quad \text{(C.19)}$$

$$\mathbf{(R)}: N_{1,i} - c_{total,i}^V \cdot \kappa_{11,i}^V \cdot a \cdot (y_{1,i} - y_{1,i}^I) - y_{1,i} \cdot N_{total,i}^V = 0 \quad \text{(C.20)}$$

$$\mathbf{(R)}: N_{2,i} - c_{total,i}^V \cdot \kappa_{22,i}^V \cdot a \cdot (y_{2,i} - y_{2,i}^I) - y_{2,i} \cdot N_{total,i}^V = 0 \quad \text{(C.21)}$$

$$\mathbf{(Q)}: y_{1,i}^I - K_{1,i} \cdot x_{1,i}^I = 0 \quad \text{(C.22)}$$

$$\mathbf{(Q)}: y_{2,i}^I - K_{2,i} \cdot x_{2,i}^I = 0 \quad \text{(C.23)}$$

$$\mathbf{(Q)}: y_{3,i}^I - K_{3,i} \cdot x_{3,i}^I = 0 \quad \text{(C.24)}$$

$$\mathbf{(S)}: x_{1,i}^I + x_{2,i}^I + x_{3,i}^I - 1 = 0 \quad \text{(C.25)}$$

$$\mathbf{(S)}: y_{1,i}^I + y_{2,i}^I + y_{3,i}^I - 1 = 0 \quad \text{(C.26)}$$

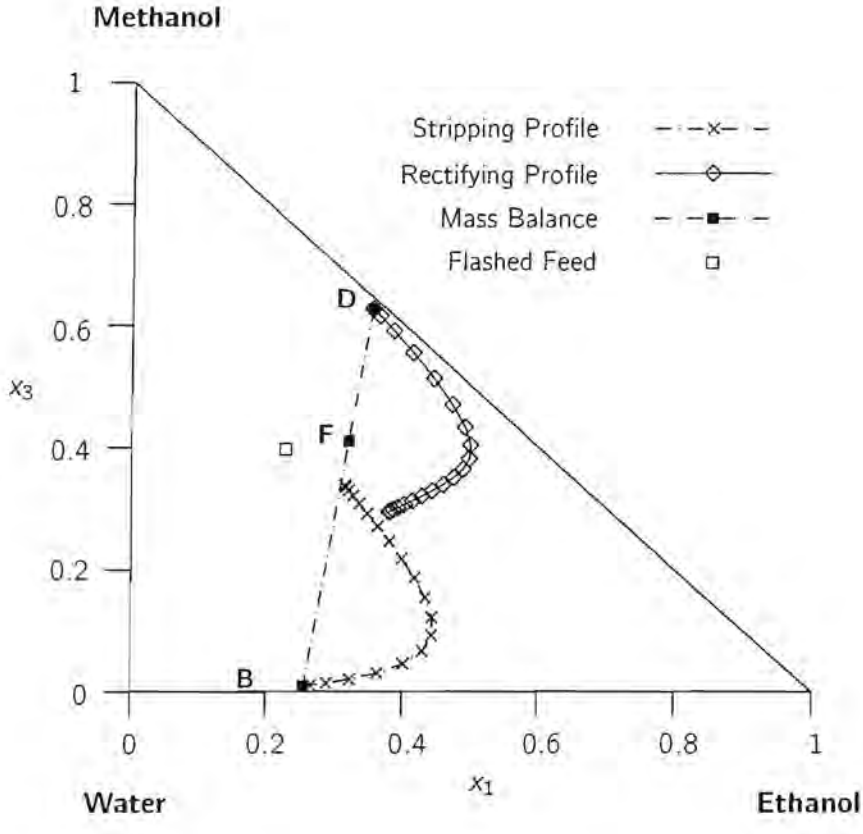

Figure D.1: Liquid phase ternary plot of Methanol versus Ethanol for **Model 2**: *Finding a feasible solution:* (Section 5.2.1)

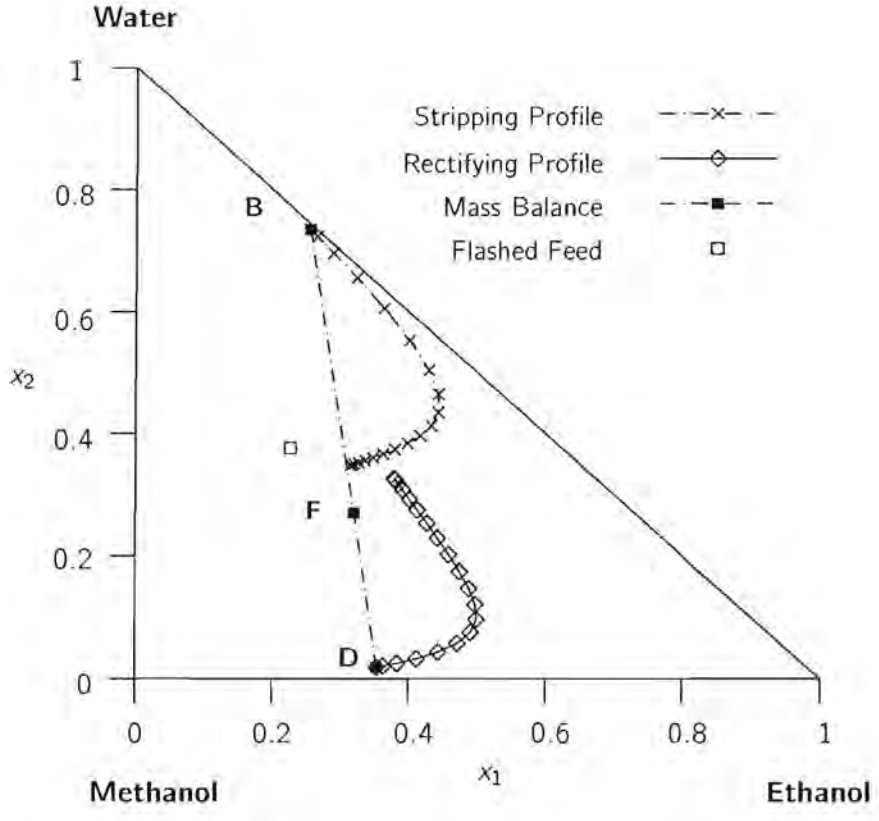

Figure D.2: Liquid phase ternary plot of Water versus Ethanol for **Model 2**: *Finding a feasible solution:* (Section 5.2.1)

D.2 Starting Point Solution: General Profiles

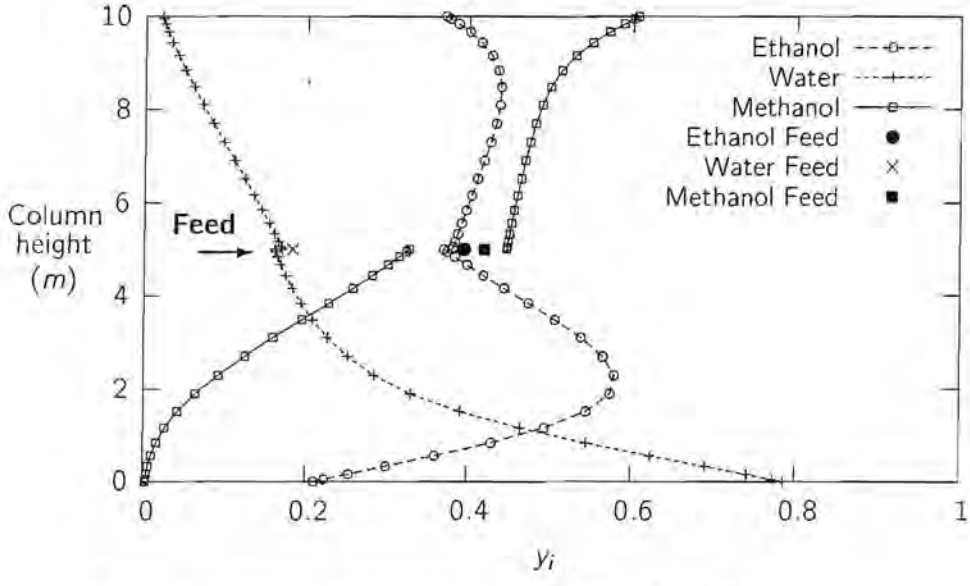

Figure D.3: Vapor Composition profiles for **Model 2**: *Finding a feasible solution:* (Section 5.2.1)

D.2.1 Optimal Feed Position using Temperature

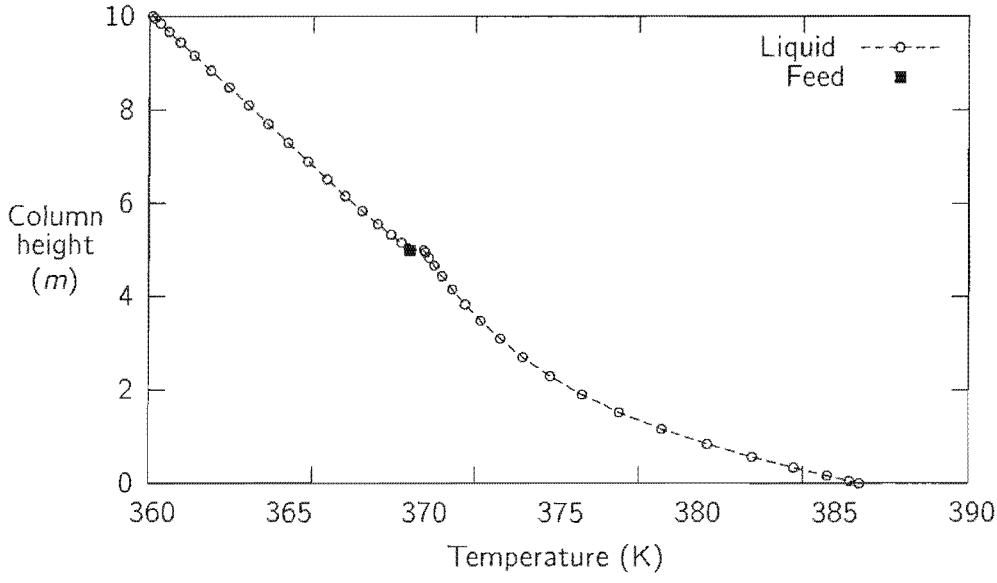

Figure D.4: Liquid Temperature plot for **Model 2**:
Adjusting the internal flows: (Section 5.2.1)

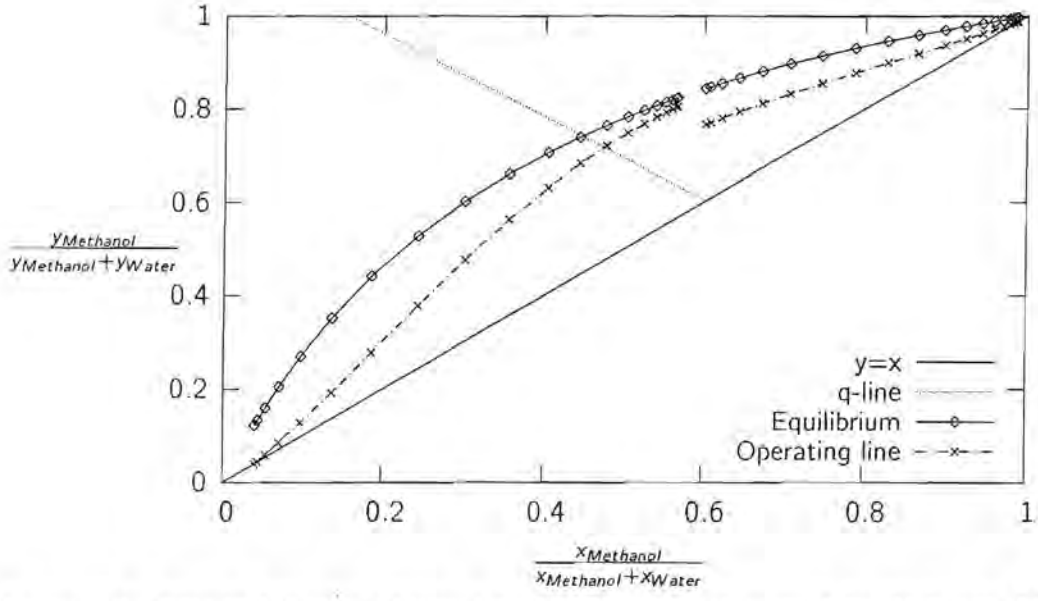

Figure D.5: Pseudo McCabe-Thiele plot of Methanol with respect to Water for **Model 2**: *Adjusting the internal flows:* (Section 5.2.1)

Appendix E

Results: Model 3

E.1 Starting Point Solution: Ternary Diagrams

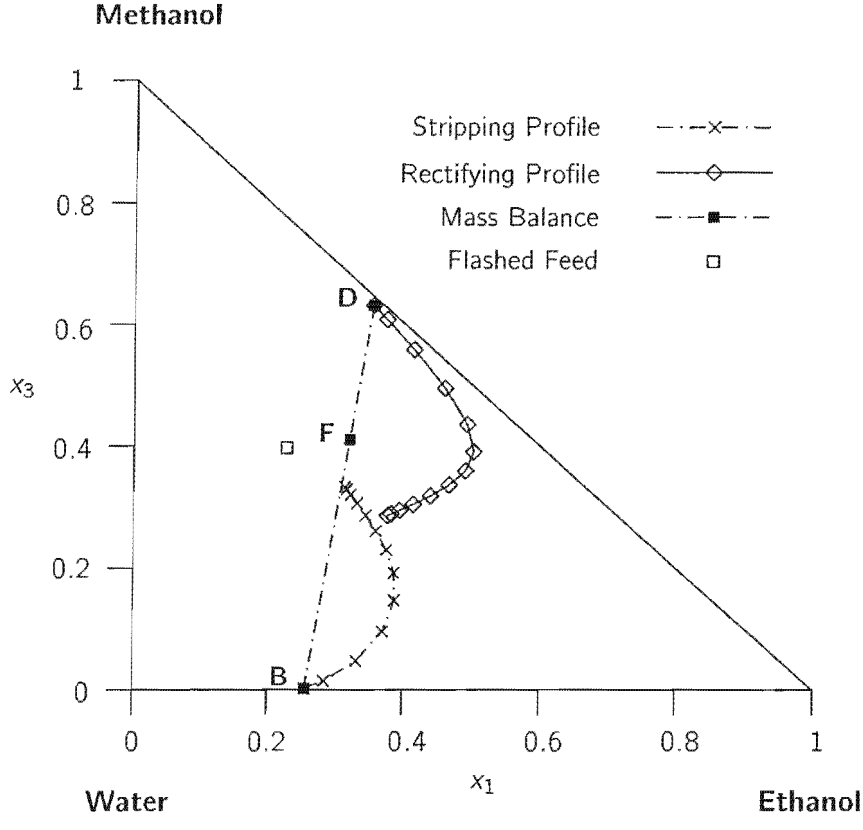

Figure E.1: Liquid phase ternary plot of Methanol versus Ethanol for **Model 3**: *Finding a feasible solution:* (Section 5.3.1)

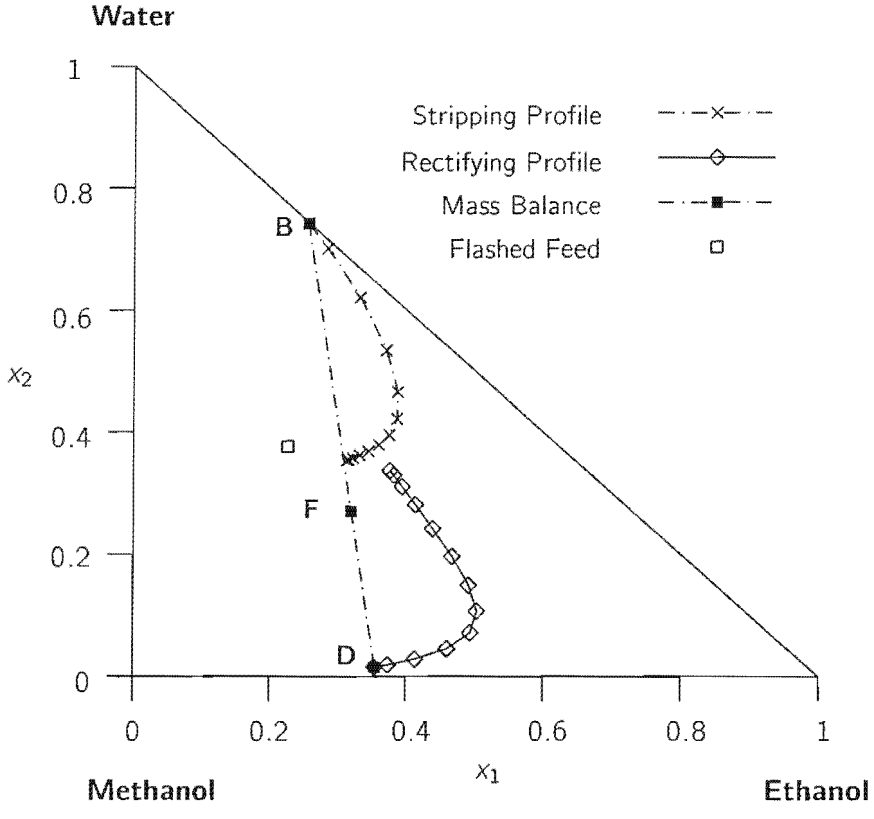

Figure E.2: Liquid phase ternary plot of Water versus Ethanol for **Model 3**: *Finding a feasible solution:* (Section 5.3.1)

E.2 Starting Point Solution: Pseudo McCabe-Thiele Diagrams

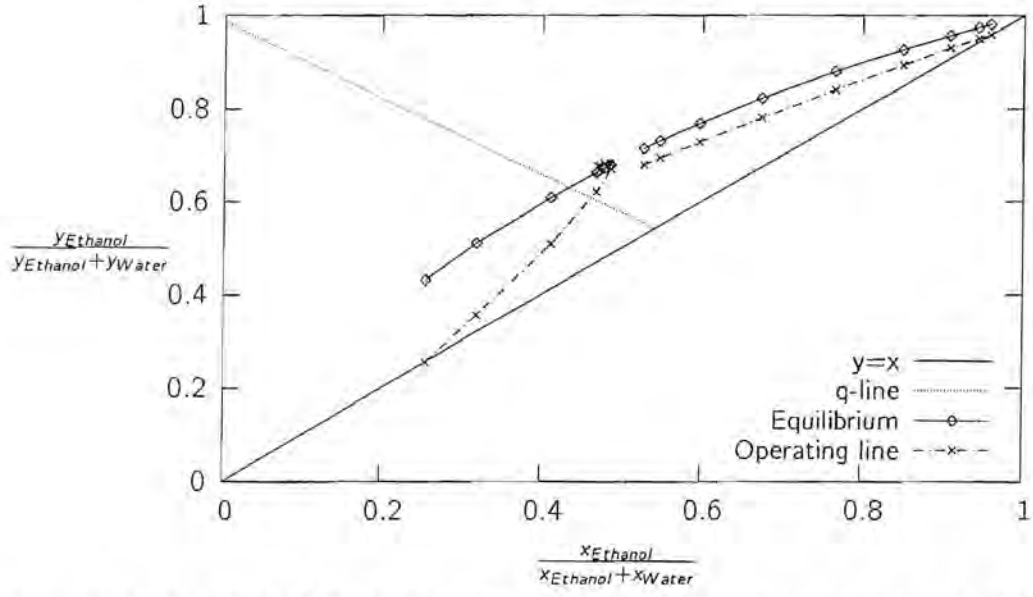

Figure E.3: Pseudo McCabe-Thiele plot of Ethanol with respect to Water for **Model 3**: *Finding a feasible solution* (Section 5.3.1)

E.3 Starting Point Solution: General Profiles

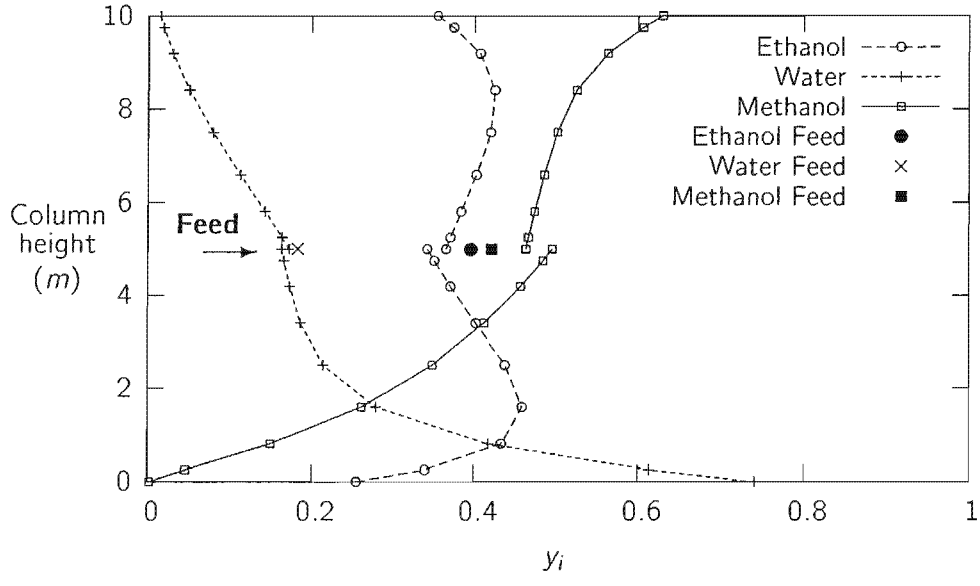

Figure E.4: Vapor Composition profiles for **Model 3**:
Finding a feasible solution: (Section 5.3.1)

E.4 Minimum Flows

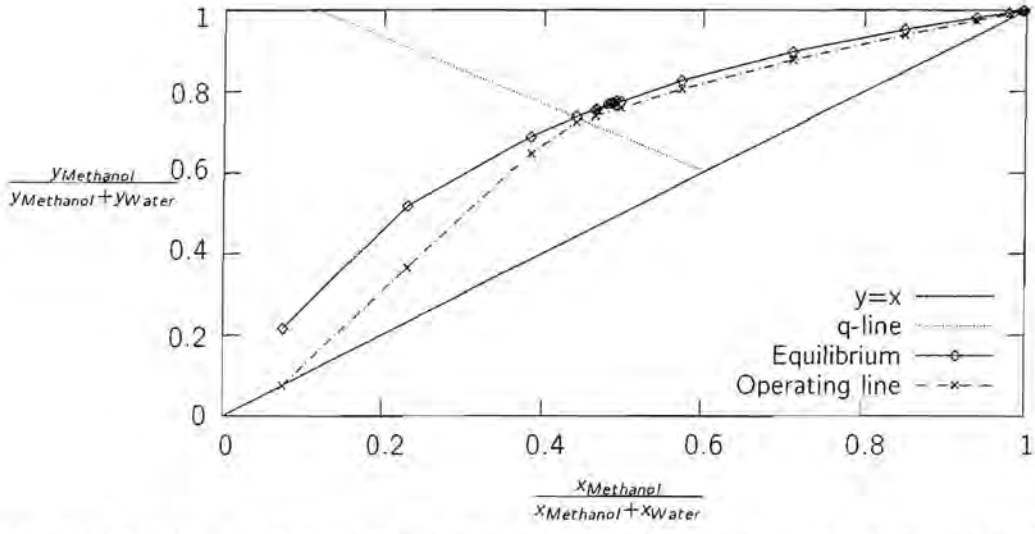

Figure E.5: Pseudo McCabe-Thiele plot of Methanol with respect to Water for **Model 3**: *Finding the minimum height for a specified separation in both the distillate and bottoms* (Section 5.3.2)

E.5 Minimum Height

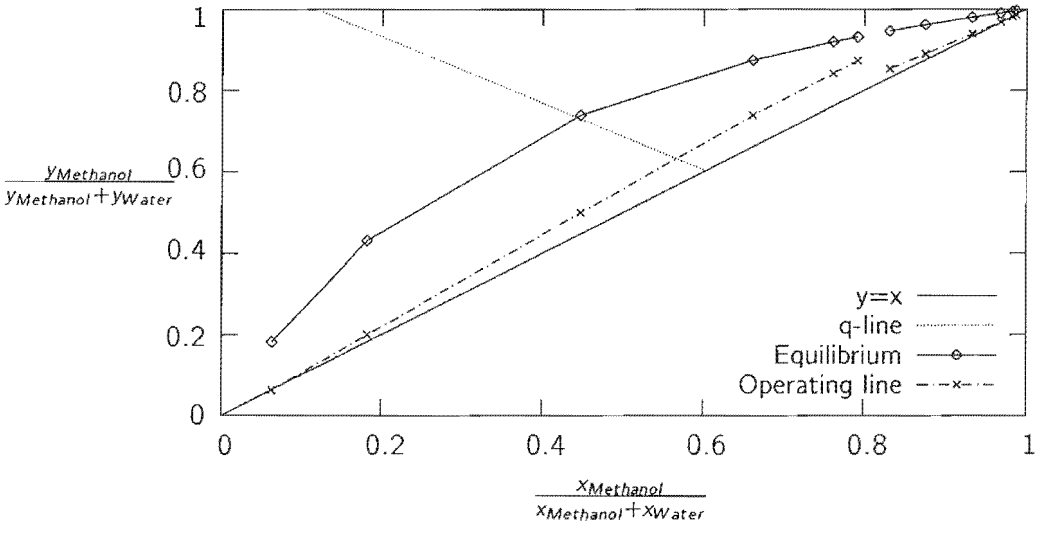

Figure E.6: Pseudo McCabe-Thiele plot of Methanol with respect to Water for **Model 3**: *Finding the minimum flows for a fixed bottoms composition of Methanol* (Section 5.3.2)

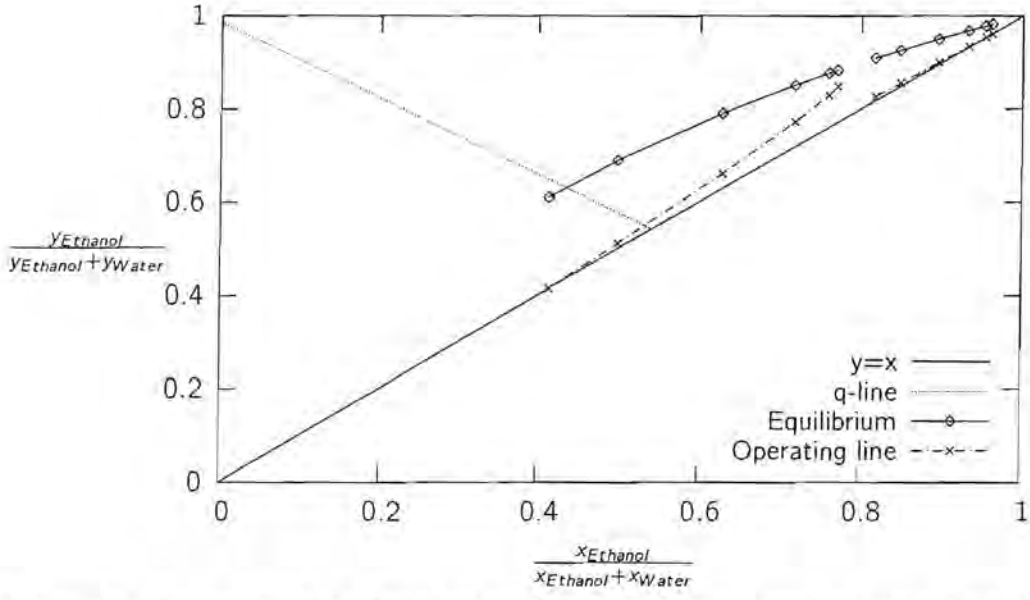

Figure E.7: Pseudo McCabe-Thiele plot of Ethanol with respect to Water for **Model 3**: *Finding the minimum height for a specified separation in both the distillate and bottoms* (Section 5.3.2)

Appendix F

Results: Investigating the Separation Feasibility

Table F.1: Solutions for **Model 3** with constant reboil ratio indicating a counter-intuitive increase in methanol purity in the bottoms with increasing reflux ratio: *ChemSep Solution*

Ratios		Methanol Purity		Separation Ratios		Methanol Recovery
Reflux	Reboil	Bottoms	Distillate	$\frac{d_{Methanol}}{b_{Methanol}}$	$\frac{D}{B}$	Distillate
1.0	2.4	0.008	0.715	86.4	1.88	99.4 %
2.0	2.4	0.031	0.846	27.4	1.17	97.0 %
2.5	2.4	0.040	0.906	22.4	0.984	95.7 %
3.0	2.4	0.048	0.965	19.9	0.852	94.4 %
3.5	2.4	0.073	0.999	13.6	0.750	91.1 %
4.0	2.4	0.117	0.999	8.55	0.666	85.1%

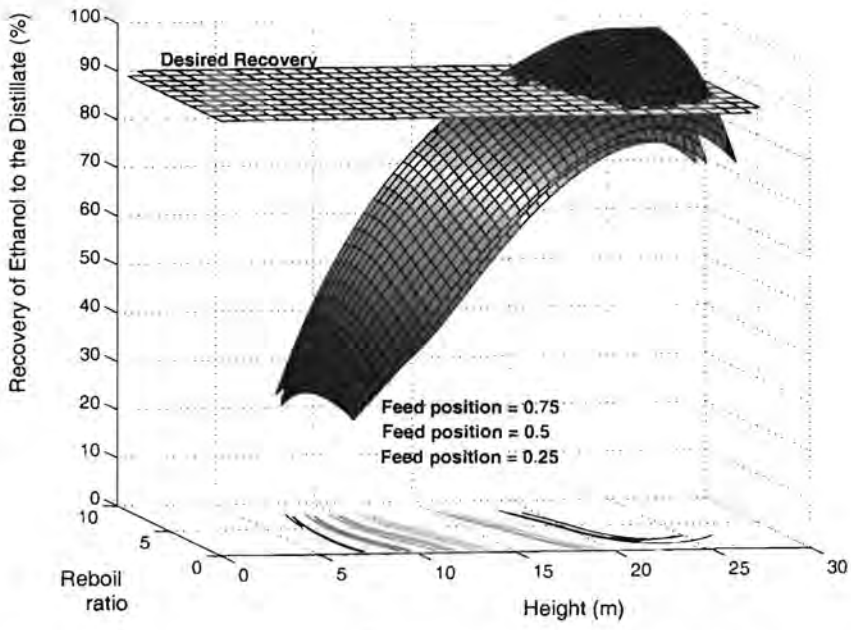

Figure F.1: Investigating the Separation Feasibility for **Model 2**: Recovery of Ethanol to the distillate as a function of the *reboil ratio*, *feed position* and the *height*. The reflux ratio is 2 with a desired recovery > 90%

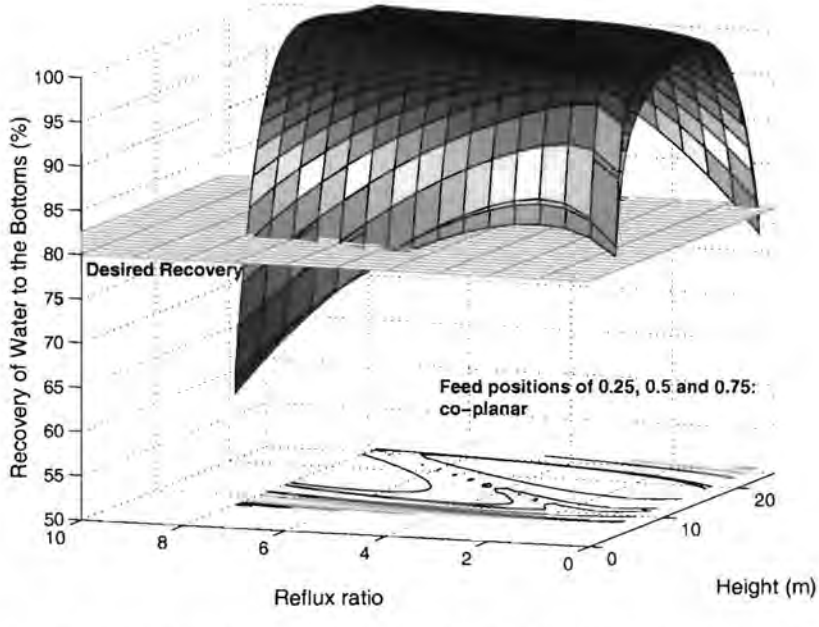

Figure F.2: Investigating the Separation Feasibility for **Model 2**: Recovery of Water to the bottoms as a function of the *reflux ratio*, *feed position* and the *height*. The reboil ratio is 1 with a desired recovery > 80%

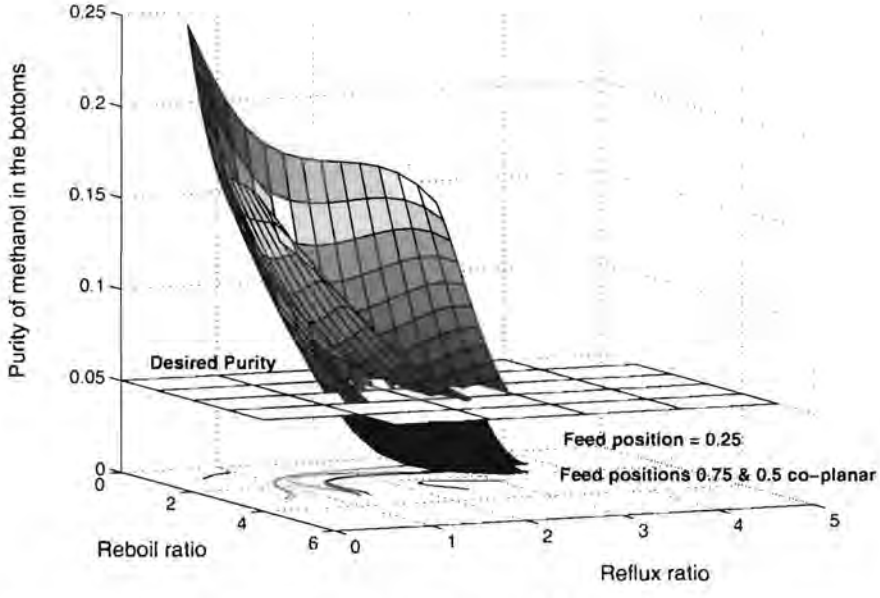

Figure F.3: Investigating the Separation Feasibility for **Model 2**: Purity of Methanol in the bottoms as a function of the *reflux ratio*, *reboil ratio* and the *feed position*. The height is 15m and the desired purity < 0.05

As per University regulations: *I know the meaning of plagiarism and declare that all the work in this document, save for that which is properly acknowledged, is my own*

Index